

November 2023

MICRO AND NANO R2R EMBOSSING OF EXTRUDED POLYMERS

Raymond S. Frenkel
University of Massachusetts Amherst

Follow this and additional works at: https://scholarworks.umass.edu/dissertations_2



Part of the [Manufacturing Commons](#), and the [Nanoscience and Nanotechnology Commons](#)

Recommended Citation

Frenkel, Raymond S., "MICRO AND NANO R2R EMBOSSING OF EXTRUDED POLYMERS" (2023). *Doctoral Dissertations*. 2883.

<https://doi.org/10.7275/36002525> https://scholarworks.umass.edu/dissertations_2/2883

This Open Access Dissertation is brought to you for free and open access by the Dissertations and Theses at ScholarWorks@UMass Amherst. It has been accepted for inclusion in Doctoral Dissertations by an authorized administrator of ScholarWorks@UMass Amherst. For more information, please contact scholarworks@library.umass.edu.

MICRO AND NANO R2R EMBOSSING OF EXTRUDED POLYMERS

A Dissertation prepared

by

RAYMOND S. FRENKEL

Submitted to the Graduate School of the
University of Massachusetts Amherst in partial fulfillment
of the requirements for the degree of

DOCTOR OF PHILOSOPHY

September 2023

Mechanical and Industrial Engineering

© Copyright by Raymond S. Frenkel 2023

All Rights Reserved

MICRO AND NANO R2R EMBOSsing OF EXTRUDED POLYMERS

A Dissertation Presented


by

RAYMOND S. FRENKEL

Approved as to style and content by:


DocuSigned by:

8774B2004924412...
Jonathan P. Rothstein, Chair

DocuSigned by:

778R3BF779D74F7
Stephen S. Nonnenmann, Member

DocuSigned by:

970A3BFC1602464...
Ching Shung Chang, Member

DocuSigned by:

3F8496455D304DC...
Sundar Krishnamurthy, Department Head
Mechanical and Industrial Engineering

ACKNOWLEDGEMENTS

I wish to acknowledge and express my appreciation for the guidance, shared experience, and general mentoring of my research and academic advisor, Professor Byung H. Kim. His patience and insight and research acumen help me succeed in this effort.

I also wish to thank my colleagues and fellow grad students for all their assistance, their encouragement and their friendship.

Many thanks also go to Richard Winn, Miles Eastman, Richard Miatowski and Colby Norwood of the College of Engineering, Engineering Technical Support Services who did machining and welding of components and helped to secure materials. Allan Rakouskas and all the professional staff of the Department of Mechanical and Industrial Engineering deserves mention for all their help. To the National Science Foundation and The Center for Hierarchical Manufacturing (CHM) at the University of Massachusetts Amherst - Professor Kenneth Carter, Professor James Watkins, and Dr. Jacob John and to John Nicholson in the Nanofabrication Clean Room. Also, Professor Donggang Yao, Professor Wen Chen for their assistance and my dear friends Scott Patashnick, J.D. and Sam Cabot, Ph.D. for their encouragement and editorial review.

Special acknowledgements are due Professor Jonathan P. Rothstein and Professor Ching Shung Chang who served as committee members.

Finally, I must acknowledge the loving support of my wife, Margaret.

ABSTRACT

MICRO AND NANO R2R EMBOSSING OF EXTRUDED POLYMERS

SEPTEMBER 2023

Raymond S. Frenkel, B.S., UNIVERSITY OF MASSACHUSETTS AMHERST

M.S.C.E., UNIVERSITY OF MASSACHUSETTS AMHERST

M.S.M.E., UNIVERSITY OF MASSACHUSETTS AMHERST

Ph.D., UNIVERSITY OF MASSACHUSETTS AMHERST

Directed by: Professor Byung Kim

This dissertation presents a process for directly imprinting or embossing extruded polymers as an advancement in roll-to-roll (R2R) embossing methods that avoids the problems of converting preformed films, increases throughput, and reduces costs. A proof-of-concept R2R apparatus was designed and constructed for directly embossing extruded polymer, and experimental results were evaluated. This laboratory scale R2R apparatus employed a thin metal ribbon belt mold with micro or nano scale features in a calendaring setup, with a close coupled induction heating (IH) coil to preheat the ribbon mold above glass transition temperature (T_g) of the polymer, prior to contact with the extrudate at the nip of the calender. This allowed the melted polymer to fully fill the mold patterns before starting to solidify. The thin ribbon mold rapidly conducted heat to the calender roller, providing an effective cooling stage. Microscale and nanoscale features were imprinted directly onto extruded polymer film at a rate of 10 to 12 meters per second, three to over one hundred times the throughput of current R2R processes and orders of magnitude faster than planar processes. Metal ribbon mold belts with nano features were needed to test the direct embossing of extruded polymers at the nano scale. Three different avenues were

taken to make such ribbon belts. First, preset nickel alloy molds were obtained. A master mold of the Book of Leviticus with letters 6 μm in width, 6 to 9 μm tall and 60-170 nm high and a nickel alloy DVD master mold with track pitch of 740 nm and 105 nm deep Pits between 400 nm and 1900 nm long. These were welded into stainless steel ribbon belts to form belt molds. Second, a process was developed using base forms or mandrels for metal-forming nickel ribbon belt molds with test patterns that included gratings from 70 to 500 nm and pillars having diameters of 1 μm , 700 nm, 500 nm and 350 nm. Third, an investigation of metal glass (MG) as a candidate mold material was undertaken and a laboratory scale mechanism was designed and constructed to emboss metal glass surfaced rollers thermally.

TABLE OF CONTENTS

	Page
ACKNOWLEDGEMENTS.....	IV
ABSTRACT.....	V
LIST OF TABLES.....	X
LIST OF FIGURES.....	X
CHAPTER 1 INTRODUCTION.....	1
1.1 Goal of Research.....	1
1.2 Problem Statement.....	1
1.3 Current state-of-the-art.....	5
1.4 Modeling Process Parameters.....	10
CHAPTER 2 MICROSCALE MOLD.....	12
2.1 Early Work.....	12
2.2 Design of Variotherm Extrusion Roller Imprinting Process.....	12
2.4 Experimental setup.....	18
2.5 Results of early testing.....	24
CHAPTER 3 NANO SCALE MOLD: METHODS.....	30
3.1 Overview.....	30

3.2 Creating a mold	30
3.3 Processes Investigated.....	31
3.4 UV Photolithography and Beyond	32
3.5 Direct Laser and Electron Beam Etching.....	36
3.6 Nano Imprint Lithography (NIL)	37
CHAPTER 4 NANO SCALE MOLD: IMPLEMENTATION	39
4.1 Experimental Setup	39
4.2 Other Mold Belts	46
CHAPTER 5 NANO SCALE MOLD: RESULTS	48
5.1 Mold Belts Made by Metal Forming.....	48
5.2 Other Ribbon Belt Molds	55
5.2.1 Alumina Ceramic Filter Discs	55
5.2.2 Master Mold of the Book of Leviticus	56
5.3 The Nickel Alloy DVD Master Mold	58
CHAPTER 6 DISCUSSION.....	60
6.1 Nickel Sulfamate Versus Nickel Sulfate Metal Forming.....	60
6.1.1 Metal Forming	60
6.1.2 Nickel Sulfate	63
6.1.3 Adding a Copper Layer	64

6.2 NOA Adhesion to Nickel	65
6.3 Removal of NOA 81	66
Chapter 7 Process For Embossing a Metal Glass Roller with Microfeatures.....	69
7.1 Introduction	69
7.2 Determining the processing protocol by experimentation	69
7.3 Testing the operating parameters with the roller hot emboss mechanism ..	77
7.3.1 Roller hot embossing mechanism design	77
7.3.2 Use of 5 mm wide rings to test the determined processing protocol parameters	81
7.3.3 Experiments	83
7.4 Roll-to-Roll embossing of extruded LDPE with the MG ring.....	91
CHAPTER 8	96
CONCLUSIONS.....	96
BIBLIOGRAPHY.....	99

LIST OF TABLES

TABLE 1: SPECIFIC COMPOSITION OF THE Zr MG EXTRUDED TUBE.	70
--	----

TABLE 2: EMBOSsing TIME, TEMPERATURE, AREA AND PRESSURE AT 100 NEWTONS.....	76
---	----

LIST OF FIGURES

FIGURE 1: FORMATION OF REPLICATION DEFECTS DURING THERMAL ROLLER IMPRINTING:	
--	--

(A) ENGAGING; (B) IMPRINTING; (C) INCOMPLETELY FILLED CAVITY; (D) DISTORTED STRUCTURES.	2
---	---

FIGURE 2: SCHEMATIC SETUP OF VARIO THERM EXTRUSION ROLLER IMPRINTING.....	13
---	----

FIGURE 3. INDUCTION HEATING OF BELT MOLD.....	17
---	----

FIGURE 3: C. W. BRABENDER TYPE 125-25HC FOUR ZONE 1.25 INCH EXTRUDER AND PID CONTROLLERS.....	19
--	----

FIGURE 4: STANDARD EXTRUDER SCREW.....	19
--	----

FIGURE 5: STANDARD TWO-PART SPLIT DESIGN RIBBON DIE.	20
---	----

FIGURE 6: COMPACT DESIGN RIBBON DIE MADE USING EDM.....	20
---	----

FIGURE 7: TWO-PIECE ROLLER FOR RIBBON MOLD CHANGING.	20
---	----

FIGURE 8: MODIFIED JEWELERS ROLLING MILL.	21
--	----

FIGURE 9: INDUCTION HEATING COIL SHOWN FROM THE BELOW AND ABOVE THE RIBBON MOLD.	22
--	----

FIGURE 10: 60 MM WIDE CLOSED LOOP FLEXIBLE RIBBON MOLD.....	22
---	----

FIGURE 11: CROSS-SECTION OF MOLD PATTERN GEOMETRY	23
--	----

FIGURE 12: PHOTOGRAPH AND FUNCTIONAL ILLUSTRATION OF THE RIBBON MOLD AND CALENDER ROLLER SETUP.	23
---	----

FIGURE 13: PATH OF EXTRUDED WEB.....	24
--------------------------------------	----

FIGURE 14: PROFILOMETER GRAPH OF EMBOSSED LDP	24
FIGURE 15: SEM IMAGE AND PROFILOMETRY OF THE RIBBON MOLD.	25
FIGURE 16: MICROSCOPY IMAGES AND PROFILOMETER GRAPHS: (A) NO HEAT, (B) 1.2 kW, (C) 1.6 kW.	27
FIGURE 17: VEECO DEKTAK STYLUS PROFILOMETER 3D FOR LDPE FILMS IMPRINTED WITH (A) NO HEAT, (B) 1.2 kW AND (C) 1.6 kW.	28
FIGURE 18: DIGITAL MICROSCOPY IMAGES AND PROFILOMETER GRAPHS OF THE NICKEL ALLOY MOLD.	28
FIGURE 19: DIFFRACTION GRATING PATTERN WITH HELIUM-NEON LASER (632.8 NM).	29
FIGURE 20: R2R UV NIL PROCESS FOR FORMING NANO FEATURES ON PET FILM.	39
FIGURE 21: PET FILM WITH THE NOA 81 FEATURES.	40
FIGURE 22: NANONEX NANOIMPRINT TOOL AND EMBOSSED TFE FROM SI MASTERS.	41
FIGURE 23: PTFE AS MOLD FOR UV NIL ON THE NANO EMBOSS 100.	41
FIGURE 24: COATING OF PET FILM WITH NICKEL IN THE SE-600 ELECTRON BEAM EVAPORATOR.	42
FIGURE 25: PET WITH SEED Ni, PLATING BATH AND 200 UM THICK NICKEL BELT.	42
FIGURE 26: RIBBON BELT MOLD BEING INSTALLED.	43
FIGURE 27: TAKE-OFF AND COOLING ROLLER.	44
FIGURE 28: POLYMER WEB LEAVING THE TAKE-OFF ROLLER.	45
FIGURE 29: COOLING ROLLERS AND WINDER	45
FIGURE 30: CURING THE GLUE IN AN OVEN TO SECURE ALUMINA FILTER DISKS TO SS RIBBON BELT AND THE BELT INSTALLED ON THE CALENDER ROLL.	46
FIGURE 31: THE BIBLE BOOK OF LEVITICUS MASTER MOLD AS A RIBBON MOLD.	47

FIGURE 32: NICKEL ALLOY DVD MASTER MOLD MICRO-WELDED INTO A SS RIBBON LOOP AND INSTALLED ON THE ROLLING MILL OR CALENDER ROLLER.	47
FIGURE 33: SEM IMAGE OF NI BELT SECTION SHOWING DIFFERENT GRATING SIZES OF THE IBM TEST PATTERN.....	49
FIGURE 34: SEM OF A SECTION OF THE 500 NM PATTERNED NICKEL MOLD SHOWING NOA 81 CONTAMINATION.....	49
FIGURE 35: SEM IMAGES OF NI COPY OF A SECTION OF IBM TEST PATTERN.	50
FIGURE 36: SEM IMAGE OF THE 500 NM GRID IN NOA 81 ON PET (71)	50
FIGURE 37: KEYENCE VK-X 200 LASER CONFOCAL MICROSCOPE IMAGES OF IBM TEST PATTERN IN NI MOLD.	51
FIGURE 38: KEYENCE VK-X 200 LASER CONFOCAL MICROSCOPE IMAGES OF EMBOSSED EXTRUDED LDPE.....	51
FIGURE 39: AFM ANALYSIS, 3D IMAGE AND A PLOT OF THE PROFILE LDPE SAMPLE.	52
FIGURE 40: SEM IMAGES OF THE UV-NIL R2R PILLARS IMPRINTED IN NOA 81 ON PET HAVING DIAMETERS, (A) 1 μ M, (B) 700 NM, (C) 500 NM AND (D) 350 NM (71).	53
FIGURE 41: AFM OF PILLAR HOLES IN NI MOLD, 3D IMAGE AND PROFILE PLOT.....	54
FIGURE 42: PILLARS ON PET FILM IMPRINTED BY UV NIL ROLL-TO-ROLL SYSTEM, THE 3D IMAGE OF THE PILLARS AND THE PROFILE OF THE PILLARS ALONG THE HORIZONTAL WHITE LINE. THE SIZE OF THE PILLARS WERE 450-500 NM DIAMETER AND 66-90 NM HEIGHT.....	54
FIGURE 43: PILLARS ON LDPE FILM IMPRINTED THERMALLY BY ROLL-TO-ROLL PRODUCTION, THE 3D IMAGE OF THE PILLARS AND THE PROFILE OF THE PILLARS	

ALONG THE HORIZONTAL WHITE LINE. THE DIAMETER AND HEIGHT OF THE COLUMNS WERE ABOUT 645-660 NM AND 120-170 NM HEIGHT.....	55
FIGURE 44: AN AFM ANALYSIS OF THE SURFACE OF AN ALUMINA CERAMIC FILTER DISK FOR 10 μ M AND 1 μ M.	56
FIGURE 45: AFM ANALYSIS OF LEVITICUS NI MASTER MOLD (TOP) AND THE EMBOSSED LDPE PRODUCED BY THE CONTINUOUS EXTRUSION-TO-EMBOSSING PROCESS (BOTTOM). THE IMAGES ON THE RIGHT ARE THE HEIGHT ANALYSIS OF THE FEATURES SHOWN ON THE LEFT. THE DEPTH OF IMPRINTED LETTERS IN THE LDPE WAS 60-170 NM AND THE GRAPH IS THE HEIGHT PROFILE UNDER THE WHITE LINE IN THE LDPE IMAGE.	57
FIGURE 46: SEM ANALYSIS OF EXTRUDED LDPE COMPARING WITH AND WITHOUT IH AT DIFFERENT HORIZONTAL WITH OF FIELD (HWF) SETTINGS.....	59
FIGURE 47: NICKEL SULFAMATE PLATING BATHS.	61
FIGURE 48: FLAWS FROM THE CONDUCTIVE SILVER PAINT.....	61
FIGURE 49: THE FLAWS AFTER REMOVING THE PET BASE WITH HEAT TREATMENT.	61
FIGURE 50: MOLD BELT BEFORE AND AFTER HEAT TREATMENT IN A VACUUM OVEN.....	62
FIGURE 51: MOLD RIBBON BELT BEING INSTALLED.....	63
FIGURE 52: WEAK SEAM, PLATING OVER SEAM, STRONGER SEAM, VIEW THROUGH MICROSCOPE.	64
FIGURE 53: BELT WITH COPPER LAYER, CRACKING AND DELAMINATING, REPAIRED WITH SOLDER.	64
FIGURE 54: REFRACTION COLORS FROM NANO FEATURES ON THE MOLD BELT AND THE REMOVED PET MANDREL.....	65

FIGURE 55: THE NICKEL SEPARATED FROM THE MANDREL UNDER PLATING TENSILE STRESS.	66
FIGURE 56: NOA 81 CONTAMINATED BELT MOLD SOAKING IN DCM AND HEATED.	66
FIGURE 57: MOLD BELT SOAKING IN DCM ON ACOUSTICALLY DRIVEN PLATFORM.....	67
FIGURE 58: THE SS TANK WITH THE TEN 40 KHZ TRANSDUCERS MOUNTED ON THE BOTTOM.	68
FIGURE 59: THE MOLD BELT SOAKING IN NMP SUSPENDED IN THE ULTRASONIC CLEANER	68
FIGURE 60: A 5 MM WIDE RING SECTION OF THE MG CYLINDER, IN THE EDM TO CUT 5 MM SECTIONS.	71
FIGURE 61: (A) THE INSTRON TEST FIXTURE AND ZR-BASED MG SAMPLES (5 MM 5 MM 1 MM) CUT FROM THE TUBE FOR IMPRINTING TESTS. (B) THE DRAWING OF THE FIXTURE AND THE HOLDING STRAP.....	72
FIGURE 62: (A) THERMOPLASTIC FORMING STAGE USING INSTRON 5969 DUAL-COLUMN TESTING SYSTEM WITH THE FORCE CAPACITY UP TO 50 kN AND HEATING TEMPERATURE UP TO 600 °C. (B) A TEST SAMPLE MOUNTED ON THE FIXTURE.	72
FIGURE 63: ZYGO PROFILOMETER SURFACE PROFILE AND LINE PROFILE OF THE NICKEL ALLOY MOLD.....	73
FIGURE 64: OM IMAGES OF ZR-BASED MG EMBOSSED AT (A) 450 °C FOR 5 s AND (B) 470 °C FOR 2 s.	74
FIGURE 65: CALCULATING AREA OF EMBOSSED PATTERNS.	75
FIGURE 66: THE RELATIONSHIP BETWEEN TEMPERATURE, PRESSURE AND DEPTH OF INDENTATION.....	76
FIGURE 67: DESIGNED ROLLER HOT EMBOSsing MECHANISM.....	78

FIGURE 68: THE BASE ASSEMBLY INCLUDING THE HOT PLATE AND THE INSULATING CERAMIC (YELLOW).	79
FIGURE 69: THE UNDERSIDE OF THE BASE ASSEMBLY SHOWING THE HEATERS.	79
FIGURE 70: THE BEARING HOUSING ASSEMBLY.....	80
FIGURE 71: SIDE WALL SHOWING REPLACEABLE CAM PLATE.	80
FIGURE 72: THE ROLLER HOT EMBOSSING MECHANISM WITH WIDER SIDE WALLS.....	81
FIGURE 73: MANDREL ROLLER FOR TESTING 5 MM MG RINGS.....	81
FIGURE 74: THE ZR RING ON THE MANDREL AND THE NI PRIMARY MOLD ON THE AL BLOCK.	82
FIGURE 75: MEASURING PRESSURE WITH FUJIFILM PRESCALE® FILM.....	83
FIGURE 76: THE MG RING OFF CENTER ON THE MANDREL TAPER, THE NI MOLD ON THE AL BLOCK AND THE HALF-EMBOSSSED RING SEGMENT.....	83
FIGURE 77: PATH OF THE FIRST EMBOSSING OF A MG RING.	84
FIGURE 78: PROFILOMETER SURFACE PROFILE AND LINE PROFILE OF EMBOSSED SEGMENTS OF 1 ST MG RING.	85
FIGURE 79: THE THREE SEGMENTS OF THE MG RING AND MOTOR CONTROLLER.....	86
FIGURE 80: PROFILOMETER SURFACE PROFILE AND LINE PROFILE OF EMBOSSED SEGMENTS OF 2 ND MG RING.....	87
FIGURE 81: GRAPH OF EMBOSSING DEPTH VS. SURFACE SPEED.	88
FIGURE 82: GLASS PLATE AND CERAMIC WOOL INSULATION UNDER THE HOT ROLLER EMBOSSING MECHANISM.	89
FIGURE 83: HOTPLATE TEMPERATURE CONTROLLER AND AL BLOCK THERMOCOUPLE DISPLAY.	89

FIGURE 84: THE NICKEL MOLD CURLED.	90
FIGURE 85: THE NI MOLD CURLED AND THE PROFILOMETER SURFACE PROFILE AND LINE PROFILE OF THE 3 RD RING.....	90
FIGURE 86: PROFILOMETER ANALYSIS OF 4 TH MG RING.....	91
FIGURE 87: ROLLING MILL WITH 40 MM DIAMETER ROLLERS ADAPTER TO SERVE AND A CALENDER.....	92
FIGURE 88: PATH OF LDPE WEB THROUGH THE CALENDER, OVER THE COOLING ROLLER AND TO THE WINDER.	93
FIGURE 89: THREE OM IMAGES OF THE LDPE RIBBON.....	94
FIGURE 90: PROFILE VIEWS OF EMBOSSED LDPE	95

CHAPTER 1

INTRODUCTION

1.1 Goal of Research

Current technologies for nano patterning complex 2-D and 3-D structures suffer inherent low productivity and consequently high costs. Processes such as Photo lithography (PL), nano imprint lithography (NIL), and direct metal imprinting (DMI) are secondary or converting operations on previously produced thin-film materials.

The motivation behind this research was the need to continuously emboss micro and nanostructures on polymer film economically on a production scale. This research developed a continuous roll to roll (R2R) process for embossing micro and nano structures onto extruded polymers at production processing speeds using a thin metallic (nickel) continuous belt mold. This process will allow the manufacture of thin-film materials with a micro or nano-structured surface. Potential uses of this technology include microelectronics, micro electromechanical systems (MEMS), specialty coatings, microfluidic systems, bio-molecular segregation, polymerase chain reaction, micro arrays, micro reactors, micro-optical devices and micro lenses, micro gratings, micro prisms, extruded polymer sheets with micro-scale and/or nano-scale hydrophobic features to support research on superhydrophobic surfaces [1] [2] [3] and any number of micro or nano products of the future.

1.2 Problem Statement

An accurate and complete rendering of the imprint mold on the surface of an extruded polymer requires precise control of the heating and cooling of the mold as well

as of the extrudate. Since the surface energies of most polymers do not substantially vary with temperature or between different polymers [4], the viscosity is of primary concern and is a function of temperature. The viscosity of the extrudate must be low enough to allow complete filling of the mold cavities. This precludes premature cooling of the extrudate with mold contact and therefore necessitates heating of the mold before application. Existing investigations on thermoplastic roller imprinting revealed poor pattern transfer fidelity, especially for high-aspect-ratio features. The standard roller imprinting process involves a constant-temperature roller mold for imprinting, leading to an undesirable thermomechanical history for the imprinted polymer. Due to the lack of effective cooling, the polymer film leaves the roller mold at a temperature higher than the polymer softening temperature. The embossed structures are thus subjected to unwanted viscoelastic recovery after pattern release. Because of viscoelastic recovery, the imprinted surface features are distorted and minimized and, in the worst case, converge to a flat surface. Figure 1 illustrates the formation of replication defects in thermoplastic roller imprinting.

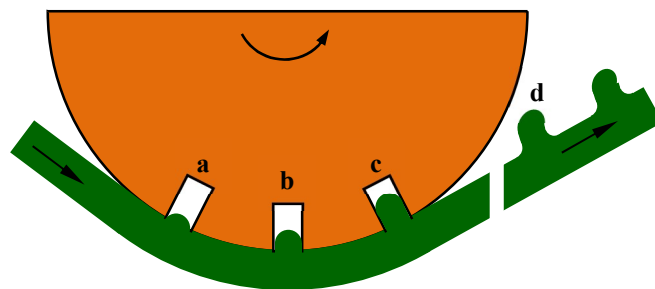


Figure 1: Formation of replication defects during thermal roller imprinting: (a) engaging; (b) imprinting; (c) incompletely filled cavity; (d) distorted structures.

To retain the geometric structures implied by the mold, the extrudate and therefore the mold must be cooled below the glass transition temperature (T_g) before mold separation [5]. It is therefore essential to control the temperature of the mold and the extrudate during the entire embossing or calendering process of extruded polymers.

Successfully forming micro or nano structures on the surface of an extruded polymer is highly dependent on developing an embossing mold. Creating a mold that can be rapidly heated and cooled poses a challenging engineering problem. A mold must be strong enough to endure embossing stresses, durable enough to withstand repeated pressings and thermal cycles, of low enough thermal mass to be rapidly heated and cooled, and have sufficient thermal conductivity to remove heat from the extrudate. A mold made from a thin metallic ribbon can satisfy these requirements. A thin metallic ribbon can be rapidly heated and cooled and is stable at temperatures in excess of 327°C , the crystallization temperature of polytetrafluoroethylene (PTFE). The form of the mold is, by necessity, closely connected to the method chosen for heating and cooling the mold. Creation of the mold is far from trivial, and is the most challenging part of the process.

Some work has been conducted to develop more effective thermal control methods in roller imprinting. Earlier, Michaeli and coworkers [6] proposed to develop tools for dynamically heating the embossing (or imprinting) roller and providing different temperatures over the circumference of the roller. With such an embossing roller, the film can be embossed (or imprinted) in a high temperature zone and then cooled in a low temperature zone on the same roller. In the follow-up studies [7] [8], Michaeli and coworkers developed two technical approaches, induction heating and radiation heating, for variothermally heating the embossing roller and successfully replicated different types

of microstructures in continuous production. Despite the promising results, the primary limiting factor in this process is the large thermal mass of the roller mold. Due to the substantial thermal inertia, rapidly heating and cooling the roller surface and achieving high take-up speed is challenging. A possible alternative to directly heating and cooling the roller is to create a separate belt mold. This belt mold has a low thermal mass and can therefore be rapidly heated and cooled. In fact, thin-shell molds have been successfully used in flat-mold hot embossing [9] [10]. Contact heating is particularly effective in heating such shell molds [11]. Similar ideas may be adapted to roller imprinting for heating belt molds. This may be accomplished by employing multiple pairs of rollers [12] [13]: for example, one pair of rollers for heating the belt mold and a second pair of rollers for cooling the belt mold. Besides contact heating, active heating methods can also be utilized to heat the belt mold. Fagan et al. [14] demonstrated that induction heating can rapidly heat a belt mold, and a temperature difference of more than 200°C can be achieved in continuous roller imprinting. With this imprinting system, they could replicate both micrometer and sub-micrometer patterns at film feed speed exceeding 1.5 m/min. Compared with the heating of the imprinting roller, heating of the belt mold benefits from the low thermal mass and the long path of the belt mold. Therefore, flexible manufacturing systems may be developed for demanding applications in micro- and nanofabrication.

Recently, interest has also emerged in integrating film extrusion with roller imprinting, leading to the development of the extrusion roller imprinting process [7] [15] [16] [17], It is believed that a number of advantages result from such system integration:

- (1) The single-step extrusion and imprinting process minimizes particle contaminant to the web surface.
- (2) Functional materials can be formulated *in situ* to meet particular requirements in specific applications.

- (3) Reheating of the polymer film is not necessary. This mitigates problems caused by the reheating process, e.g., film wrinkling.
- (4) Film tension and temperature can be better controlled. This can reduce residual stress in the imprinted film as well as producing more uniform properties.

The extrusion roller imprinting process essentially bears close similarities with classical film extrusion and post processing. It utilizes the typical viscoelastic behavior of polymer for achieving the optimal process dynamics. The extrusion speed and the roller speed can be independently controlled yet synchronized so as to impart a suitable tension and microstructural development on the film. Due to these similarities, the broad knowledge base developed in conventional polymer processing may be adapted to the new micro- and nanofabrication process.

In this work, we designed and constructed a new extrusion roller imprinting system with a variotherm belt mold and tested its suitability for continuous microfabrication. The system's major components include an extruder, a belt mold, a roll-to-roll setup, and an induction heating unit. The extruded polymer film is imprinted between the belt mold and the pressure roller. Due to the variotherm capability, the imprinted film is effectively cooled before released from the belt mold. The feasibility of the overall manufacturing system was tested, and continuous production of microstructured polyethylene film was established.

1.3 Current state-of-the-art

Micro and nano embossing are forms of microfabrication aimed at streamlining the process of manufacturing micro or nanostructures. Standard lithographic methods evolved from the fabrication of microelectronics, so all the incumbent chemistry was used to create

a master from which copies could be made in a more straightforward printing like process. In the 1980s, Erwin Willy Becker and Wolfgang Ehrfeld of the Institute for Nuclear Process Engineering (*Institut für Kernverfahrenstechnik, IKVT*) in Germany expanded on work done at IBM by Romankiw and coworkers in the late 1960s and early 1970s [18], to develop a process they called Lithographie, Galvanoformung, Abformung (Lithography, Electroplating, and Molding) or LIGA for the manufacturing of high-aspect-ratio structures with lateral precision below one micrometer. They used highly collimated x-rays from a synchrotron accelerator radiation source to expose a thick resist coating of polymethylmethacrylate (PMMA) through a shadow mask. The exposed photoresist was chemically removed in a developing process allowing the exposed electrically conductive substrate to be electroplated, filling in the spaces in the PMMA with metal [19] [20]. After chemically stripping away the remaining PMMA, the electroformed metal microstructure could be used as a mold insert for injection molding or embossing [21]. Prof. Stephen Chou coined the term "Nanoimprint Lithography" (NIL) in 1986 [22]. Early imprint lithography was done mainly as a hot embossing process with thermoplastics and was designated T-NIL when used to create sub-micron feature sizes. In later developments UV curable liquid photo resists were used for low temperature -low pressure, imprint lithography and were designated P-NIL for photo nanoimprint lithography for sub-micron work [23] [24].

Although Lin et al. (1998) reported shorter cycle times when using an electroformed nickel mold insert over directly using the PMMA structure on silicon [25], Wang et al. (2004) claimed that the direct use of micromachined silicon as a tool material for hot embossing of polymers represented a significant reduction in cost and fabrication time for producing embossing masters [26]. Bala Ganesan and David Hardt (2004) showed

the importance of controlling the temperature of the mold and workpiece during the entire forming process, the rate of cooling of the mold and substrate, the mold and substrate platen displacement and displacement rate, and the force applied on the platen and distribution of that force [5]. Kim et al. (2006) reduced the total embossing cycle time to around 20 seconds by applying their rapid thermal response (RAR) mold technology, developed for injection molding in 2002, to the hot embossing process [27]. Nugen et al. (2008) used copper rather than nickel both because its higher thermal conductivity should allow for shorter embossing times and to avoid the high stiction nickel can cause during de-embossing which can disturb channel and structure integrity of the embossed polymer [28].

Chen et al. (2007) describe a novel, simple and inexpensive parallel technique for fabricating nanoscale pattern molds by silicon etching followed by thermal oxidation. The mask pattern was made by Direct photolithography for submicron scale features and photolithography followed by metal over-etching for nano-scale features. The nanomold, when passivated with a Teflon-like layer, was used for first-generation replication using P-NIL and second-generation replication in other materials, such as polydimethylsiloxane (PDMS) [29].

Xinxin Fu et al. (2019) Demonstrated the feasibility of a rapid thermal nanoimprint process by developing a thermal imprint apparatus through induction heating of a nickel mold and suggested that the rapid induction heating of a nickel mold is suitable for fast nanoscale feature replication as a promising means for mass production of flexible devices with micro/nanostructures [30].

To overcome the problem of air entrapment encountered in applying NIL to larger areas or whole wafers, Lee et al. (2007) constructed a roll type UV-nanoimprint lithography

tool by wrapping a PDMS stamp around a transparent quartz cylinder. This allowed any air present to escape as the cylindrical mold contacted the resin covered substrate during the UV-NIL process [31]. A cylindrical mold was used by Osamu Nezuka and Byung Kim (2007) to demonstrate a continuous roll-to-roll (R2R) micro-embossing or P-NIL apparatus that embossed and UV-cured a liquid polymer resin onto a continuous sheet of polyethylene terephthalate (polyester) or PET film [32]. Se Hyun Ahn (2010) used a similar setup for P-NIL but with a flexible fluoropolymer, ethylene-tetrafluoroethylene (ETFE) mold. The ETFE mold was formed by hot embossing to a Si master with a 200 nm pitch pattern formed by laser interference lithography [33].

A hot roller embossing setup was used by S. H. Ng and Z. F. Wang (2008) to make microfluidic devices. A 50 μm thick nickel mold with raised microstructures was fabricated by an electroplating process and wrapped around a heated stainless steel roller. A rubber cylinder was mounted to turn against the hot roller mold and 1.5 mm thick sheets of cast PMMA were run between the rollers. The hot roller temperature, nip force, and temperature were varied to determine optimum operating conditions. There was found to be an optimum temperature for achieving a high embossing depth [34]. Suzuki et al. (2008) fed a thermoplastic sheet onto a nanostructured cylindrical mold and thermally imprinted by vacuum pumping between the mold and the sheet [35]. Yeo et al. (2009) performed a similar investigation using PMMA substrates [36].

Velten et al. (2010) created a cylindrical mold by thinning silicon masters (fabricated using UV lithography) to a thickness that guaranteed mechanical flexibility (40 μm) and sticking the thinned and diced nub wafers with a thin epoxy glue layer (thickness

20 μm) onto a steel carrier foil. The Invar foil with the flexible silicon chips was mounted on the embossing roller and served as embossing master [37].

In Previous efforts in this laboratory (2009) an electroformed nickel ribbon mold was heated by induction before passing it through the nip of a rolling mill with a thermoplastic sheet in a continuous roll-to-roll (R2R) hot nano-embossing process [14]. Temperature, pressure and viscosity were used to calculate the time needed to fill micro and nano features and ultimately to calculate the maximum roll to roll embossing speed. A 250 nm line width, 375 nm period grid with a feature height of 200 nm was successfully duplicated.

Ahn et al. (2009) used a flexible fluoropolymer, ethylene tetrafluoroethylene (ETFE) mold material to replicate 300 nm line width, 600 nm height gratings. The ETFE mold was formed from an original Si mold by a thermal NIL process at 220°C. Several pieces of the ETFE molds were replicated, wrapped, and fixed onto a 6 in. wide tensioned belt to form a ribbon mold which was used to construct a R2R P-NIL apparatus [38].

The effects of mold coatings and injection molding conditions on the final nanostructure quality were explored by Matschuk et al. (2009) who found that optimization of molding parameters only led to slight improvements in replication quality (feature depth and width) but that the application of an antistiction coating resulted in significant improvements that were mainly insensitive to variations in the molding parameters. Nickel mold inserts containing 50 and 100 nm wide pillars with aspect ratios of 1:2 and 1:1 were produced as a replica relief by electroplating of nickel on a silicon wafer based master structure. Microstructures were formed by UV lithography and the Nanostructured holes

were fabricated by electron beam lithography. Some of the mold inserts were coated with 10 nm fluorocarbon polymer by plasma-polymerization of CHF₃ monomer [39].

Shan et al. (2010) heated the surface of a mold using a thin-film heater at the back of a Ni stamp while filling the cavity with polymer to avoid the formation of a solidified layer on the contact surface of the polymer during injection molding. 800- and 200-nm-pitch nanostructures with an aspect ratio of 1–2 were replicated, and the effectiveness of mold surface heating was demonstrated [40].

1.4 Modeling Process Parameters

Worgull et al. (2005) employed detailed process simulation using MOLDFLOW and ANSYS to analyze the parameters influencing demolding forces and contact stresses between the mold and microstructures for large scale (200 mm diameter) hot embossing machines [41]. Taylor et al. (2008) implemented two computationally efficient, simplified material models in Matlab, a purely elastic model and a visco-elastic model, to predict the fidelity of embossed topography given to an arbitrary stamp layout and chosen embossing temperature, pressure and loading duration [42]. A model using nonlinear finite element analysis, along with contact analysis was reported by Stoyanov et al. (2011) to provide insights into the optimal imprint process control [43].

Yao Ren and J. K. Good studied NIP mechanics and highlighted the need to control shear and slip and the stresses that induce them when imprinting thermoplastic webs in NIL converting processes [44].

What is missing in the state of the art is a scalable high speed R2R process to directly imprint or emboss an extruded polymer in the web forming process. R2R NIL processes can be generally separated into two groups: thermoplastic roller imprinting and

UV-curing roller imprinting. As the names suggest, the former involves a thermoplastic polymer as a replicating material while the latter uses a UV-curable resin. High speed R2R UV-NIL processes exist but use expensive UV curable resists to form the nano features and many applications are more suited to having the features directly embossed on the polymer film. In theory, the heating and cooling time required for the T-NIL process makes it slower than UV-NIL [45] but the process developed in this research eliminates the heating time by directly embossing extruded polymer, which is already hot. The throughput of the developed R2R embossing of extruded polymers process should be very competitive with that of UV-NIL.

CHAPTER 2

MICROSCALE MOLD

2.1 Early Work

Prior research at the UMASS Polymeric Materials Manufacturing Lab has shown the superiority of using a continuous closed loop ribbon mold in the micro/nano embossing process. A thin nickel alloy Ribbon mold exhibited better heat transfer capabilities both in heating and in cooling, superior induction heating efficiency by moving through the induction coil and a lower force interface release due to its relatively lower coefficient of temperature expansion when compared to most polymers.

2.2 Design of Variotherm Extrusion Roller Imprinting Process

A simple filling model can be established to understand the micro- and nanocavity filling difficulty in thermal roll imprinting. By assuming constant viscosity and pressure driven flow, one can arrive at the following equation governing the filling process,

$$\mathfrak{R}(t) = \sqrt{\frac{P \cdot t}{6\eta(T, \alpha)}} \quad (1)$$

where \mathfrak{R} is cavity fill ratio, P is pressure, t is time, T is temperature, α is representative cavity size, η is viscosity that is temperature dependent. This equation reveals that to improve cavity fill, one has to increase contact pressure and contact time and reduce viscosity. Qualitatively speaking, the viscosity decreases with an increase in temperature. Since suitable contact pressure is typically limited to a few MPa's and the cavity size is fixed in a specific case, the remaining parameters to adjust are temperature

and contact time. Therefore, it becomes apparent that both temperature and contact time need to be raised to achieve better replication. Besides incorporating an effective filling stage, creating a sufficient holding stage is essential so that viscoelastic recovery after pattern release can be minimized. This requires the imprinted film to be cooled under imprinting pressure and solidified or vitrified before departure from the imprinting roll.

The design of the variotherm extrusion roller imprinting (VERI) process is illustrated schematically in Figure 2. This process is specially designed to create a suitable thermomechanical history for continuous thermal imprinting. It is characterized by several novel features including a variotherm module for controlling the heating and cooling of the polymer film and an endless belt mold for improving contact and creating an effective holding process, as elaborated below.

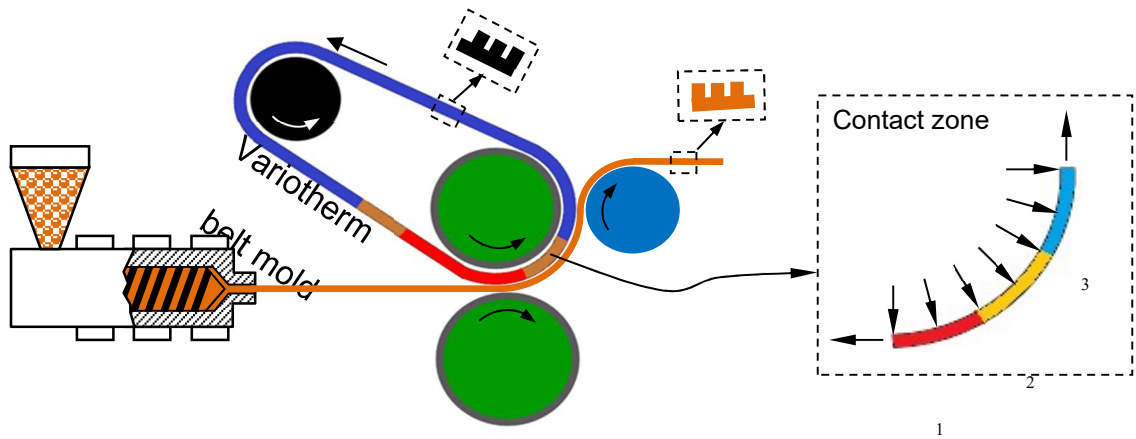


Figure 2: Schematic setup of variotherm extrusion roller imprinting

- The extended contact zone is highlighted on the right, showing decreasing temperature from T_1 to T_3 , and a pressure applied over the entire contact area.

- An extrusion unit for melting and mixing the polymer(s) allows functional materials to be in situ compounded during micro- and nanofabrication. Moreover, with the extruder, reheating of the polymer film is not required. This mitigates problems caused by the reheating process (e.g., film wrinkling, difficulty in tension control, and other factors). Furthermore, the extrusion process allows a film with a desired structure and morphology suitable for roll imprinting to be produced. This can be done by in situ control of the jet stretch, drawing and heat setting stages of the film formation process.
- A belt mold for enlarged contact between the polymer film and the master pattern. Standard roller imprinting processes rely on a tiny contact zone for applying pressure to the polymer film. This results in a short contact time for microcavity filling, causing short shot or underfilled cavities. The belt mold provides a possible solution to this problem by producing pressure in a large contact zone.
- A rapid heating and cooling capability. The belt mold is heated to the polymer softening/melting temperature before reaching the imprinting zone and then gradually cooled along the path of the polymer film. This not only provides a hot mold for filling micro- and nanocavities but also a cold mold for cooling the polymer under holding pressure.

The critical section in the VERI setup is the contact zone, as highlighted in Figure 2. Besides the normal imprinting pressure applied between R1 and R2, the contact pressure generated in the entire contact zone is due to the tension in the extruded viscoelastic film.

An additional carrying film can be placed underneath the extruded film to generate high contact pressure by applying high film tension. The enlarged pressure zone has been considered useful for high-speed imprinting since the polymer gains more time to fill the cavity. The temperature in the contact zone decreases along the film path. This is also an important feature of the new process. The decreasing temperature emulates the typical thermoplastic protocol needed for precision patterning, as used by injection molding and compression molding. The polymer will be deformed primarily in the high temperature zone, T1, held under pressure at reduced temperatures along the polymer path, and finally cooled and released from the belt. The undesired viscoelastic effects can be suppressed by incorporating in-mold holding and cooling stages. This design of the thermomechanical history is considered necessary for precision micro/nano patterning, particularly at high-speed production.

2.3 Rapid Thermal Cycling of Belt Mold

For flat molds, thermoplastics have been extensively used as substrate receivers for transferring micro- and nanostructures. The resulting process is often called “hot imprinting” or “hot embossing.” As its name implies, hot imprinting relies on a mold heated above the glass transition temperature (T_g) for an amorphous polymer or the melting temperature (T_m) for semicrystalline polymers. This elevated temperature is necessary for filling micro- and nanocavities, since the polymer melt would otherwise rapidly freeze or vitrify against a cold mold, leaving an unfilled cavity. After the imprinting stage, the mold is cooled for pattern release. Thermal cycling of a hot imprinting mold is a time consuming process, and cycle times exceeding several minutes are typical in hot embossing and imprinting. [46]

The necessity for thermal cycling in flat-mold imprinting helps us understand the limitation of roller-based processes in thermoplastic patterning. Due to its large thermal mass, a roller mold is difficult to thermally cycle. As a result, when a roller mold is used in patterning, the common practice is to set the mold to a constant temperature. [47] [48] The lack of an in-mold cooling stage is the primary reason why thermoplastic roller imprinting processes have only demonstrated limited capability in precision micro/nano patterning. Currently, limited success has only been demonstrated for roller imprinting of microstructures with relatively low aspect ratios. [12]

Several efforts to improve the thermal cycling efficiency in flat-mold hot imprinting have been reported. The reported methods include contact heating, fluid heating, infrared heating, ultrasonic heating, high frequency and induction heating, and resistive heating. In particular, Kimerling et al. [46] showed that short cycle times of about 10 seconds can be achieved in hot imprinting with high-frequency heating. With proper modification, these methods may be adapted to the heating of the belt mold.

Yao et al. [11] have discussed the general strategies for design and fabrication of a rapidly heatable and coolable mold. The two main building blocks are a low-thermal-mass mold and a means for rapid heating. The belt mold design, rather than the use of a roller mold, conforms well to the first requirement due to the extremely small thermal mass carried by the belt. The long strip design and the thin wall section of the belt also permit some of the heating methods mentioned above to be more effectively implemented. The objective was to determine a robust heating and cooling solution in a continuous process. The induction heating method stands out for this application for its effectiveness and versatility compared with other methods.

Figure 3 shows a setup involving induction heating. Passing a high-frequency current in the induction coil induces an eddy current in the belt for rapid heating. This so-called skin effect [49] helps generate electrical current concentrated at the surface of the belt, thus facilitating effective resistive heating. Since induction heating is not energy limited, rapid heating rates can be readily achieved by raising the heating power. The heated belt then engages with a pair of pressure rollers, R1 and R2, set at a low temperature. The belt starts to cool upon wrapping around the pressure roller R2. In this case, cooling is mainly facilitated by heat conduction. Since both the belt mold and the main pressure roller, R2, are preferably made of metal, the contact cooling process is expected to be fast. After leaving R2, the belt mold is under air cooling. If necessary, one can enhance cooling between R2 and R4 by employing forced convection.

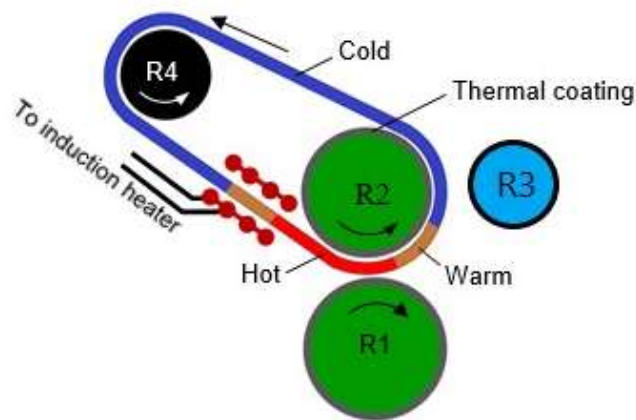


Figure 3. Induction heating of belt mold.

The cooling time t_c required for the surface of a belt to reach temperature T_f can be estimated by

$$t_c = \frac{4H^2}{\pi^2\alpha} \ln\left(\frac{4}{\pi} \frac{T_i - T_r}{T_f - T_r}\right) \quad (2)$$

where H is the belt thickness, T_i is the initial temperature, T_r is the roller temperature, and α is the diffusivity. For a representative case of a 0.5-mm thick nickel belt with $\alpha = 2.3 \times 10^{-5} \text{ m}^2/\text{s}$, $T_i = 225^\circ\text{C}$, $T_f = 125^\circ\text{C}$, and $T_r = 25^\circ\text{C}$, the calculated cooling time is on the order of 0.1 s. On the other hand, the time needed to fill an aspect ratio of 1 is calculated to be 0.6 s according to Eq. (1) assuming representative conditions of $\eta = 10^5 \text{ Pa}\cdot\text{s}$ and $P = 1 \text{ MPa}$. Therefore, it seems that the cooling process is too fast to achieve filling of high-aspect-ratio features. This can be rectified by increasing the belt thickness and/or adjusting the contact condition between the belt and the pressure roller. For example, a thermal coating can be applied to the main pressure roller that directly contacts with the belt mold, as illustrated in Figure 3. In reality, there is always a contact interface between the belt and the roller even with no coating applied, and this greatly impedes the cooling process.

2.4 Experimental setup

A 1 ¼ inch single screw extruder was refurbished and adapted for this research project to show the viability of a continuous extrusion-to-embossing process. The extruder was a C. W. Brabender Type 125-25HC four zone 1.25-inch extruder (Figure 3) driven by a 7 ½ Horsepower DC motor through a 17:1 reduction gearbox. A General Electric GP100 motor control unit controlled the speed of the motor. The temperature of each zone of the extruder barrel was controlled by a PID controller connected to electric resistance heaters

and a high-pressure air Solenoid valve for cooling. A standard screw similar to the one shown in Figure 2, with an L/D of 25:1 and a compression ratio of 2:1, was used.



Figure 3: C. W. Brabender Type 125-25HC four zone 1.25 inch extruder and PID controllers.



Figure 4: Standard extruder screw.

Two ribbon dies with a 25.4 mm x 0.254 mm opening were designed and built for the extruder; one of conventional two-part design (Figure 5) and the other a compact design (Figure 6) machined using EDM.



Figure 5: Standard two-part split design ribbon die.



Figure 6: Compact design ribbon die made using EDM.

In this design the extrudate passes through a calender with the heated ribbon mold, embossing the web with the features on the mold. The ribbon mold runs around the upper roller of the calender which both presses the extrudate into the mold surface and cools the web to set the features and harden or solidify the web. The calender in the experimental setup was constructed using a modified Pepetools 189.00 rolling mill with 139 mm wide, 65 mm diameter flat rollers. The upper roller was replaced with a two-part roller (Figure 7) that can be easily removed to change the ribbon mold.

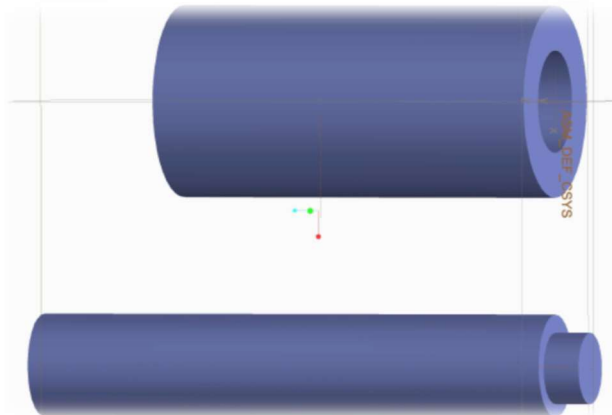


Figure 7: Two-piece roller for ribbon mold changing.

The rolling mill was mounted on an adjustable speed gear head DC motor and the hand crank was replaced with a timing belt pulley to couple with the motor used to drive the mill at up to 40 RPM. (Figure 8). To heat the ribbon mold, a close coupled induction heating (IH) coil (Figure 9) was designed and built using 3.125 mm OD soft copper tubing. The IH coil was powered by an Ameritherm Novastar 3 kW IH power unit. The 60 mm wide closed loop flexible ribbon mold (Figure 10) was assembled from strips of 230 μm thick electro-formed nickel alloy sheets using heat tolerant polyimide (Kapton) tape. A 30 μm pitch and 6 μm height saw tooth pattern feature was on the mold surface (Figure 11).

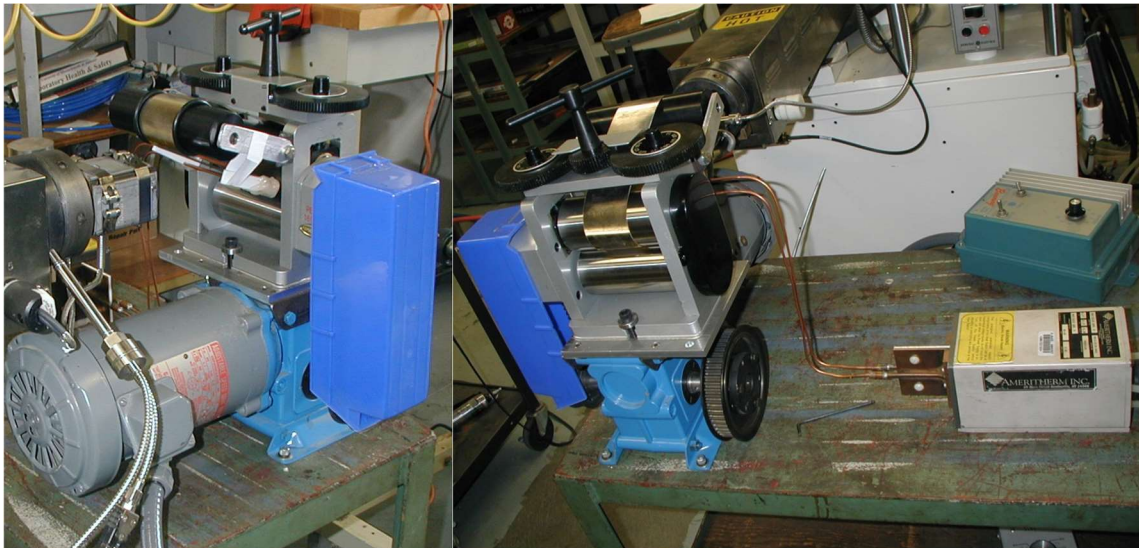


Figure 8: Modified jeweler's rolling mill.

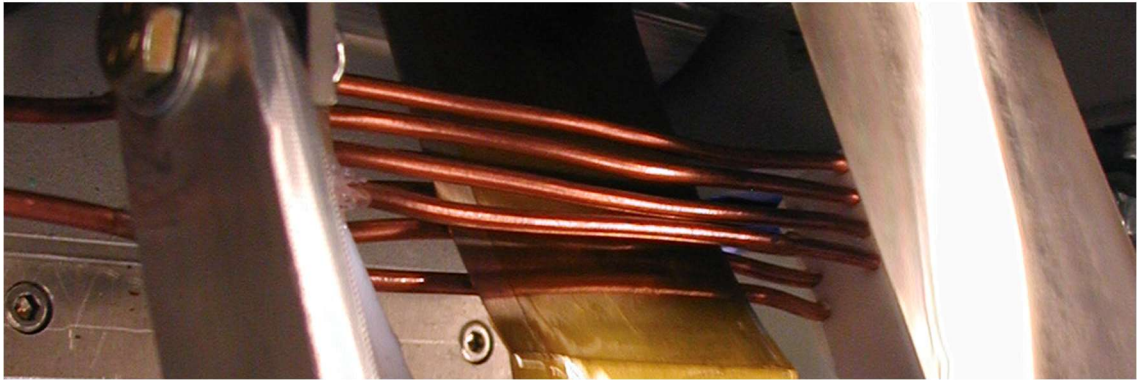
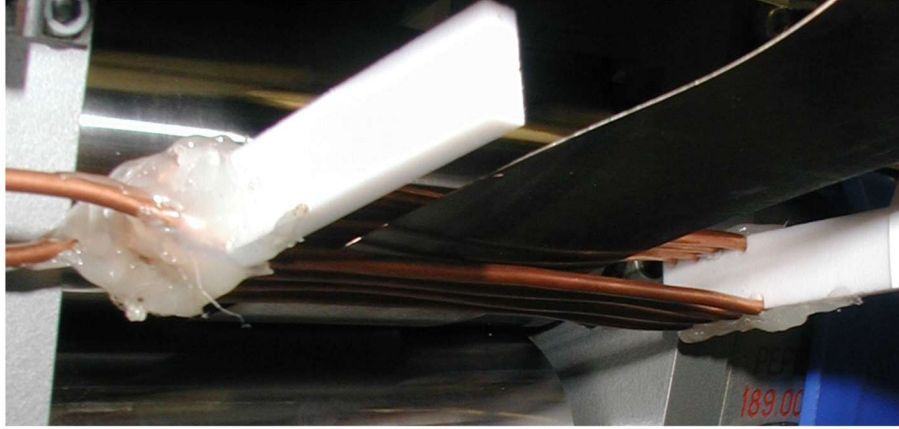


Figure 9: Induction heating coil shown from the below and above the ribbon mold.

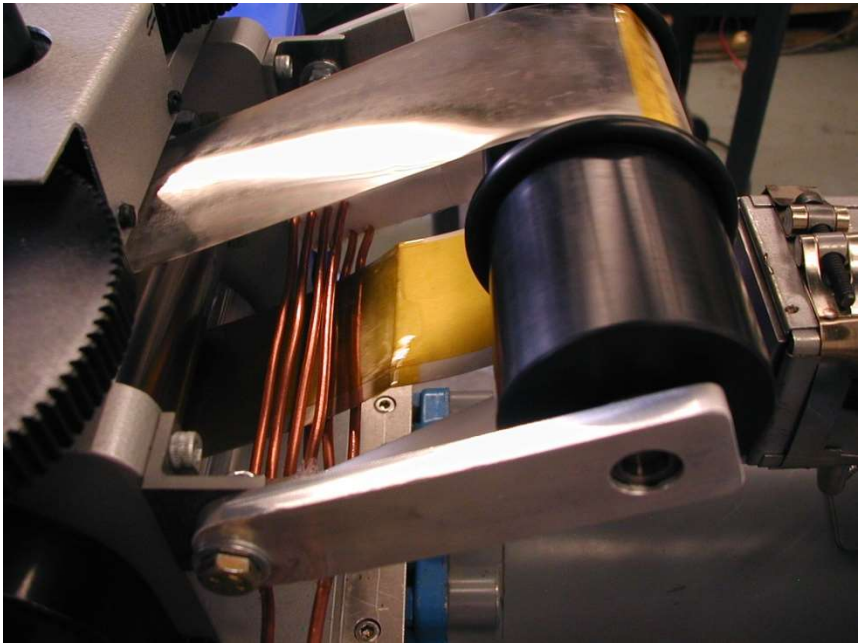


Figure 10: 60 mm wide closed loop flexible ribbon mold.

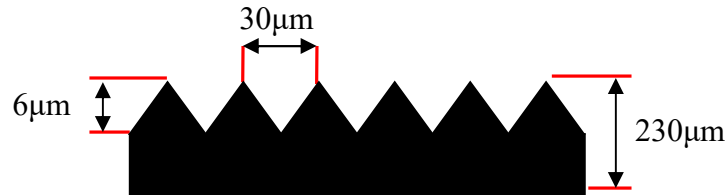


Figure 11: Cross-section of mold pattern geometry

High density polyethylene (HDPE) was used for the test. The temperatures of the four extruder barrel zones were set to span 180°C to 200°C. The first zone or loading zone was set to one 180°C. The second of zone was set to 190°C. The third and fourth zones as well as the die zone were set to 200°C. The extruded HDPE web exiting the die was run below the IH coil to meet the heated mold at the roller nip, through the rollers with the mold and then through about 2 feet of air to a take up shaft (Figure 12 & Figure 13).

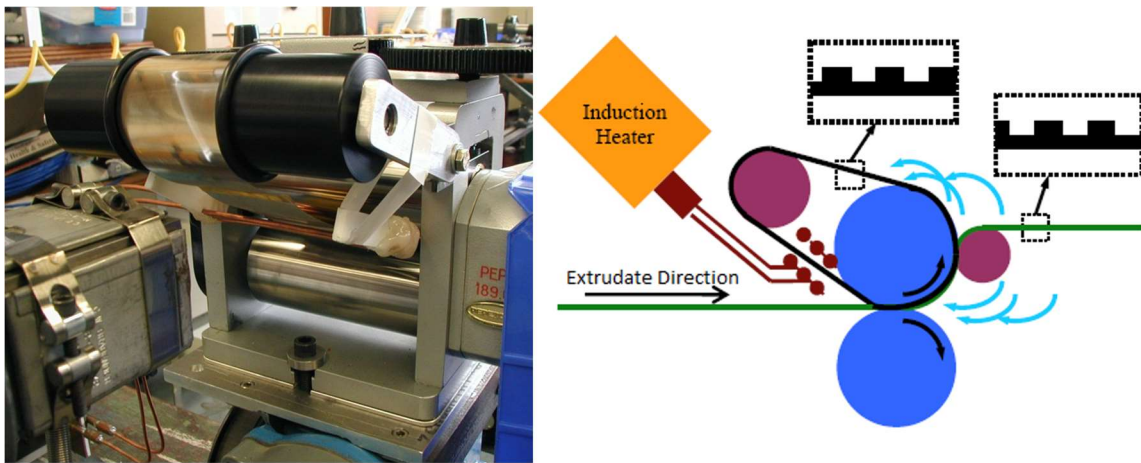


Figure 12: Photograph and Functional Illustration of the ribbon mold and calender roller setup.



Figure 13: Path of extruded web.

2.5 Results of early testing

The result of this test was full replication of the 30 μm saw tooth pattern of the mold on the LDPE as can be seen from the profilometer graph in Figure 14, which shows the peak to trough distance to be 6 μm . The SEM image and profilometry of the ribbon mold shows the same peak to trough distance and is presented in Figure 15.

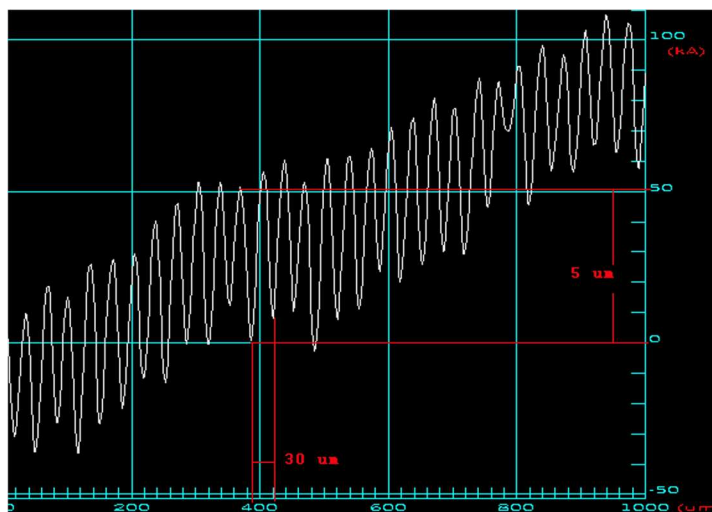


Figure 14: Profilometer graph of embossed LDP

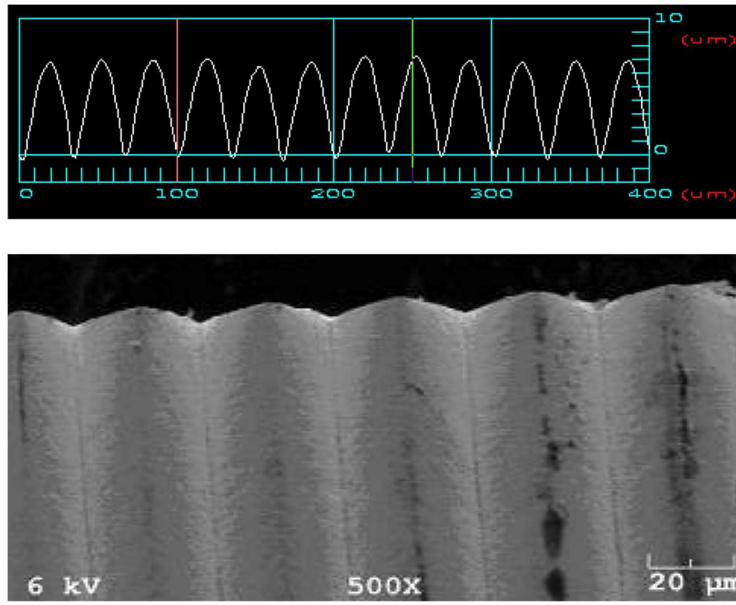


Figure 15: SEM image and profilometry of the ribbon mold.

The extruder screw was run at 18 to 20 rpm producing a melt pressure before the die of around 30 MPa. The gap between the lower roller and the mold was set to approximately 0.25 mm after the web was running smoothly. The linear speed of the produced ribbon was measured using a stop watch and the embossed ribbon was produced at a rate of around 10 to 12 m/min, three to over one hundred times the throughput of current R2R processes and orders of magnitude faster than planar processes [34] [37] [45]. The speed of the rolling mill was adjusted to match the rate of extrusion and the speed of the take-up shaft was adjusted to minimize stress defects in the extruded ribbon. The temperature of the ribbon mold was maintained at around 210 C by running the induction heater at 1.6 kW power output and around 190 C at 1.2 kW. The mold temperature was measured with a Raytek MI infrared pyrometer - a noncontact temperature sensor.

Although adjustments in the different speeds and settings of the equipment produced variations in the dimensions of the extruded ribbon, during steady-state operation the embossed ribbon had a thickness of 0.22 mm and a width of 44 mm.

During the test the induction heating unit was turned on and off several times to determine the effect of heating the ribbon mold. In Figure 16, digital microscopy images and 2D profilometer graphs of the embossed web are presented for the case with no induction heating, with induction heating power set at 1.2 kW and with induction heating at 1.6 kW. The 3D Veeco Dektak Stylus Profilometry is shown in Figure 17. These can be compared to the actual mold material in Figure 18. The improvement in feature pattern replication with the heating of the ribbon mold by induction heating is very apparent in the images. However the 2D profilometry clearly shows the difference even between using a power setting of 1.2 kW and 1.6 kW. The fidelity of the saw tooth pattern is excellent in both the peaks and troughs at 1.6 kW. At 1.2 kW the troughs are good but the peaks are distorted and without heating both the peaks and the troughs are distorted. The peaks represent the deepest part of the mold features so good fidelity indicates the polymer melt fully filling the mold features.

Heating the mold belt at power settings higher than 1.6 kW caused the polymer film to break on exiting the calender NIP so there is a balance between heating the mold belt enough to get full replication of the features and heating it so much that the polymer melt is overheated.

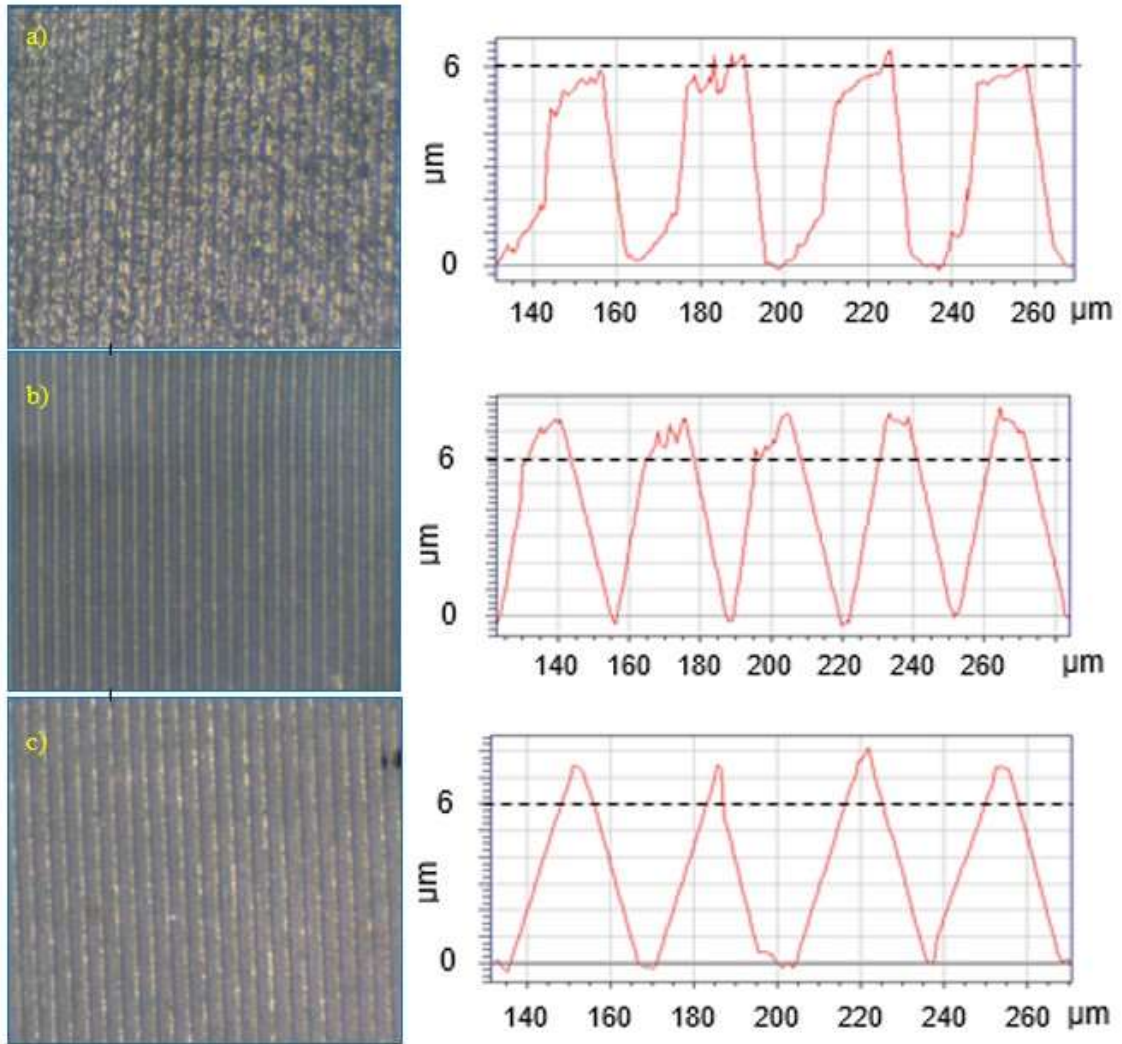


Figure 16: Microscopy images and Profilometer graphs: (a) no heat, (b) 1.2 kW, (c) 1.6 kW.

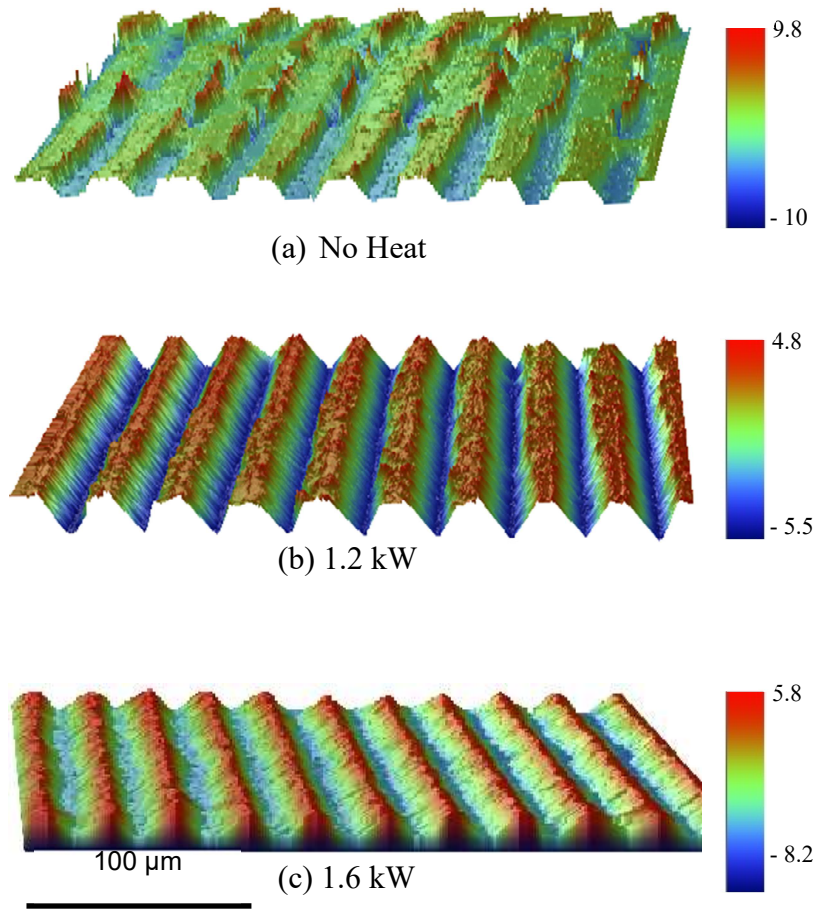


Figure 17: Veeco Dektak Stylus Profilometer 3D for LDPE films imprinted with (a) no heat, (b) 1.2 kW and (c) 1.6 kW.

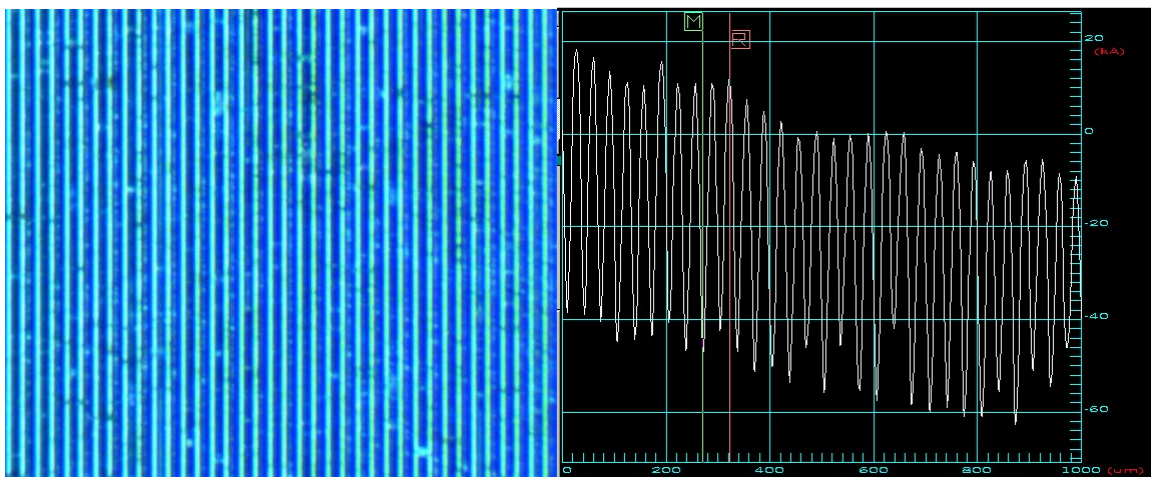


Figure 18: Digital microscopy images and Profilometer graphs of the nickel alloy mold.

Further analysis of the embossed extruded ribbon was performed using a sample of the ribbon as a diffraction grating with a helium neon laser (Figure 19). With the ribbon sample held 1 meter from the target, the distance between the first order spots was 74 mm indicating a grating spacing of 34 μm .

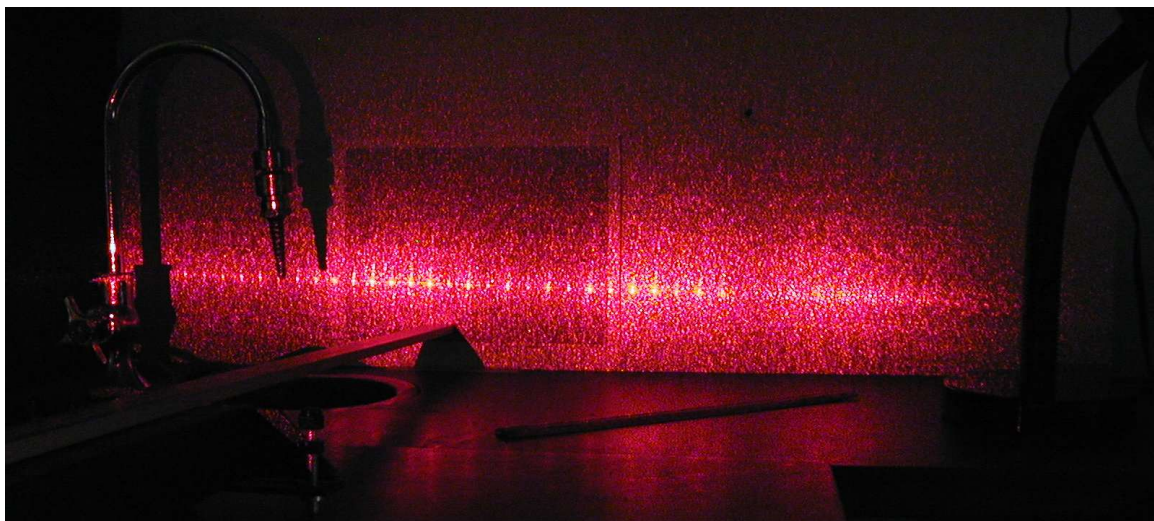


Figure 19: Diffraction grating pattern with helium-neon laser (632.8 nm).

The embossing of microstructures on extruded polyethylene has successfully been shown by this research. Next, nano structured molds were fabricated by adapting the various methods found in the literature and the molds were used to impart nano structures to extruded polymers in a manner consistent with mass production practices.

CHAPTER 3

NANO SCALE MOLD: METHODS

3.1 Overview

With the successful use of a continuous closed loop ribbon mold in the micro embossing process a belt mold with nano features was constructed. The investigation was divided into three different tasks. First, different methods of creating a mold belt with nanostructures were investigated. Second, a suitable method was used to construct the mold belt. Third, the mold belts were evaluated using low-density polyethylene (LDPE) as the extrudate, and the results were evaluated..

3.2 Creating a mold

The mold successfully used in the earlier experiments was a belt or closed loop ribbon made from 230 μm thick electro-formed nickel alloy sheets with a 30 μm pitch and a 6 μm height saw tooth pattern feature on the surface. A thin metal belt has a relatively small thermal mass along its length and can therefore be readily heated by induction and cooled by intimate contact with a cool high thermal mass roller. This property makes it possible to heat the mold above the T_g of the polymer just before contact with the extrudate and to cool the mold and the extrudate before separation. This ensures full imprint depth when the mold and the extrudate pass through the nip allowing control of the molten polymer's cooling rate during cell assembly. The coefficient of expansion differential between the metal ribbon mold and the polymer extrudate aids in reducing separation forces.

3.3 Processes Investigated

Electroforming is a process by which metal parts are fabricated using electrodeposition, a form of electroplating where a metal skin is deposited on a conductive base form in an electrolytic solution. The base form can then be dissolved, leaving the electroformed part. This process requires creation of a base form or mandrel of suitable precision so electroforming alone is not the solution to creating a ribbon mold with micro or nano features. A method of constructing micro or nano features, either on the surface of a mandrel form or directly on a metal ribbon surface, was needed and was the subject of this investigation.

Hot embossing can be employed to fabricate a Flexible mold from a rigid silicon mold using thermoplastic polymers [33] and Thermoplastic forming (TPF) of bulk metallic glass (BMG) can be used to make a thin metallic mold with a T_g higher than that of most thermoplastics [16] [50].

Advances in photolithography have been the driving factors in advancing micro and nanotechnologies. Since 1995 the minimum feature size for semiconductor production, measured in nanometers, has shrunk from 350 nm to 32 nm in 2010 with a projected 2 nm by 2024 [51] [52]. This decrease in feature size results from a synergy of advancements in optics, photo resists, chemistry, purity of chemicals and materials and advances in processes, including the use of shorter and shorter wavelengths in the lithographic process. Without a doubt, a successful micro and nano embossing of extruded polymers must adopt many of the advances made in the semiconductor industry. Historically, micro and nanostructures have been created in a clean room environment on silicon wafers 4 to 12 inches in diameter, and most current processing equipment is oriented to wafer processing.

Creating continuous micro or nanostructures on the surface of a relatively long and wide belt poses unique challenges requiring custom equipment and processes.

3.4 UV Photolithography and Beyond

Three forms of UV photolithography are generally used, contact, proximity and projection lithography. All three use a photomask with a one-dimensional image of the structures to be created. UV lithography uses shorter wavelength ultraviolet light, rather than visible light, to obtain higher resolution. The resolution of proximity lithography, where there is a gap between the mask and the photoresist, is approximately the square root of the product of the wavelength and the gap distance [53], so as the gap distance goes towards zero, as in contact lithography, the resolution theoretically gets better. Nevertheless, contact lithography is subject to distortion from contaminating particles between the mask and the resist surface and from contact damage to the mask from repeated use.

Projection lithography uses a reduction lens system to project an image of the reticle (photomask) onto the photoresist. The smallest feature size that can be resolved or the critical dimension (CD) is approximately:

$$CD = k_1 \frac{\lambda}{NA} \quad 3$$

where CD is the critical dimension or minimum feature size, k_1 is a process related coefficient, λ is the wavelength of light used and NA is the numerical aperture of the lens system. Projection lithography is limited in the area it can cover and is usually employed to project a complex mask onto a small segment of a wafer repeatedly as the position of the wafer relative to the focal point of the lens is moved or stepped.

The practical resolution limit for contact/proximity ultraviolet lithography is around 2.5 μm using Fresnel (near-field) diffraction with 200 nm wavelength radiation and a 25 μm or smaller gap. Resolutions as low as 125 nm are achievable using contact print lithography with Fresnel diffraction, 160 nm wavelength radiation, a gap of 100 nm or less and 100 nm thick resist [54]. Applying such conditions to form a ribbon-mold poses a significant challenge but Jang et al. showed that higher aspect ratio patterns are possible in thicker resist coatings using techniques to avoid the undercutting effect of the interaction between the incident beam and the beam reflected from the surface of the substrate [55].

Projection UV lithography can achieve 150 nm resolution using Fraunhofer (far-field) diffraction, 175 nm wavelength radiation, a high NA lens and a phase shift mask. The resolution of optical projection lithography can be further improved using polarized light, interference lithography, and liquid immersion. Sub 100 nm structures are possible with deep ultraviolet (DUV) radiation using vacuum UV interference lithography and interference immersion lithography with excimer laser exposure at 157 nm has achieved 30 nm feature size [56].

For feature sizes in the tens of nanometers and below, the wavelength of the electromagnetic radiation used for exposure can be reduced to extreme UV (EUV), soft x-rays (10 nm), x-rays (1 nm), electron beam and ion beam radiation. These technologies require catoptric optics (instead of refraction optical systems) and resist polymers sensitive to the respective shorter wavelengths [56].

This study investigated various lithographic techniques to determine their applicability to producing ribbon molds with micro or nano features. This included an investigation of available photopolymer resists and their possible adaptation for ribbon

mold production. Each lithographic technique requires photoresist with properties compatible with that technique. The spectral sensitivity or absorption spectrum of a photoresist must match the radiation used for exposure and the form and method of application must be compatible with the material, form and structure sizes desired. Many common resists are designed to match the emission spectrum of mercury (Hg) light sources, that is the G-line (436 nm), H-line (405 nm), and I-line (365 nm), with the I-line composing approximately 40% of the total emissions between 440 and 340 nm [57]. These can be considered for producing molds with microstructures but for nano structured molds, resists sensitive to shorter wavelengths will be required. One exception is laser interference lithography (LIL). Regular arrays of sub-micron features with a minimum achievable period of half the exposure wavelength ($\lambda/2$) can be created in a thin layer of photo resist using LIL but the feature shape and complexity are limited because the patterns are formed by standing wave interference patterns, not masks and complex optics [58] [59].

Coating systems for liquid resist materials and laminating systems for thin-film products were studied, adapted and developed to produce ribbon molds. Since spin coating is not readily applicable to a closed loop ribbon/ belt or long narrow strips, focus will be placed on spray coating, dip or Meniscus coating, roller, curtain and extrusion Coating, electrodeposition (ED), plasma-deposited photoresist, and dry film lamination in this investigation. Much work on spray coating for MEMS and 3-D patterning has been done by Pham et al. at Delft University of Technology, including a comparison of the spin coating, spray coating, and electrodeposition however the focus was on silicon wafer processing [60] [61]. Cooper et al. employed newer spray coating techniques to overcome challenges in creating 3-D structures on non-planer surfaces [62]. Meniscus or capillary

coating has been used for processing large rectangular substrates like those used in flat-panel displays [63] and inkjet type fluid ejectors can be used to deposit resist film as thin as 0.5 μm [64]. In extrusion coating a thin curtain of resist is expelled from an extrusion nozzle onto the substrate as the substrate moves underneath at a controlled rate. Film thicknesses less than one micrometer have been demonstrated using this method [65]. Electrodeposition is similar to electroplating. Photoresist particles are dispersed in an aqueous solution and become negatively charged. With the application of an electric current, deposition of resist film occurs at the anode. The uniformity and thickness of the coating can be precisely controlled by varying the current, voltage, and time [66].

Plasma-deposited and vacuum-deposited photoresists are applied using special vacuum chambers, electric current and gases or vapors [67] [68]. The process can deposit thin-films with excellent conformity and is considered dry and environmentally friendly, because it eliminates wet chemistry processes. This process accommodates large and odd shaped substrates, but has the disadvantage of requiring specialized hardware to perform the process. Lines and spaces of 350 nm have been demonstrated using a wavelength of 248 nm on 250 nm thick plasma polymerized methylsilane [68].

Dry film photoresist was originally developed over 30 years ago for the processing of printed circuits. It is usually applied by hot lamination and after exposure is easily developed with simple chemistry. Although dry film photoresist has been used for MEMS applications, the lithographic resolution is limited by the polyester or mylar cover sheet which protects the photoreactive layer [69]. Dry film resist offers the advantage of good conformability, excellent adhesion to most surfaces, short processing time, excellent uniformity of thickness, low exposure energy and near vertical structure sidewalls but it

suffers from lower resolution and lower aspect ratio than SU8 and liquid resists [70]. Typically 15 μm lines and spaces are the minimum feature size for dry film photoresist [71].

3.5 Direct Laser and Electron Beam Etching

Laser micromachining has been used in MEMS manufacturing and has the advantage over silicon lithography of fewer processing steps, high three-dimensional shape flexibility, and independence from crystallographic planes. It can be used on almost any material, including polymers, ceramics, metals and even glasses and is compatible with traditional lithographic processes. In laser micromachining, high-intensity pulsed lasers are focused on a material surface and cause ablation or mini-explosions that eject solid and gaseous particulates from the irradiated site without significant thermal degradation of the surrounding material [72] [73]. Feature size resolution of 5 μm has been achieved using 308 nm excimer lasers [74] and 2 μm using a 157 nm F_2 laser with a mask and reducing optics [75]. Nano machining by ultra-fast laser ablation uses very high peak laser intensities, greater than 10^{14} W/cm^2 , and pico-second pulse durations. Oxford Lasers has achieved spot diameters as small as 4 μm with 100 nm depth using a 532 nm, 9 ps laser [76]. These processes may be useful for micropatterning a ribbon mold, but true nano structuring will require higher resolution.

Focused electron beam etching and lithography (EBL) use a modified transmission electron microscope to direct a beam of electrons, with a spot size of about 1 nm, to scan a target substrate in a vacuum chamber. The EBL patterning technique can readily produce patterns down to 10 nm, and with cold development and ultrasonic assist, 5 nm patterns have been produced [77] [78] [79]. In EBL projection printing parallel electron beams

patterned by a mask are projected onto a substrate using a high precision lens system. Direct writing EBL is the more mature technology and has proven versatility and flexibility in making a variety of nano devices with critical dimensions below 10 nm [80] [81].

X-ray lithography is similar to other projection lithography, but its short wavelength radiation gives it the advantage of low diffraction effects and high depth of focus in imaging small features. Highly collimated x-ray radiation makes the process relatively insensitive to the mask distance from the source and enables the forming of high aspect ratio microstructures thick resist layers [82]. High-resolution masks for x-ray lithography are usually pattern by EBL and then enhanced by a multistep process.

A wholly mechanical process for creating micro and nanostructures, invented by Emanuel F. Barros, precisely controls microscopic and nanoscopic supersonic jet of liquid to cut and shape features less than 50 nm in size. This technology is being marketed by NanoMatrix, Inc. of Scotts Valley, California and will be investigated for this research [83] [84].

3.6 Nano Imprint Lithography (NIL)

The term "nanoimprint lithography" was coined in 1996 by Prof. Stephen Chou and his students [22]. NIL is a method of fabricating nanometer scale patterns by mechanical deformation of imprint resist, typically a monomer or polymer formulation that is cured by heat or UV light during the imprinting. When the resist is cured by UV light the process is called UV-NIL. A R2R version of UV-NIL which created 3D nano features on the surface of a polymer web, was developed by Jacob John et al. and The Center for Hierarchical Manufacturing (CHM) [85]. That polymer web, with 3D nano features imprinted on the surface by R2R UV-NIL was an ideal candidate for use as a base form for metal forming a

metal ribbon belt mole with nano features to use in the continuous extrusion to nano embossing process.

A combination of R2R UV-NIL and nickel metal forming are the methods primary methods chosen for this research. Both of these methods were readily doable at the University of Massachusetts campus in Amherst.

CHAPTER 4

NANO SCALE MOLD: IMPLEMENTATION

4.1 Experimental Setup

The Center for Hierarchical Manufacturing (CHM) at the University of Massachusetts – Amherst [86] developed a R2R UV NIL process for forming nano features on Polyethylene terephthalate (PET) film (Figure 20) using Norland Optical Adhesive 81 (NOA 81) as a UV NIL resist for replicating nm features [85]. Nano test patterns obtained from IBM were imprinted on the film that included gratings from 70 to 500 nm and pillars having diameters of 1 μm , 700 nm, 500 nm and 350 nm. The PET film with the NOA 81 features (Figure 21) filled the need for a base form or mandrel for creating a nickel belt mold by metal forming.

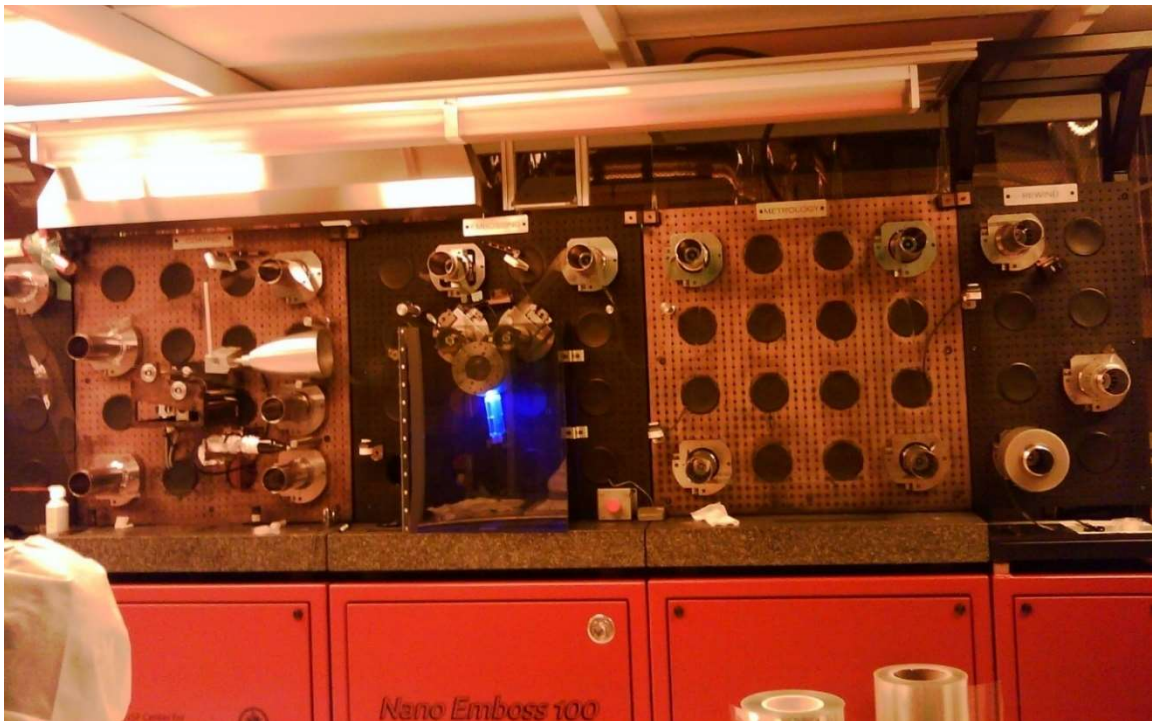


Figure 20: R2R UV NIL process for forming nano features on PET film.

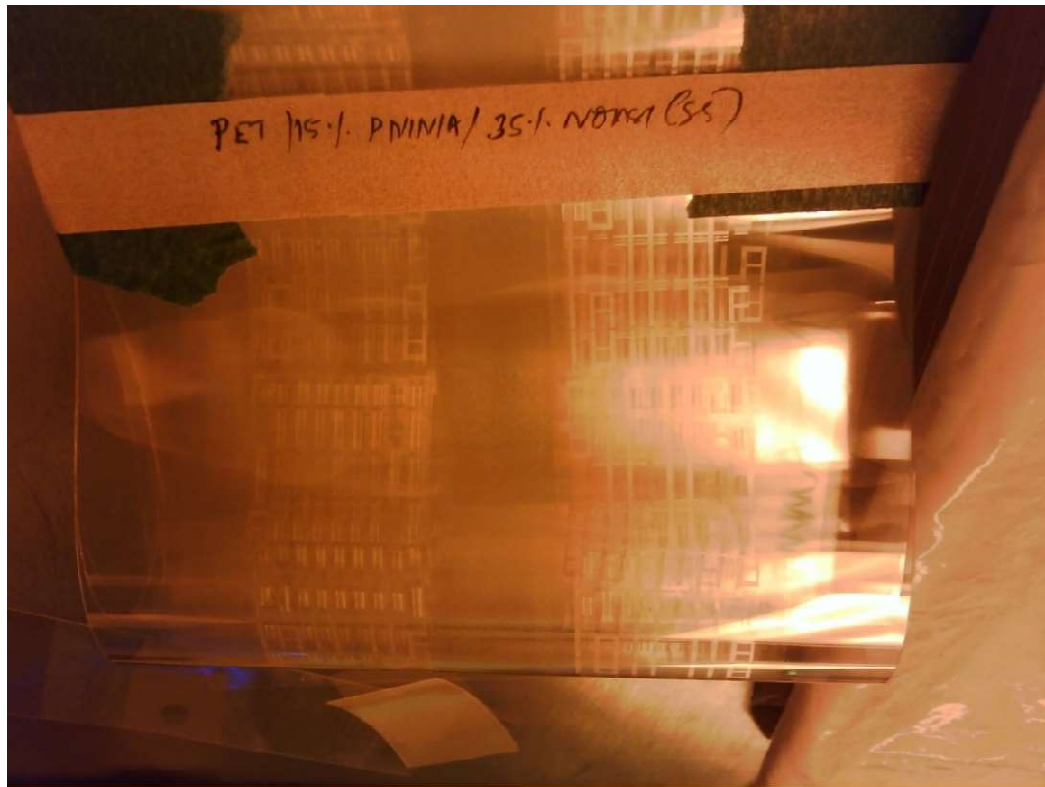


Figure 21: PET film with the NOA 81 features.

The nickel mold belt was the result of four distinct processes.

1. The creation of nano features on silicon (positive) by electron beam etching or lithography.
2. The transfer of the nano features to PTFE (negative) in a Nanonex Nanoimprint Tool (heat and pressure).
3. The transfer of the nano features from the PTFE to UV cured epoxy (positive) using the Nano Emboss 100 by Carpe Diem Technologies at the NSF Center for Hierarchical Manufacturing (CHM) at UMASS Amherst.
4. The creation of a nickel mold belt (negative) using nickel forming techniques.
5. Roll to roll production of nano features on an extruded polymer ribbon (positive) using the nickel mold belt with induction heating.

The first three steps of the process were accomplished with the help of CHA and lab manager Dr. Jacob John. The nano featured Silicon chips were obtained from outside sources including IBM. The features were transferred to PTFE by placing pieces of PTFE on top of the silicon chips and applying heat and pressure in the Nanonex Nanoimprint Tool (Figure 22).

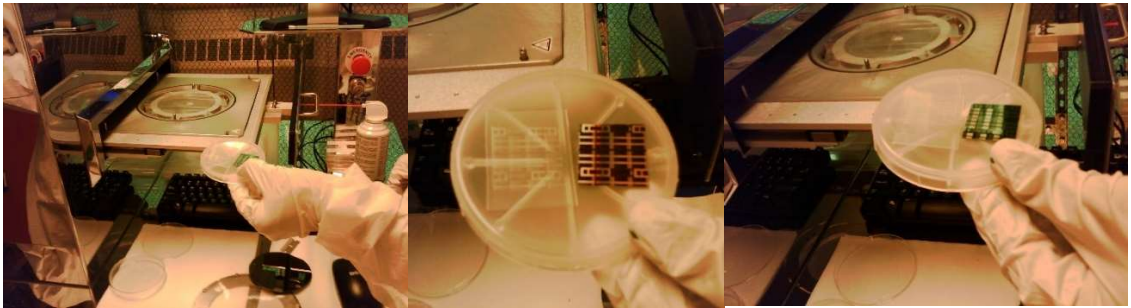


Figure 22: Nanonex Nanoimprint Tool and embossed TFE from Si masters.

The PTFE negative molds were then stuck onto the imprinting cylinder of the Nano Emboss 100 (Figure 23) to transfer of the nano features from the PTFE to the surface of the PET film by UV NIL with NOA 81 (positive).



Figure 23: PTFE as mold for UV NIL on the Nano Emboss 100.

Step 4 was accomplished by preparing a 3-inch wide by 20-inch-long section of the PET film, with the nano features, to be coated with 200 nm of nickel in the CHA SE-600

electron beam evaporator in the Conte Nanotechnology Cleanroom Lab. This took over 3 hours and most of that time was the evacuation of the chamber. To minimize the pump down time, each PET film was put into a vacuum chamber the evening before plating and left under vacuum all night to remove any moisture from the material (Figure 24).



Figure 24: Coating of PET film with nickel in the SE-600 electron beam evaporator.

The nickel coated film was formed into a continuous belt by attaching the ends together with the nickel coated surface on the inside. The belt was then prepared and suspended in a nickel-plating bath where nickel was added to the thin coating until the nickel was approximately 200 μm thick (Figure 25).



Figure 25: PET with seed Ni, plating bath and 200 μm thick nickel belt.

The PET film was then stripped off the nickel belt and the UV cured epoxy was removed from the belt. The nickel belt was then installed on the Roll-to-Roll extruder/thermal embosser (Figure 26).



Figure 26: Ribbon belt mold being installed.

The completed belt mold was approximately 70 mm wide, 50 cm long, and 250 μm thick. It was installed onto the modified rolling mill through the upper roller.

To heat the belt mold, a closely coupled induction heating (IH) coil was designed and built using 3.125 mm OD soft copper tubing (Figure 26). The IH coil was powered by a high-frequency power unit (Model: Nova Star 3H from Ameritherm Inc., Scottsville, NY). This power unit was able to deliver a maximum power of 3 KW, with a maximum voltage of 220 V and a maximum current of 17 A, over a frequency range of 215 kHz to 1.0 MHz

Low-density polyethylene (Westlake Chemical EC808 LDPE) was used in the processing tests. The temperatures of the four extruder barrel zones were set to span from 180 to 200°C. The first zone or feeding zone was set to one 180°C. The second zone was set to 190°C. The third and fourth zones as well as the die zone were set to 200°C. The extruded HDPE web exiting the die runs below the IH coil to meet the heated belt mold at the roller nip, then wraps around the belt mold on the upper roller, and finally travels about 70 cm in air to a take-up beam.

The extruder screw was run at 18 to 20 rpm producing a melt pressure before the die of around 30 MPa. The gap between the lower roller and the belt mold was set to approximately 0.25 mm after the web was running smoothly, and the embossed film was produced at a rate of around 10 to 12 m/min, three to over one hundred times the throughput of current R2R processes and orders of magnitude faster than planar processes [34] [37] [45]. The speed of the rolling mill was adjusted to match the rate of extrusion, and the speed of the take-off roller (Figure 27) was adjusted to minimize defects in the extruded film. The temperature of the belt mold was maintained at about 210°C by running the induction heater at 1.6 kW power output and around 190°C at 1.2 kW. The temperature of the mold was measured right before the belt enters the imprinting nip using a Raytek MI infrared pyrometer – a noncontact thermometer. For reference, the temperature of the mold right before the belt enters the HI coil was also measured. This latter temperature was found to be close to room temperature, indicating that sufficient cooling of the belt was achieved.

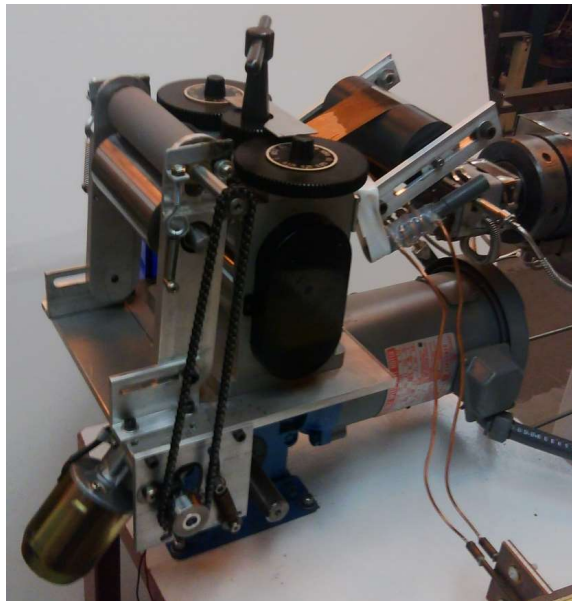


Figure 27: Take-off and cooling roller.

After leaving the take off and cooling roller the embossed polymer web traveled approximately 1 m through the air for further cooling (Figure 28) to the winder (Figure 29).



Figure 28: Polymer web leaving the take-off roller.



Figure 29: Cooling rollers and winder

Although adjustments in the different speeds and settings of the equipment produced variations in the dimensions of the extruded film, during steady-state operation the imprinted film had a thickness of 0.22 mm and a width of 44 mm.

During the test the induction heating unit was turned on and off several times to determine the effect of heating the belt mold.

4.2 Other Mold Belts

Stainless steel (SS) ribbon 50.8 mm wide and 114 microns thick (2" x 0.0045") was welded to form closed loops to be used in the developed continuous extrusion-to-embossing process as the basis for making closed loop ribbon mold belts that could be heated by induction. For the first ribbon mold attempt, Alumina filter disks were glued with SU8 to the surface of such a belt in an attempt to transfer the nanopattern of the surface of the filter disk to a LDPE ribbon (Figure 30).



Figure 30: Curing the glue in an oven to secure Alumina filter disks to SS ribbon belt and the belt installed on the calender roll.

For the second ribbon mold belt, a master mold containing the Book of Leviticus, with letters 6 μm in width, 6 to 9 μm tall and 60-170 nm high, was cut, welded to the surface of a SS ribbon and welded into a SS ribbon mold loop (Figure 31).



Figure 31: The Bible Book of Leviticus master mold as a ribbon mold.

A third ribbon mold was made from a nickel alloy DVD master mold, with track pitch of 740 nm and 105 nm deep Pits between 400 nm and 1900 nm long, which was micro-welded into a SS ribbon loop (Figure 32).

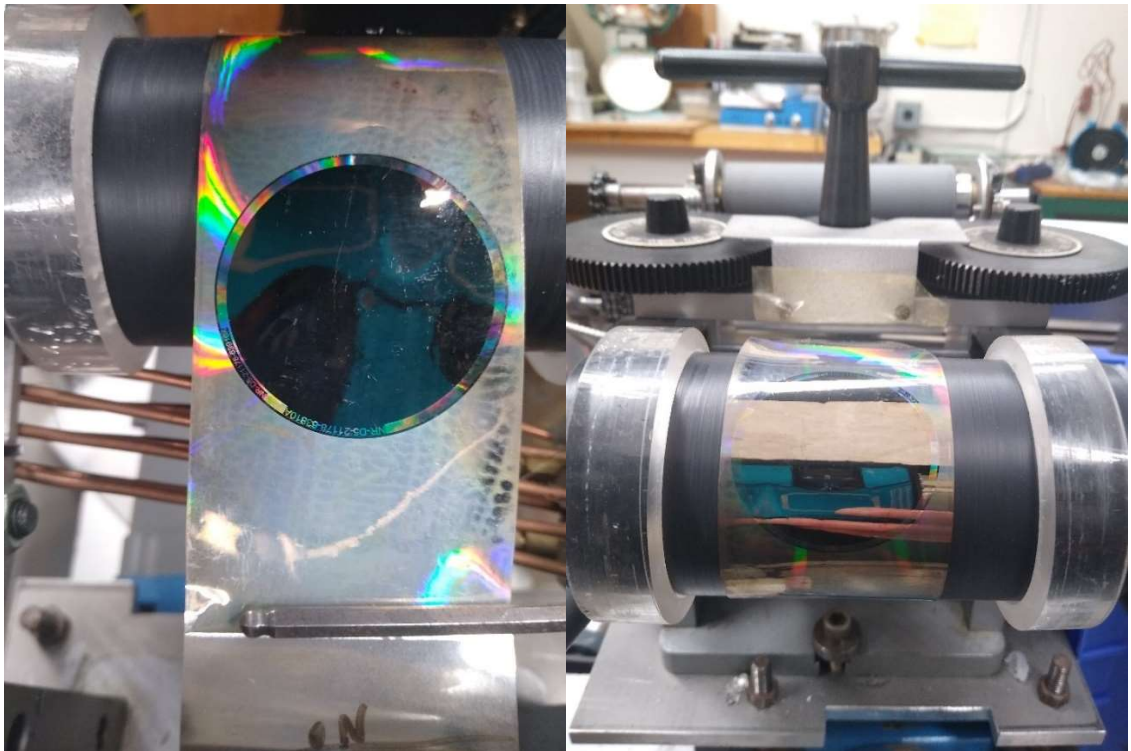


Figure 32: Nickel alloy DVD master mold micro-welded into a SS ribbon loop and installed on the rolling mill or calender roller.

CHAPTER 5

NANO SCALE MOLD: RESULTS

5.1 Mold Belts Made by Metal Forming.

Nanometer scale patterns were successfully created in electroformed nickel mold belts but removing the UV curable epoxy NOA 81 from the nickel was problematic. An SEM analysis of pieces of a nickel mold belt was performed showing both the successfully copied nanostructures and the NOA 81 contamination of part of the mold. A range of grating sizes in the IBM test pattern is shown in the SEM image of a 50 μm section of a Ni belt mold in Figure 33. In Figure 34, the SEM image of the copied 500 nm grating pattern was clearly visible where the NOA 81 was removed. SEM images of clean sections of a nickel mold belt clearly show the sections of the 500 nm grating in Figure 34 and Figure 35. The top edges of the square wave pattern were crisp, indicating that the metal forming process produced good fidelity in reproduction of the 500 nm grating that was on the base form (NOA 81 on PET) shown in Figure 36. Figure 37 shows the 500 nm grating in a section of nickel mold belt as obtained from a Keyence VK-X 200 Laser Confocal Microscope. The features in this image generally looked good but the evidence of lingering resist was also apparent. These images show that the metal forming process copied the nano features on the PET base form with good fidelity.

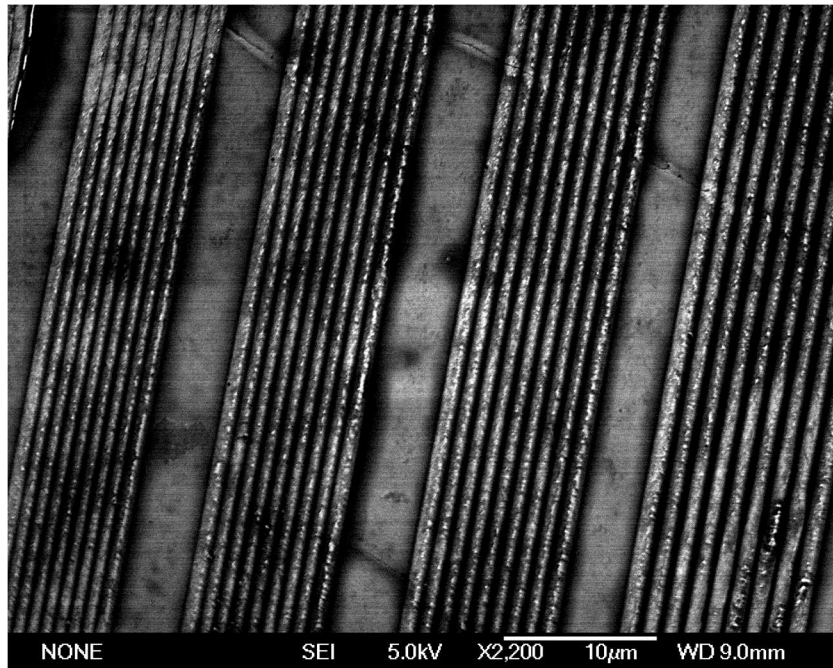


Figure 33: SEM image of Ni belt section showing different grating sizes of the IBM test pattern.

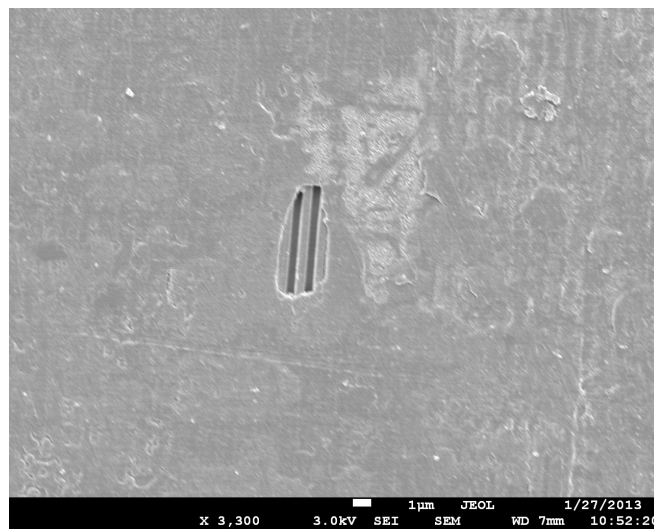


Figure 34: SEM of a section of the 500 nm patterned nickel mold showing NOA 81 contamination.

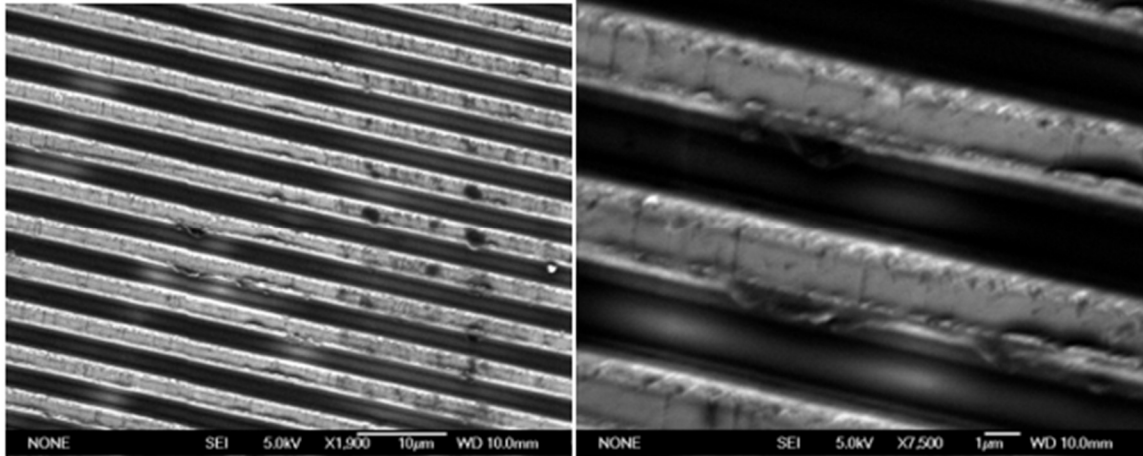


Figure 35: SEM images of Ni copy of a section of IBM test pattern.

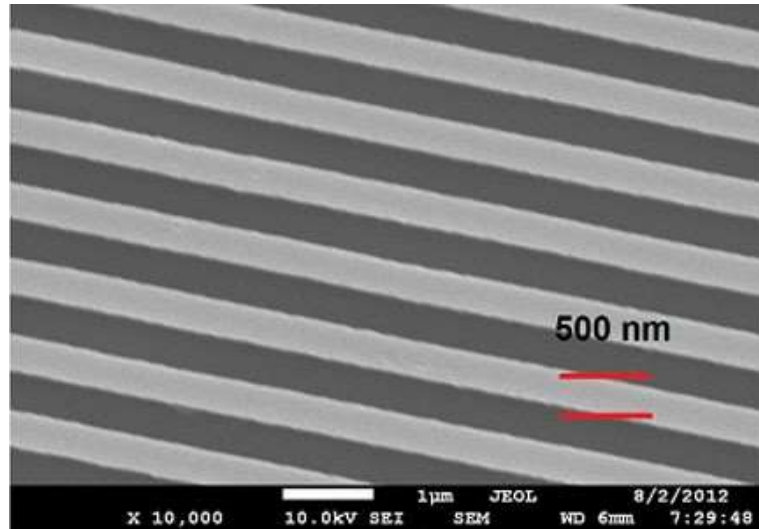


Figure 36: SEM image of the 500 nm grid in NOA 81 on PET [85]

A piece of embossed extruded LDPE was also analyzed with the Keyence VK-X 200 Laser Confocal Microscope and the resulting image, shown in Figure 38, can be compared with Figure 37. This was from one of the small areas where the NOA 81 had come off of an otherwise covered nickel mold belt. The effects of residual resist were apparent but the profile plot did not show the flat tops of the

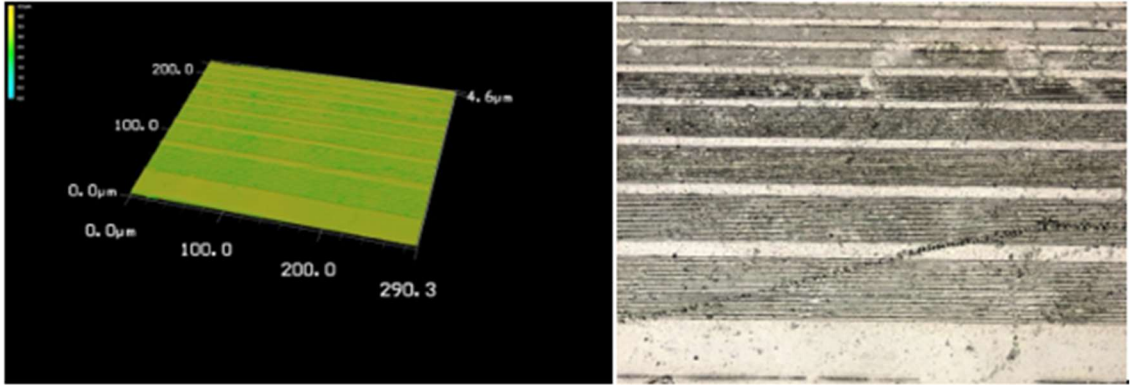


Figure 37: Keyence VK-X 200 Laser Confocal Microscope images of IBM test pattern in Ni mold.

grating as seen in the nickel mold. The grating form was apparent in the 2D image however the crisp fidelity was not there.

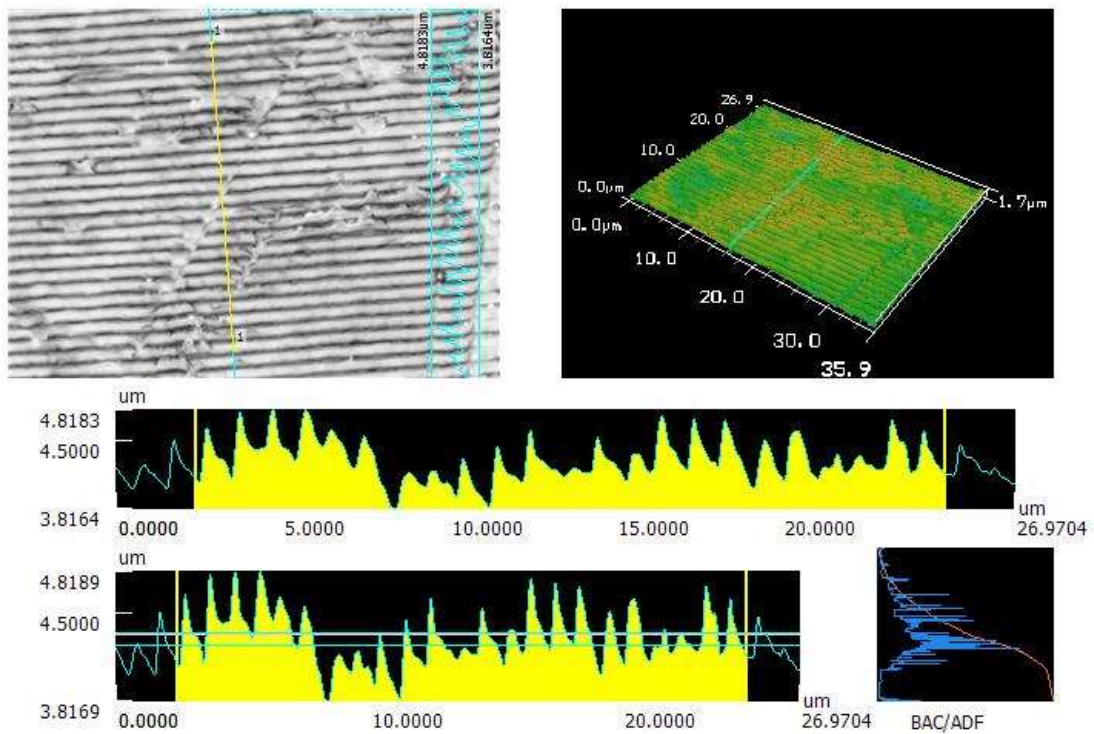


Figure 38: Keyence VK-X 200 Laser Confocal Microscope images of embossed extruded LDPE.

Figure 39 is an AFM analysis, a 3D image and a plot of the profile along the line in the AFM image of an embossed extruded LDPE sample showing the rectangular grooves of the test grating pattern. The size of a rectangular groove in the AFM image was 630-670 nm in width (about 650 nm), 310-370 nm spacing (about 350 nm) and 70-125 nm in height (depth). The 3D image is of a 30 μm x 30 μm section with 0.2119 μm thickness and shows the effect of residual resist contamination. Parts of the grating structure in the LDPE looked good but the overall fidelity was inconsistent.

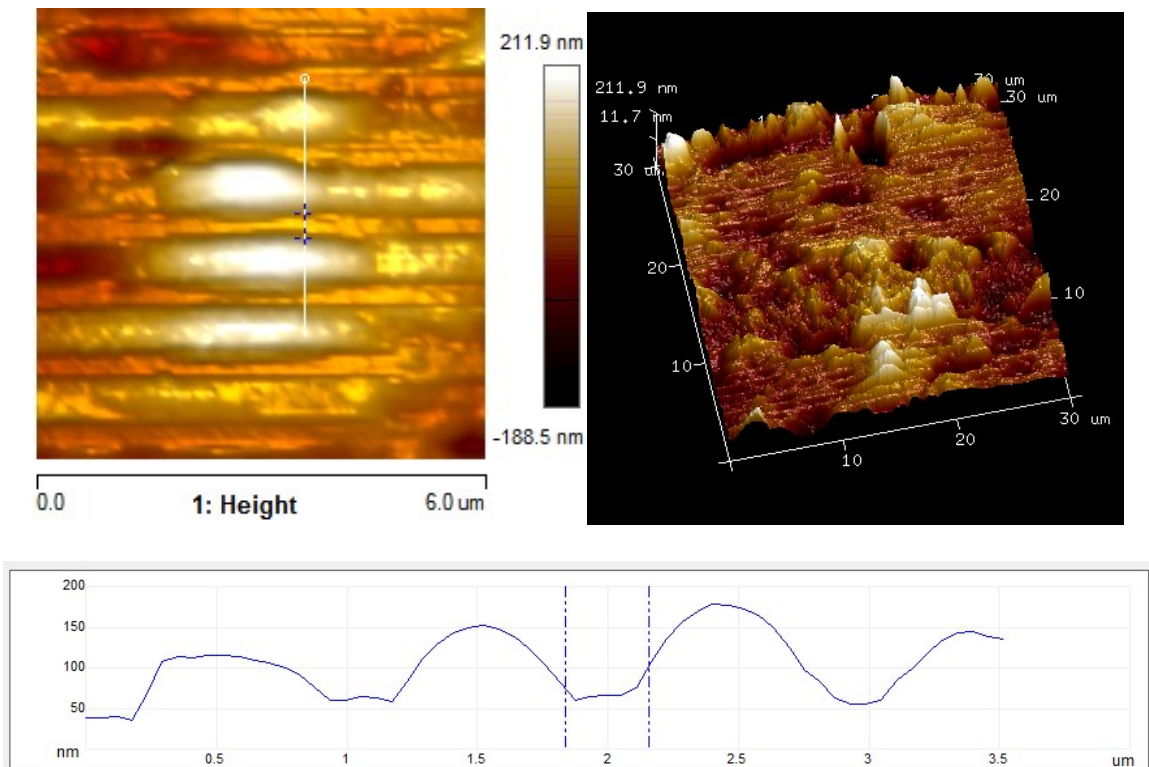


Figure 39: AFM analysis, 3D image and a plot of the profile LDPE sample.

The test patterns on the PET base form also included sections of pillars having diameters of 1 μm , 700, 500 and 350 nm (Figure 40). The negative or reverse of the pillars (wells) was what was formed in the Ni ribbon mold as seen in Figure 41. The wells in the

figure were 510-620 nm in diameter and 46-60 nm deep. Some of the wells were filled with UV cured resist residue that came off the PET base form.

The AFM analysis of the pattern of pillars printed on PET film by the CHM R2R UV NIL process is shown in Figure 42 and can be compared with the AFM analysis of the pattern produced on extruded LDPE, by the nickel belt electroformed using a similar PET film as a mandrel, in Figure 43. The pillars were egg shaped and taller than the depth of the wells due to the tension during separation from the mold belt while the extrudate was still relatively hot. Reducing calender speed would give more cooling time.

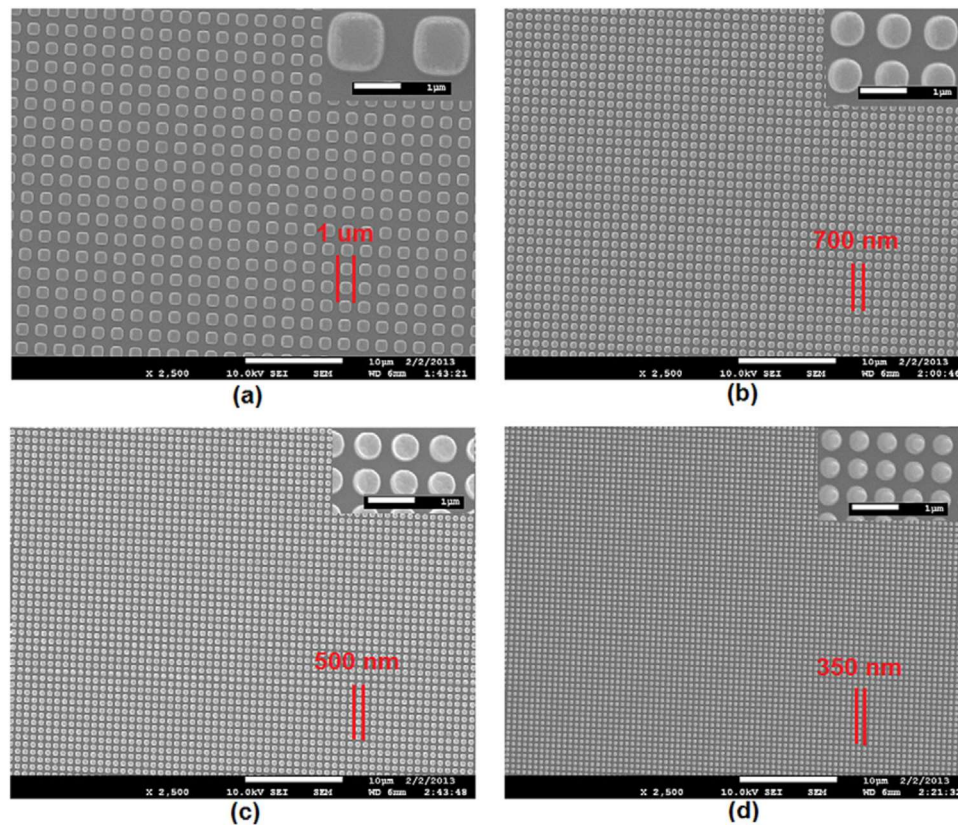


Figure 40: SEM images of the UV-NIL R2R pillars imprinted in NOA 81 on PET having diameters, (a) 1 μm, (b) 700 nm, (c) 500 nm and (d) 350 nm [85].

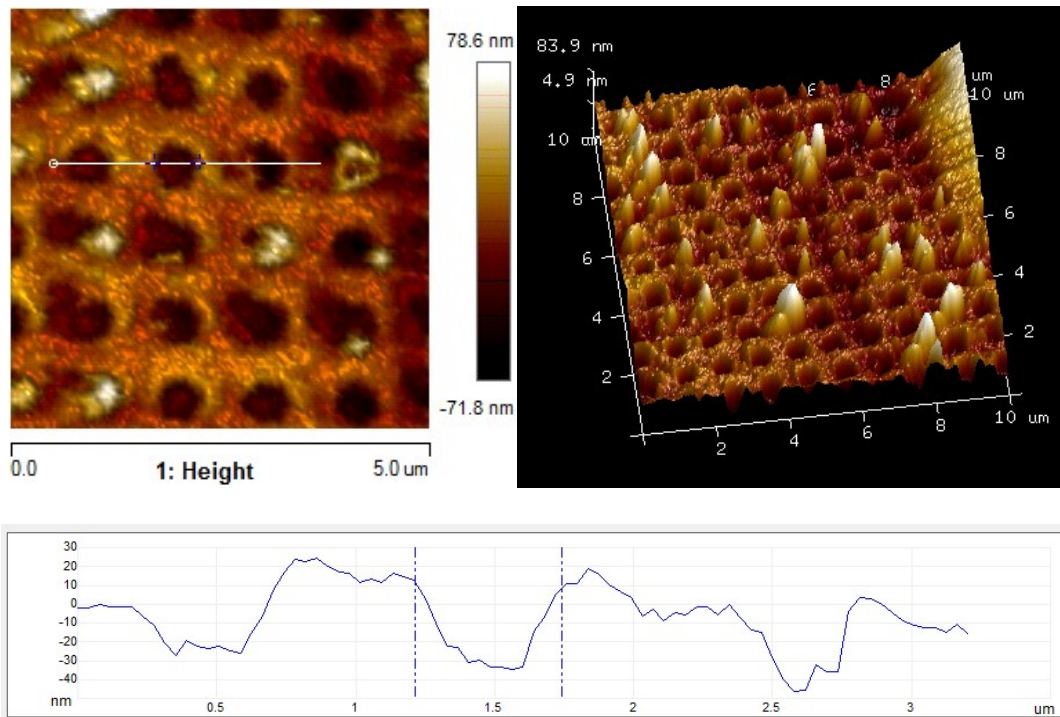


Figure 41: AFM of pillar holes in Ni mold, 3D image and profile plot.

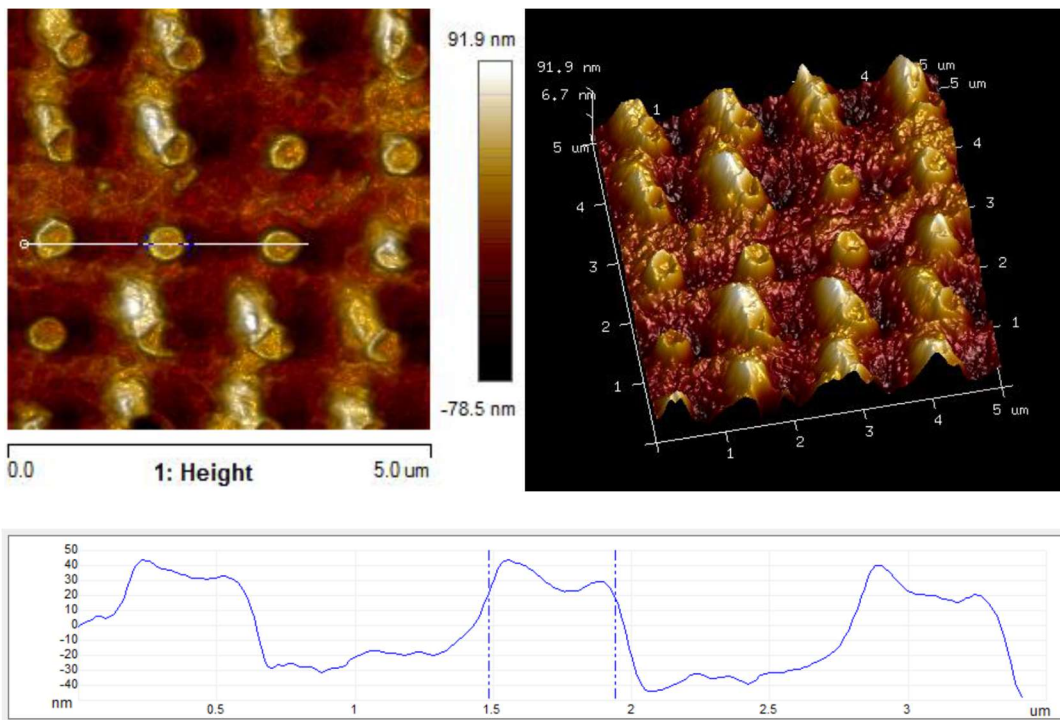


Figure 42: Pillars on PET film imprinted by UV NIL Roll-to-Roll system, the 3D image of the pillars and the profile of the pillars along the horizontal white line. The size of the pillars were 450-500 nm diameter and 66-90 nm height.

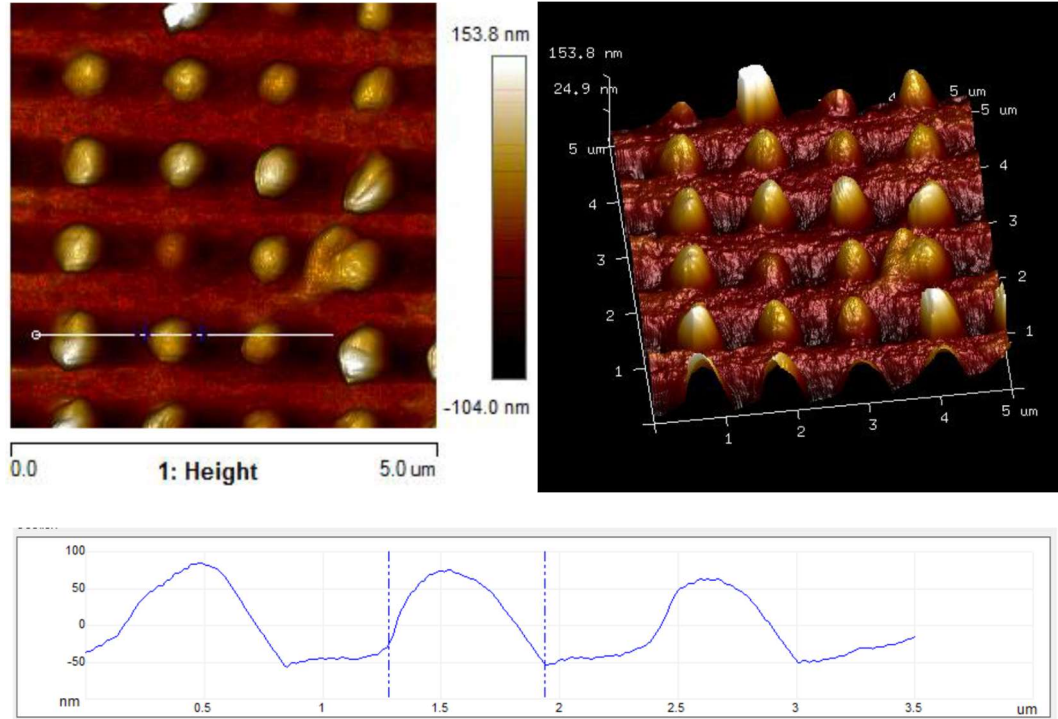


Figure 43: Pillars on LDPE film imprinted thermally by Roll-to-Roll production, the 3D image of the pillars and the profile of the pillars along the horizontal white line. The diameter and height of the columns were about 645-660 nm and 120-170 nm height.

5.2 Other Ribbon Belt Molds

5.2.1 Alumina Ceramic Filter Discs

The use of ceramic filter disks was not successful. The induction heating of the SS ribbon did not adequately heat the ceramic disks and the surface structure of the disks was very small and irregular as seen in Figure 44.

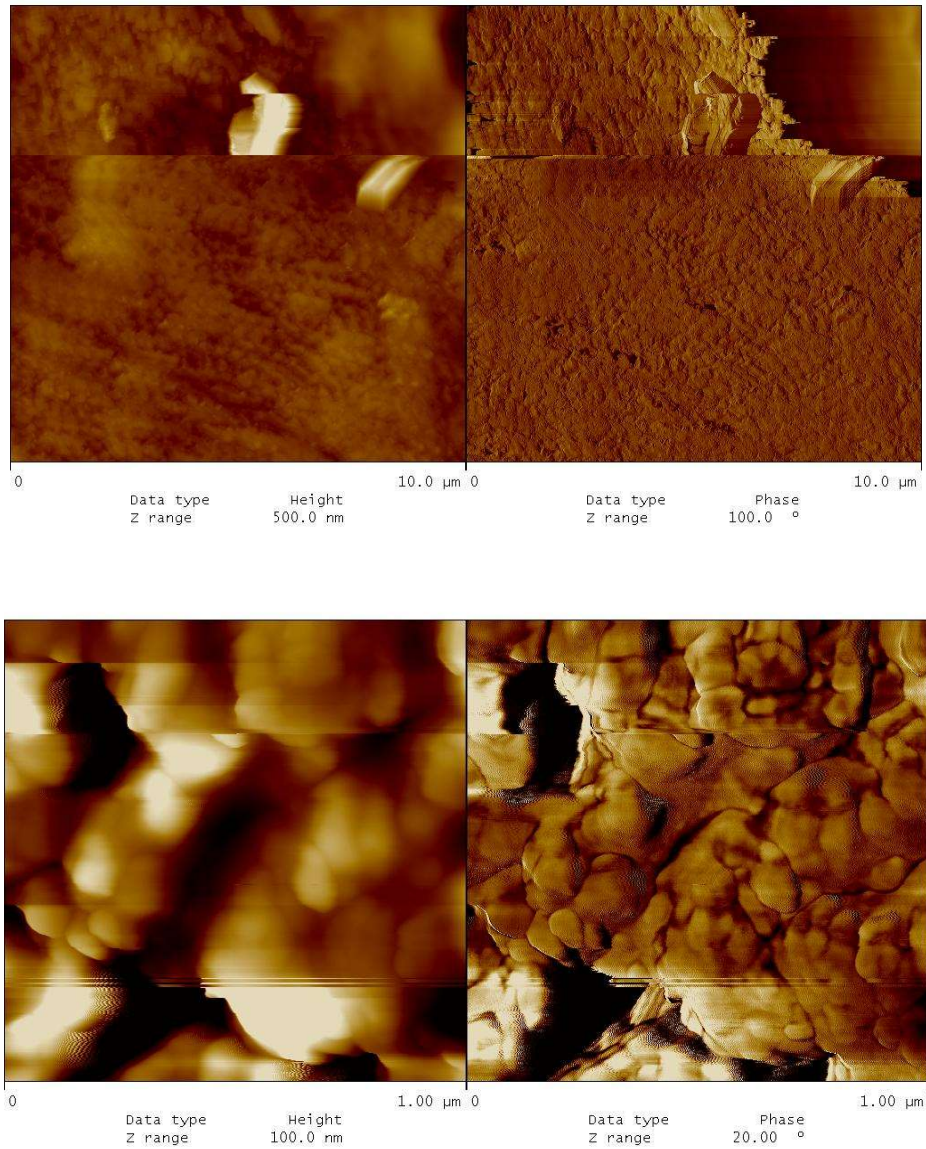


Figure 44: An AFM analysis of the surface of an alumina ceramic filter disk for 10 μm and 1 μm .

5.2.2 Master Mold of the Book of Leviticus

The ribbon mold belt with the master mold of the Book of Leviticus successfully embossed a negative or mirror image of the text of the Book of Leviticus onto extruded LDPE as seen in the AFM analysis in Figure 45. The size of the letters was 6 μm in width,

6 to 9 μm in height and 60-170 nm deep. Replication of the text was clear and no distortion was visible.

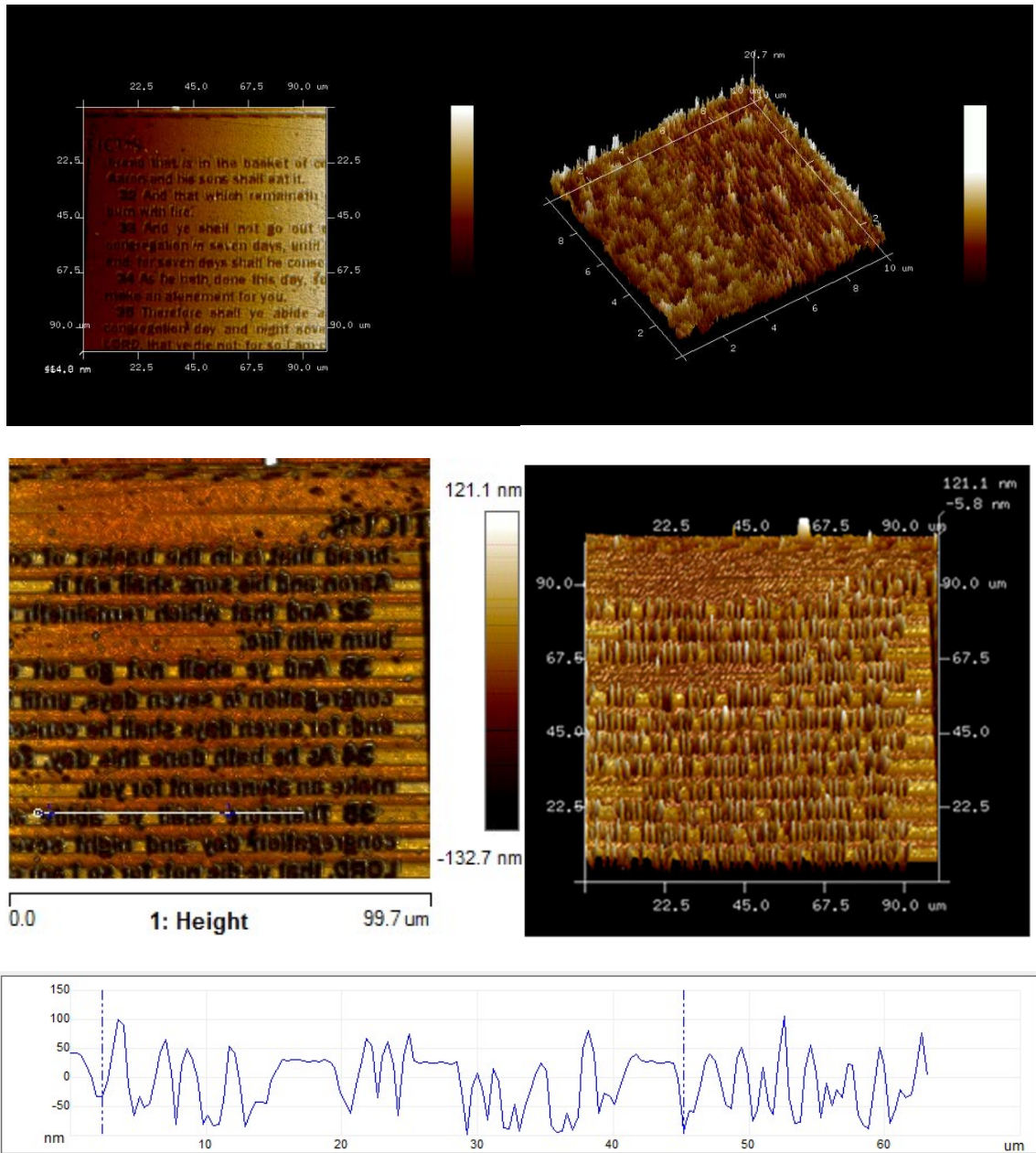


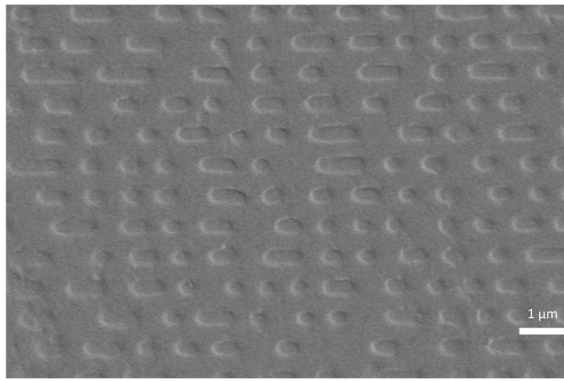
Figure 45: AFM analysis of Leviticus Ni master mold (top) and the embossed LDPE produced by the continuous extrusion-to-embossing process (bottom). The images on the right are the height analysis of the features shown on the left. The depth of imprinted letters in the LDPE was 60-170 nm and the graph is the height profile under the white line in the LDPE image.

5.3 The Nickel Alloy DVD Master Mold

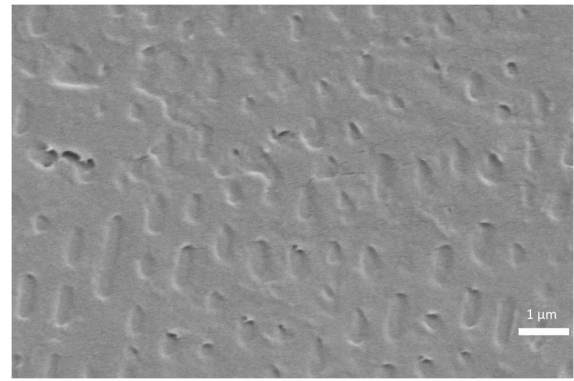
The ribbon mold made with the nickel alloy DVD master mold not only successfully embossed the extruded LDPE but proved to be ideal for showing the necessity of heating the ribbon mold above T_g of the extruded polymer prior to it contacting the melt at the nip point of the calender.

In Figure 46, the effect of IH the nickel belt is compared with not heating. The embossing results with the mold belt heated show clear intaglio patterns in A, C and E. (The fine cracks observed in E and F are due to the gold sputtering or coating necessary to prevent the reflection of the film (LDPE) surface in SEM. The thickness of the gold layer was 2 nm.) This demonstrates the necessity of mold heating before contact with the polymer extrudate.

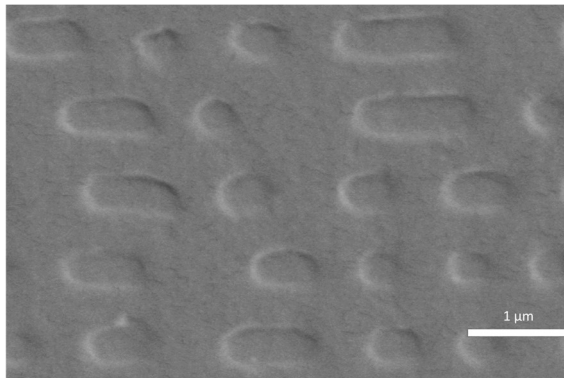
The reproduction of the DVD patterns on the extruded LDPE film was without visible flaws when the mold belt temperature was maintained at or slightly above 210 C. The LDPE film was produced at a rate of 10 to 12 m/min. DVD track pitch is 740 nm. Pits are 105 nm deep and the pits and lands are between 400 nm and 1900 nm long.



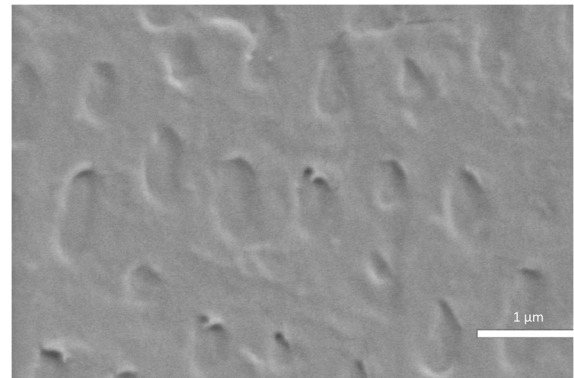
A. HWF-14.9µm - heat on



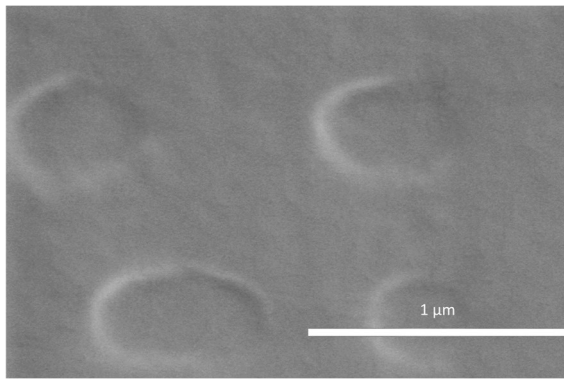
B. HWF-12.5µm - heat off



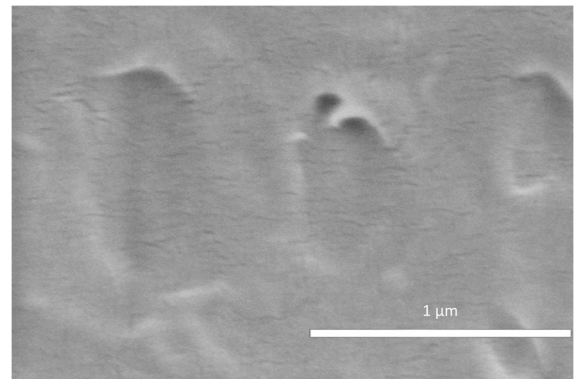
C. HWF-5.97µm - heat on



D. HWF-5.97µm - heat off



E. HWF-2.29µm - heat on



F. HWF-2.29µm - heat off

Figure 46: SEM analysis of extruded LDPE comparing with and without IH at different horizontal with of field (HWF) settings.

CHAPTER 6

DISCUSSION

Although the accomplishments of this research have advanced state of the art, T-NIL embossing of extruded polymers and the making of micro and nano featured molds, some rough spots were encountered along the way. In this section those difficulties are discussed so that other researchers might avoid them.

6.1 Nickel Sulfamate Versus Nickel Sulfate Metal Forming

6.1.1 Metal Forming

Electroforming with nickel sulfamate was used and recommended by a majority of published literature on the subject [87] [88]. The touted “advantages of nickel electroforming from sulfamate solutions are the low internal stress of the deposits and the high rates of deposition” [89]. Also, Caswell Inc. (<https://caswellplating.com>) sells a Nickel Electroforming Kit that supplied all the chemical components needed for a nickel sulfamate bath and a plating manual with instructions.

For the first electroforming attempt the PET substrate was seeded with a 50 nm coating of nickel and any flaws, the butt seam to form a loop and the connection to copper tape electrodes were touched up with conductive silver paint. This base form or mandrel was placed in a nickel sulfamate plating bath (Figure 47) as the cathode and about 200 microns of nickel was deposited on it at a current of approximately 700 mA or 11mA/in². The bath temperature was kept at 113°F, pH at 4-4.5 and the circulator pump continuously running. The conductive silver paint caused flaws (Figure 48) in the surface. The plated nickel formed with high sulfur content making the belt stiff and somewhat brittle.



Figure 47: Nickel Sulfamate plating baths.



Figure 48: Flaws from the conductive silver paint.

Heat treating at 350°C in a vacuum oven did not appreciably improve the stiffness of the belt but did exasperate the flaws as seen in Figure 49.



Figure 49: The flaws after removing the PET base with heat treatment.

Forming a nickel ribbon mold with Nickel Sulfamate ($\text{Ni}(\text{SO}_3\text{NH}_2)_2$) without using conductive paint appeared to reproduce the features but was still very stiff. Heat treating at 500°C and 730°C in a vacuum oven destroyed the mold presumably because of the sulfur content [89] (Figure 50).



Figure 50: Mold belt before and after heat treatment in a vacuum oven.

A new nickel sulfamate bath was set up after a temperature controller failed and boiled out the previous bath. A belt was formed using this new bath and was installed on the calender setup (Figure 51) without heat treating. The belt failed at the seam before any extrusion could be tried. An attempt was made to have the mold belt seam laser welded but Joining Technologies said the material was too brittle to be successfully welded. The nickel formed using the sulfamate process lacked ductility and was brittle due to the high sulfur content.



Figure 51: Mold ribbon belt being installed.

6.1.2 Nickel Sulfate

A nickel sulfate ($\text{NiSO}_4 \cdot 6\text{H}_2\text{O}$) or Watts bath was set up and a mold belt was formed using the bright nickel-plating solution from Caswell. This belt proved to be more flexible than the ones made with nickel sulfamate but the plated joint cracked and failed on this belt also. Joining Technologies attempted to laser weld this belt but was not successful. The ends of the mold belt were then joined with high temperature polyimide (kapton) tape and an attempt at embossing extruded LDPE was made. This attempt resulted in the transfer of only small areas of the nano features to the LDPE. On further examination of the nickel ribbon mold surface, it was found that although the PET carrier readily separated from the nickel, the Norland Optical Adhesive 81 (NOA 81) had actually separated from the PET and was still stuck to the nickel. In the process of running this test the tape failed and the mold belt cracked in another place.

A new mold belt was made in the Watts bath and after the belt was formed, the area of the belt adjacent to the butt connection was insulated with plastic tape and the exposed seam was further plated to strengthen the joint. The process added material to the joint but the result was not smooth (Figure 52).



Figure 52: Weak seam, plating over seam, stronger seam, view through microscope.

6.1.3 Adding a Copper Layer

Another mold belt was formed in the nickel sulfate bath and in an attempt to add durability, the inside of the belt was plated with copper before removing the PET {Figure 53}. This was not successful as the copper separated from the nickel under stress and the copper cracked. An attempt was made to repair the cracks by soldering but the cracking and delamination continued to progress when running the belt around the rollers and heating it with IH.



Figure 53: Belt with copper layer, cracking and delaminating, repaired with solder.

Reverse pulse current plating was also tried using a Dynatronix, Inc. MicroStar power supply but the improvement was found to be minimal. Further research into a nickel metal forming process that will increase ductility is needed.

6.2 NOA Adhesion to Nickel

The most challenging problem with the mold belts made by metal forming was an unanticipated surprise. The continuous extrusion-to-embossing process had successfully embossed extruded LDPE with micro and nano features using mold belts made from commercially electro-formed, saw-toothed patterned nickel alloy sheets, from a master mold of the Book of Leviticus and from a nickel alloy DVD master. The refraction colors from the nano features on the metal formed mold belt were plainly visible yet the extruded LDPE was not being embossed with the nano features. Examination of the PET mandrel removed from the belt gave a clue to the cause as seen in Figure 54. Most of the NOA 81 features were no longer on the PET film. The adhesion of the NOA 81 to the deposited nickel was stronger than the adhesion to the PET film and although not visible to the naked eye, the nano features on the nickel belt were covered with NOA 81 (Figure 34).

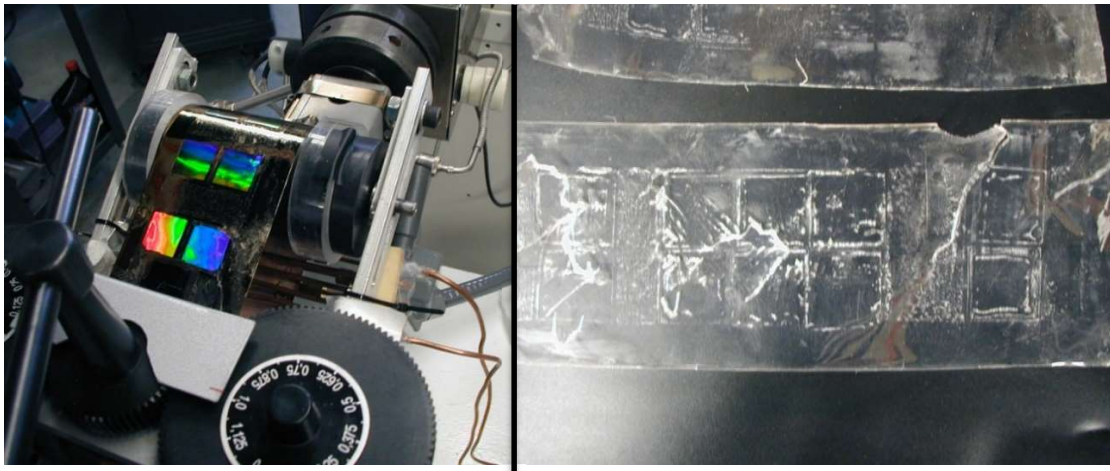


Figure 54: Refraction colors from nano features on the mold belt and the removed PET mandrel.

In an attempt to solve this adhesion problem a modified PET substrate base form or mandrel, with PTE added to the Norland Optical Adhesive 81 as a release agent, was fabricated. A seed layer of nickel was applied to the mandrel in the electron beam evaporator and the mandrel was placed in the electroplating bath. In the metal forming

process the tensile stress that developed in the plated nickel was stronger than the adhesion of the NOA 81-PTE to the PET and caused it to separate from the form as seen in Figure 55.



Figure 55: The nickel separated from the mandrel under plating tensile stress.

6.3 Removal of NOA 81

When fully cured (polymerized) NOA 81 is not soluble. Norland was consulted and recommended soaking in N-Methyl-2-pyrrolidone (NMP) to swell the NOA 81 to assist in removal. A contaminated mold belt was soaked in NOA for days without success. The NMP was heated but kept below its boiling temperature of 202°C (296°F) without effect (Figure 56).



Figure 56: NOA 81 contaminated belt mold soaking in DCM and heated.

The next attempt to remove the NOA 81 from the belt mold without disturbing the nickel nano features was to use agitation of the DCM. A spring mounted platform was constructed and fitted with acoustic drivers. The container holding the mold belt soaking in NMP was placed on the platform and the acoustic drivers were driven by an amplifier with multiple frequencies (music) for days and then at 15 kHz for days (Figure 57) but the NOA 81 was not removed.



Figure 57: Mold belt soaking in DCM on Acoustically driven platform.

Next a large ultrasonic cleaner was constructed. The stainless-steel (ss) tank was 12 inches by 24 inches and 12 inches deep. Ten 60-Watt 40 kHz ultrasonic transducers were attached to the bottom of the tank in a pattern that separated the transducers by an acoustic wavelength (40 kHz in ss) from each other (Figure 58). The transducers were driven by a Beijing Ultrasonic generator and the tank was filled with distilled water. The container holding the mold belt soaking in NMP was suspended in the ultrasonic cleaner (Figure 59) and run through multiple 15-minute cleaning cycles but this also failed to remove the NOA 81 from the nickel mold belt.



Figure 58: The ss tank with the ten 40 kHz transducers mounted on the bottom.

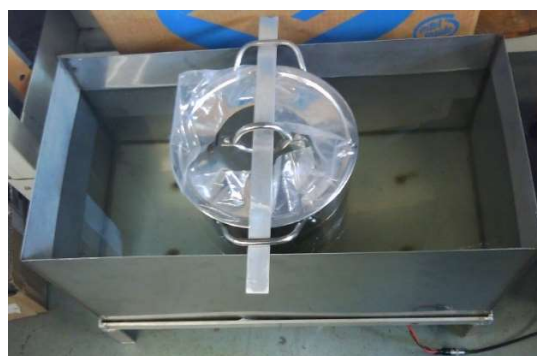


Figure 59: The mold belt soaking in NMP suspended in the ultrasonic cleaner

The NOA 81 documentation stated “The cured adhesive can be separated by soaking in a chlorinated solvent such as methylene chloride” so the mold belt was then soaked in Tetrachloroethylene, another chlorinated solvent, for over 24 hours and then sprayed with a high-pressure steam gun using 110 psi saturated steam. That successfully removed the NOA 81 from the nickel mold belt without damaging the nano features of the mold. The ribbon mold belt was then installed on the Roll-to-Roll extruder/thermal embosser and successfully embossed the LDPE with the features.

CHAPTER 7

PROCESS FOR EMBOSSING A METAL GLASS ROLLER WITH MICROFEATURES

7.1 Introduction

Metallic glasses (MGs) have unique advantages as a mold material. The featureless amorphous structure endows MGs with exceptional attributes such as high strength (>2 GPa), high elasticity (up to ~2%), high toughness, paired with superior wear, corrosion resistance, and smooth surface. Unlike crystalline metals, whose properties such as grain size make nanomoulding infeasible [90], MGs can be thermoplastically formed or shaped like thermoplastic polymers, at their supercooled liquid state above the glass transition temperature, T_g [91]. In this investigation the optimal operating parameters for embossing a MG roller with micro or nano features are explored, presented and evaluated.

7.2 Determining the processing protocol by experimentation

The key parameters to successfully embossing the surface of a MG roller without causing crystallization of the MG are the temperature of the primary mold, the applied force or pressure of the mold against the surface and the time of contact of the surface with the mold [92]. A temperature above the glass transition temperature (T_g) of the MG was necessary to quickly transfer sufficient heat to the MG surface to soften it for embossing without melting it or causing crystallization. The time required for the heat transfer will govern the rotational speed of the roller over the primary flat mold. The pressure applied to the roller should be sufficient for accomplishing the embossing without distorting the

roller surface. The focus of this study was to establish an appropriate processing protocol by which practical time, temperature, stress, and strain rate can be applied to achieve precise nanoimprinting of an MG surfaced roller without crystallization.

The material used in this part of the investigation was an injection molded MG cylinder with 40 mm OD and 1 mm thick walls (Figure 60). The constituent elements include Zr (56.6 wt%), Ti (25.4 wt%), Cu (8.1 wt%), Be (4.6 wt%), Hf (3.3 wt%), and other microelements such as Dy, Sn, Ni, Al, etc. (Table 1). It has a glass transition temperature of 305°C and a crystallization temperature of 450°C measured by DSC at a heating rate of 20 °C/min. The large thermoplastic forming ability of this material endows it with a great advantage of imprinting.

Table 1: Specific composition of the Zr MG extruded tube.

elements	Zr	Hf	Ti	Cu	Ni	Be	Mg	Dy	Al	Sn	Ta, Nb
(wt%)	56.64	3.26	25.36	8.12	0.21	4.61	0.04	1.48	0.05	0.22	margin

To determine the optimal operating parameters for embossing a MG roller with micro or nano features, a curvature-based imprinting process was developed to simulate and identify the process window for roll-based imprinting. A 5 mm ring was cut from the extruded MG cylinder and the ring was cut into approximately 5 mm segments (Figure 60) using a wire electric discharge machine (EDM). A fixture for the Instron testing machine, that matched the inner diameter curvature of the extruded cylinder, (Figure 61a) was designed to hold the 5 mm test specimens with a thin steel strap. The tests simulated the roll-based imprinting process to estimate the practical temperature, time, and pressure required during roll-based imprinting. Figure 61b shows the drawing of the fixture and the

strap. This test fixture was mounted on the upper part of the Instron and a hot plate to support the primary flat mold on the lower part of the Instron testing machine (Figure 62).



Figure 60: A 5 mm wide ring section of the MG cylinder, in the EDM to cut 5 mm sections.

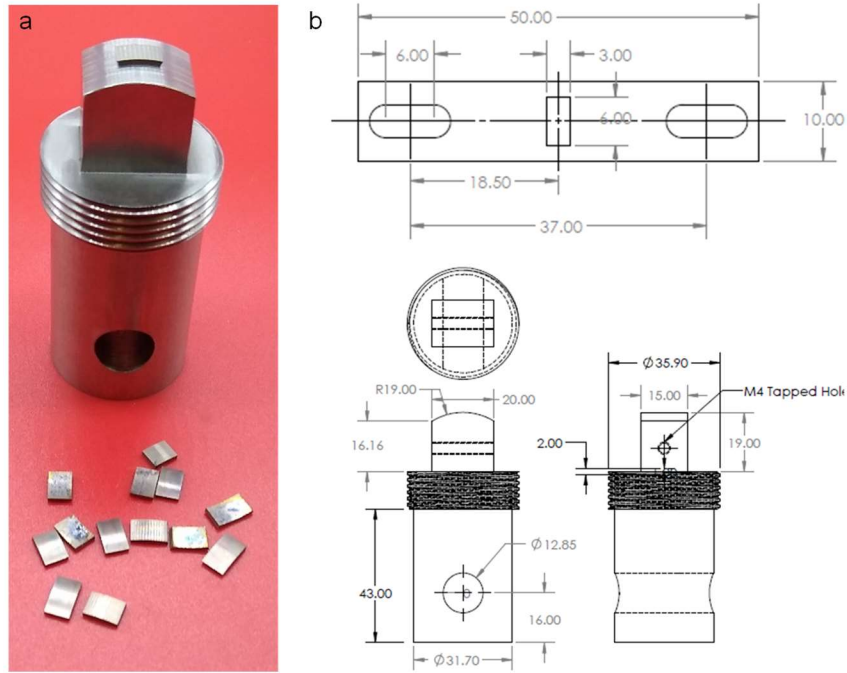


Figure 61: (a) The Instron test fixture and Zr-based MG samples (5 mm 5 mm 1 mm) cut from the tube for imprinting tests. (b) The drawing of the fixture and the holding strap.

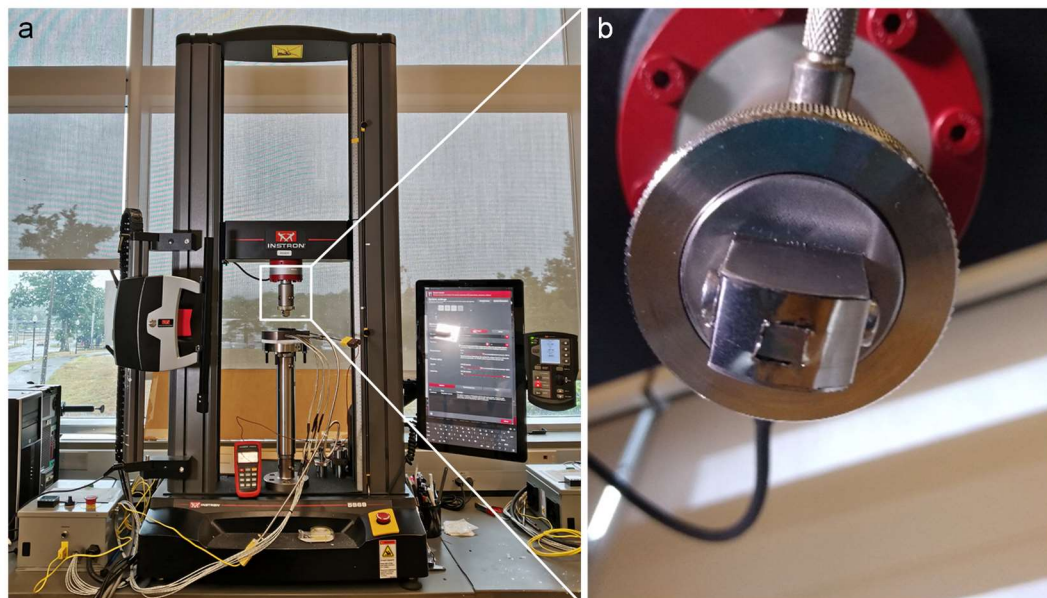


Figure 62: (a) Thermoplastic forming stage using Instron 5969 dual-column testing system with the force capacity up to 50 kN and heating temperature up to 600 °C. (b) A test sample mounted on the fixture.

The Instron testing machine was programmed to thermoplastically imprint MG into a nickel primary mold placed on the hot plate. The MG test piece was lowered 149 mm, to 1 mm above a nickel primary mold placed on the hotplate, at high speed. It was then slowly lowered down to the mold until a set force was reached. The force was held for a set time and then the test sample was returned to the starting position.

The mold used for experimentation was a nickel alloy mold with sawtooth type features 12 μm in height and 30 μm pitch and was 230 μm thick (Figure 63).

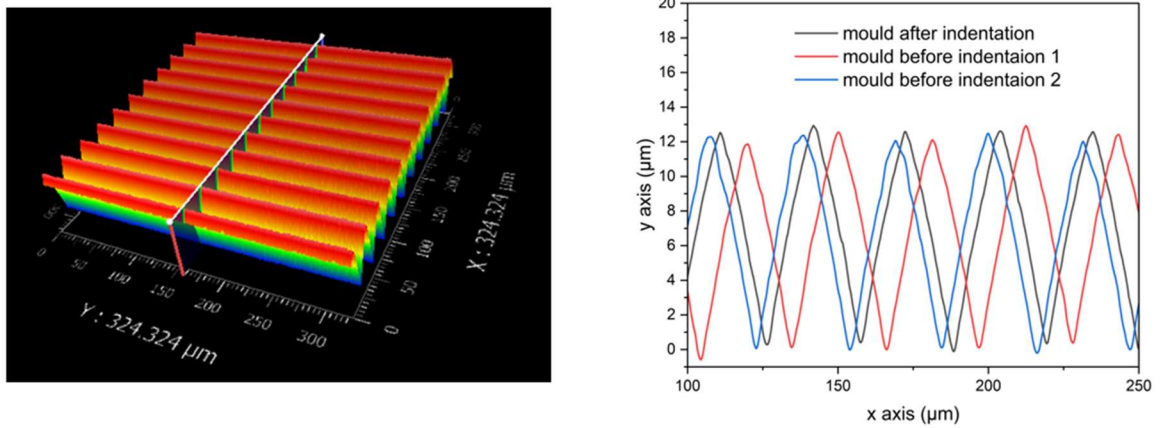


Figure 63: Zygo Profilometer surface profile and line profile of the nickel alloy mold.

During thermoplastic imprinting, the force/pressure was held for a duration of time until the imprinting process was completed. The calculated pressure for the area embossed at 450 $^{\circ}\text{C}$ for 5 seconds was between 43 and 50 MPa. The calculated pressure for the area embossed at 470 $^{\circ}\text{C}$ for 2 seconds was between 61 and 75 MPa. Testing was conducted at different temperatures of 410 $^{\circ}\text{C}$, 430 $^{\circ}\text{C}$, 450 $^{\circ}\text{C}$, and 470 $^{\circ}\text{C}$. A force of 100 N was used and times between 2 and 20 seconds were attempted. Successful embossing was achieved at 450 $^{\circ}\text{C}$ and 5 s and at 470 $^{\circ}\text{C}$ and 2 s as seen in the optical microscopy (OM) images in Figure 64.

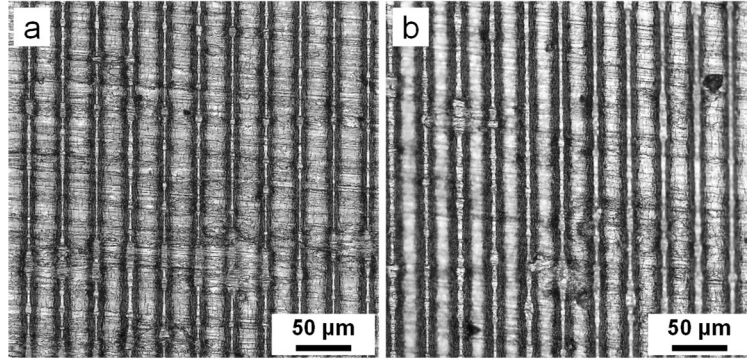


Figure 64: OM images of Zr-based MG embossed at (a) 450°C for 5 s and (b) 470°C for 2 s.

The calculated pressure for the area embossed at 450°C for 5 seconds was between 43 and 50 MPa. The calculated pressure for the area embossed at 470°C for 2 seconds was between 61 and 75 MPa. Figure 65 illustrates how the areas were derived to calculate the embossing pressure.

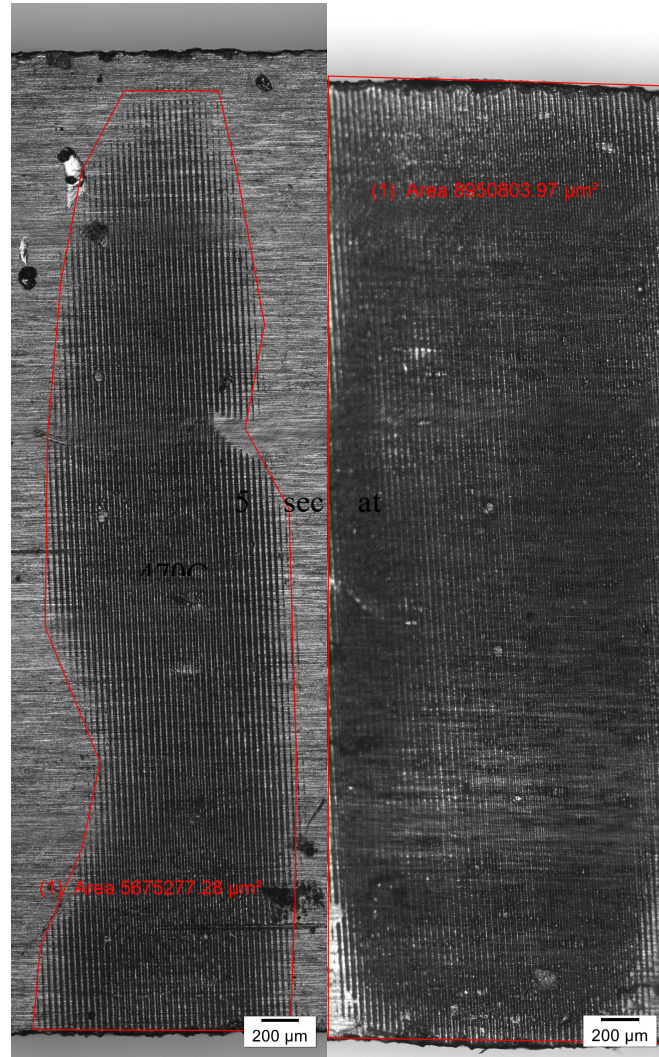


Figure 65: Calculating area of embossed patterns.

The embossing time, temperatures, area embossed and calculated embossing pressure at a force of 100 N are shown in Table 2. Three temperatures are shown, the temperature of the hot plate as displayed on the Omega controller, the temperature of the aluminum block supporting the nickel mold, and the temperature of the mold as measured with a noncontact infrared hand-held instrument. The analysis of the 2 second and 5 second embossing at 100 N force indicated that a 2 second contact time with the hotplate at 500°C would achieve full indentation of the MG in a shorter time. The relationship between the

temperature of the hotplate, embossing pressure and the depth of embossing is shown in Figure 66.

Table 2: Embossing time, temperature, area and pressure at 100 Newtons.

Time (s)	Temperature (°C)			Area (μm^2)	Pressure (Mpa)	Depth (μm)
	Controler	Hotplate	Pyrometer			
2	390	396	307	0.7	136.5	0.5
	410	418	324	1.5	66.4	0.6
	430	437	345	2.1	48.5	1.6
	450	457	363	2.3	42.9	2.7
	470	477	384	3.7	26.8	3.5
	490	500	399	9.0	11.2	12
5	370	376	295	0.5	220.8	0.5
	390	396	307	1.0	99.3	1.6
	410	418	324	1.7	59.2	0.6
	430	437	345	3.2	30.8	1.7
	450	457	363	4.5	22.5	4.8
	470	477	384	5.7	17.6	6.4

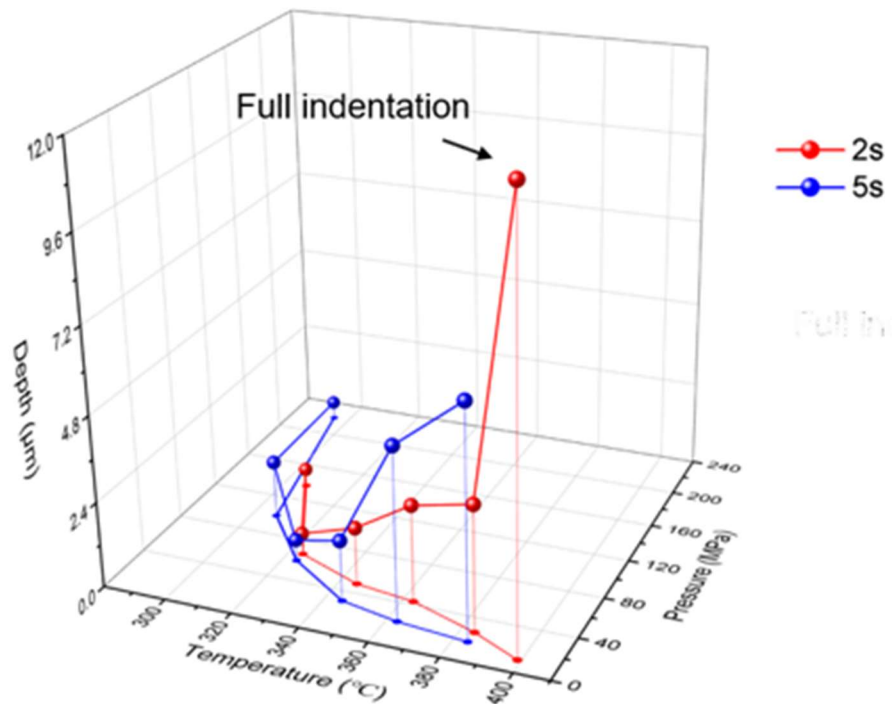


Figure 66: The relationship between temperature, pressure and depth of indentation.

7.3 Testing the operating parameters with the roller hot emboss mechanism

7.3.1 Roller hot embossing mechanism design

The function of the designed mechanism is to bring a roller into contact under pressure with a heated flat primary mold, roll the roller over the heated mold for one revolution of the roller, and then remove the roller from the heated mold. The speed (timing), temperature of the primary mold and applied pressure are all adjustable to conform with an appropriate processing protocol by which practical time, temperature, stress, and strain rate can be applied to achieve precise roller nanoimprinting of an MG without crystallization.

The mechanism was designed to function inside an inert gas oven just below T_g , the glassine temperature of the MG ($\sim 400^\circ\text{C}$). The high operating environment temperature imposed severe constraints on the design of the mechanism as well as the method for driving the mechanism.

The mechanism was designed to be able to function inside an inert gas oven just below T_g of the MG (e.g., $\sim 400^\circ\text{C}$). The high operating environment temperature imposed severe constraints on the design of the mechanism as well as the method for driving the mechanism. The material used for the structural frame had to maintain sufficient strength and rigidity at this elevated temperature. The bearing material also had to be able to withstand a high temperature operating environment. The drive motor and controller cannot withstand such high temperatures, so the driving lead screw had to be long enough to extend through the oven wall. For these reasons the basic structure of the mechanism

(Figure 67) is formed from steel plate. The bearings are high temperature tolerant brass and the support insulation for the hot plate in ceramic and refractory cement. The lead screw that drives the mechanism is long enough to extend through an oven wall where the drive motor can operate at room temperature.

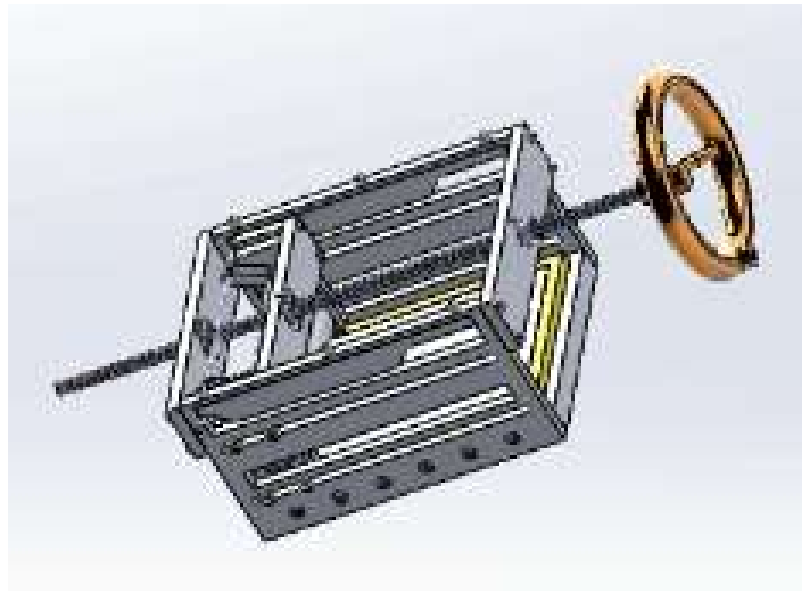


Figure 67: Designed roller hot embossing mechanism

Specifically, the base of the mechanism (Figure 68) supports the hot plate and frame walls. The hotplate is designed to support three 500-Watt heaters (Figure 69). The hot plate is 10” by 7” to accommodate up to a 6” long by 3” diameter roller. The bearing housings (Figure 70) are attached to guide slots in the walls and are driven back and forth in the guide slots by a leadscrew. The bearings for the roller are supported between two springs in the housings a weaker spring below the bearing to lift the roller off the hotplate and a stiffer spring above the bearing which is compressed by a cam to press the roller against the master mold which is placed on the hotplate. Replaceable cam plates, mounted in the walls (Figure 71), drive the follower shaft which operates the pressure cams in the bearing

housings to lower and raise the roller for embossing. The cam plates are machined to match the outer diameter of the roller being embossed.

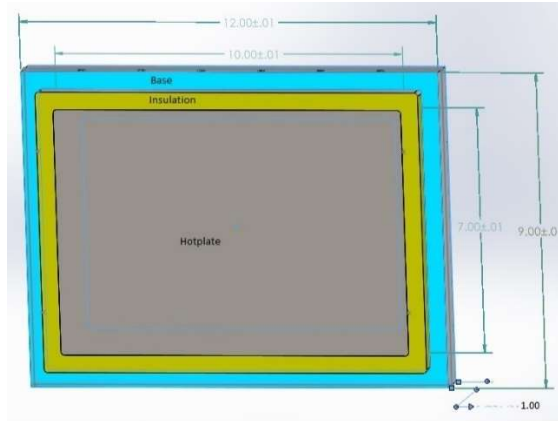


Figure 68: The base assembly including the hot plate and the insulating ceramic (yellow).

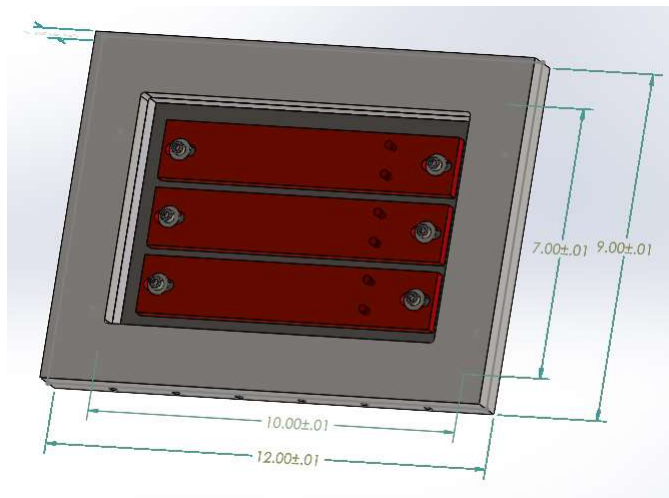


Figure 69: The underside of the base assembly showing the heaters.

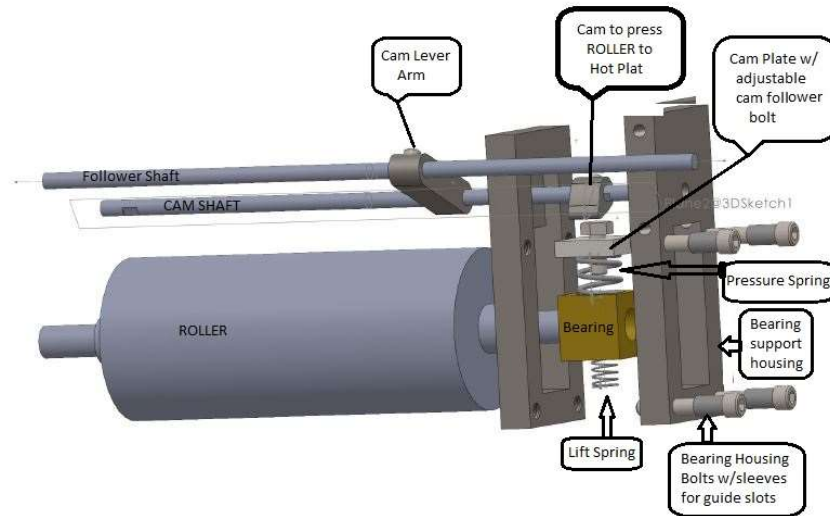


Figure 70: The bearing housing assembly.

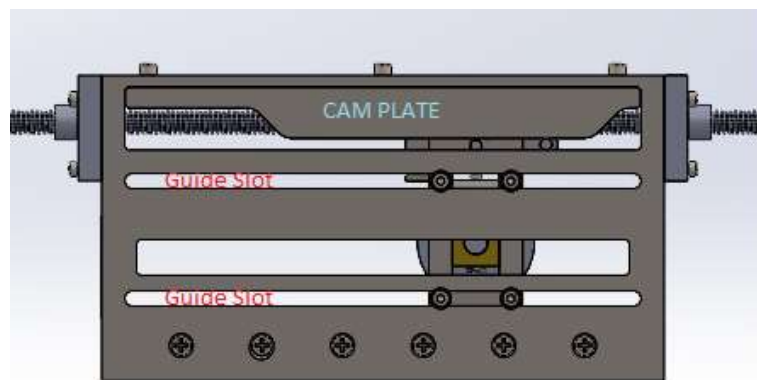


Figure 71: Side wall showing replaceable cam plate.

The initial testing of the MG embossing mechanism was to be done using the micron scale features without an inert gas oven so new longer side plates were constructed. Three inches was added to each end of the new side plates to enable the test roller to move totally away from the hot plate and to facilitate the installation and removal of the test specimens away from the hot plate (Figure 72). A variable speed gearhead motor was used to drive the 10 tpi leadscrew which moved the roller spindle over the hotplate.



Figure 72: The roller hot embossing mechanism with wider side walls.

7.3.2 Use of 5 mm wide rings to test the determined processing protocol parameters

To facilitate the testing of the determined processing parameters at a reasonable scale and cost, 5 mm rings were cut from the extruded MG tube and mounted at the longitudinal center of a custom mandrel that tapered to a 38 mm outer diameter for 10 mm at the center (Figure 73: Mandrel roller for testing 5 mm MG rings.). The mandrel was installed onto the roller hot Embossing mechanism by sliding a 12.7 mm (1/2") shaft through the bearings



Figure 73: Mandrel roller for testing 5 mm MG rings.

into the mandrel. The Ni primary mold was placed on a 17 mm thick aluminum block to compensate for the small, 40 mm outer diameter, of the Zr-ring (Figure 74). The roller hot embossing mechanism was initially designed for the 65 mm rollers of the rolling mill/calender used in the continuous extrusion-to-embossing system making the aluminum block necessary.

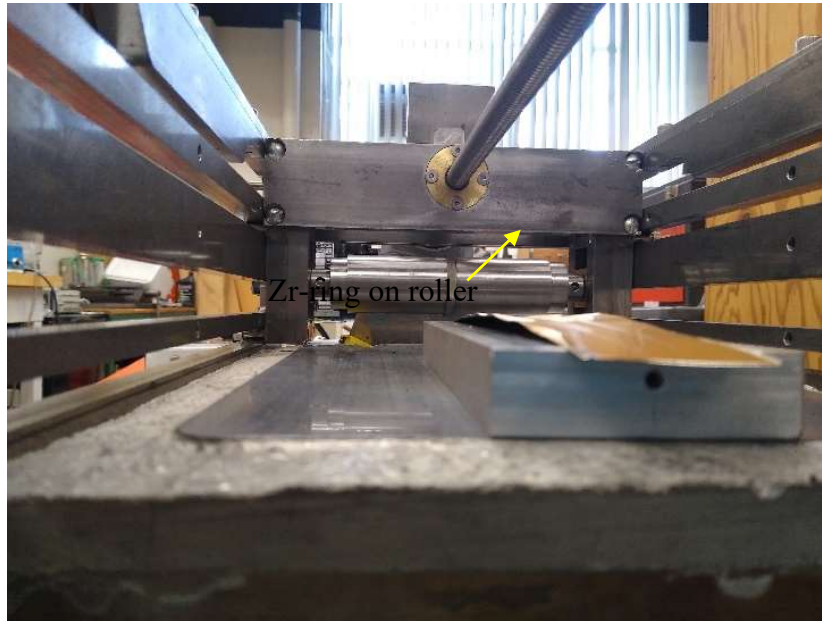


Figure 74: The Zr ring on the mandrel and the Ni primary mold on the Al block.

The pressure applied to the Zr ring was measured with Fujifilm Prescale® Film. High pressure film covering the range of 7,100 to 18,500 psi was used and indicated the pressure to be about 14,222 psi (Figure 75).

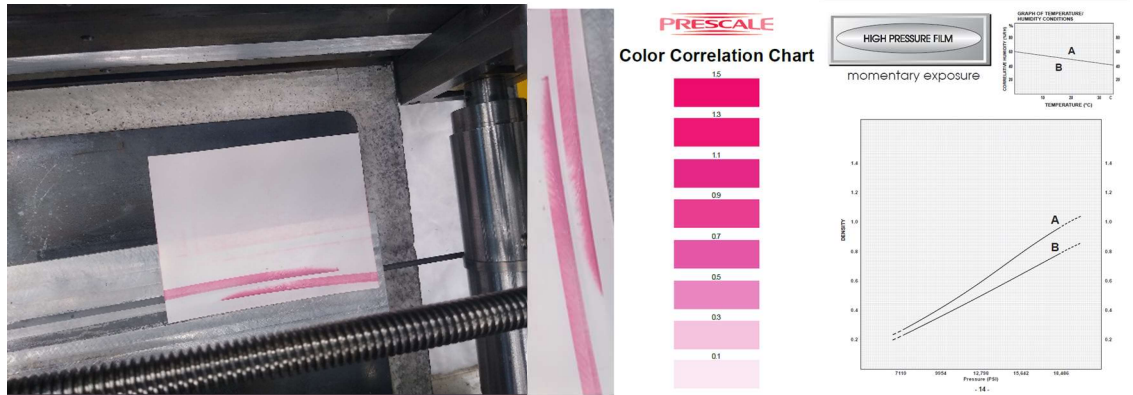


Figure 75: Measuring pressure with Fujifilm Prescale® Film.

7.3.3 Experiments

The first 5 mm wide MG ring was pushed on to the custom mandrel using a section of 29 mm ID steel tube and a mallet but could not be pushed all the way up the taper to the center where the diameter was 38 mm. The result was that embossing only occurred on the surface of the ring that was furthest up the taper as

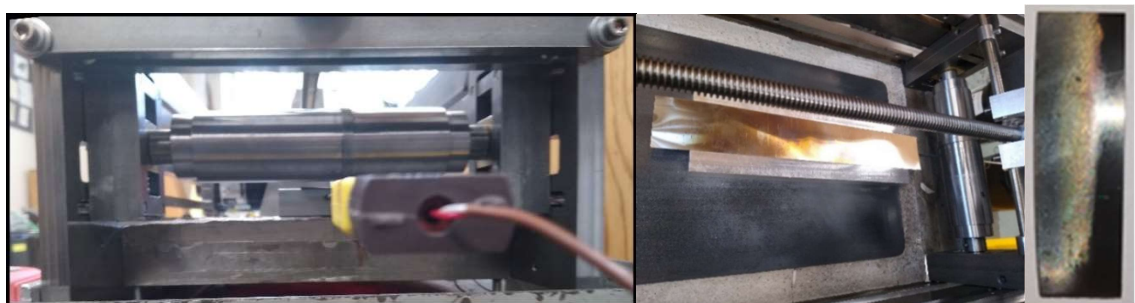


Figure 76: The MG ring off center on the mandrel taper, the Ni mold on the Al block and the half-embossed ring segment.

seen in Figure 76. With the hot plate heated to 500°C the aluminum block was at 450°C. The embossing was started with the motor controller set at 100 for roughly the first third of the circumference, slowed down to 50 for the second third and finished at 25

(Figure 77). The depth of embossing was only 2-2.5 μm at the fast speed, 6-7 μm at the medium speed and nearly the full 12 μm at the low speed (Figure 78).

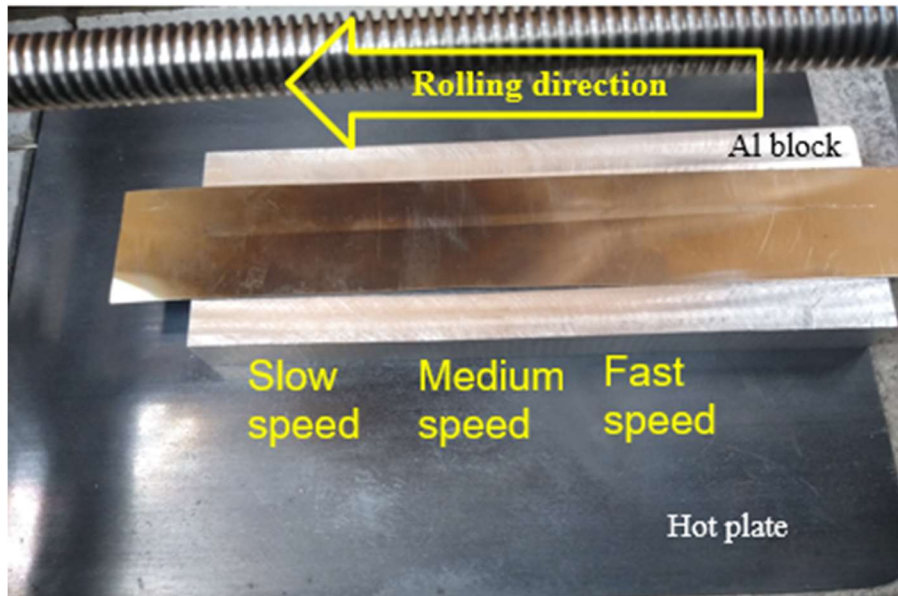


Figure 77: Path of the first embossing of a MG ring.

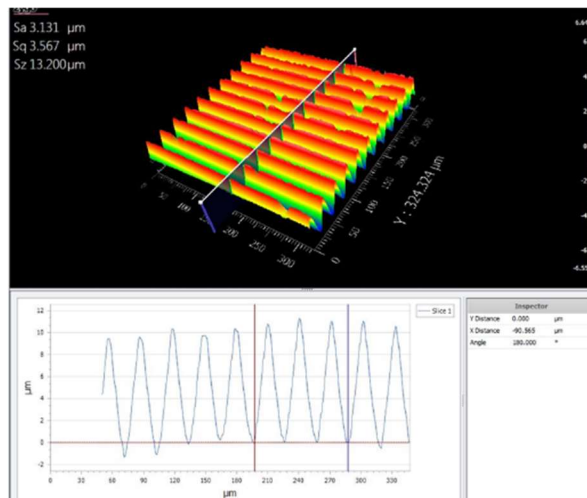
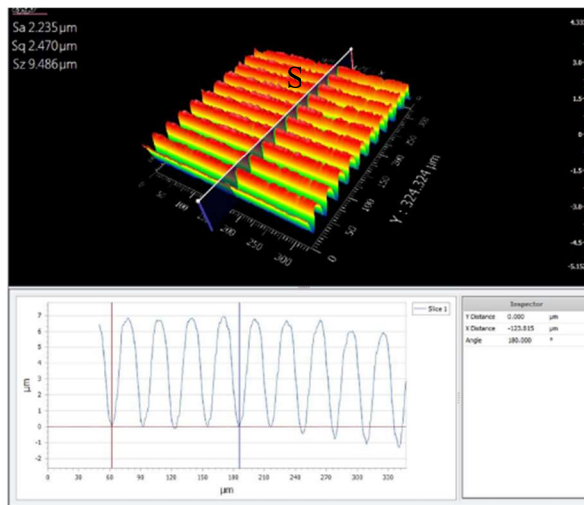
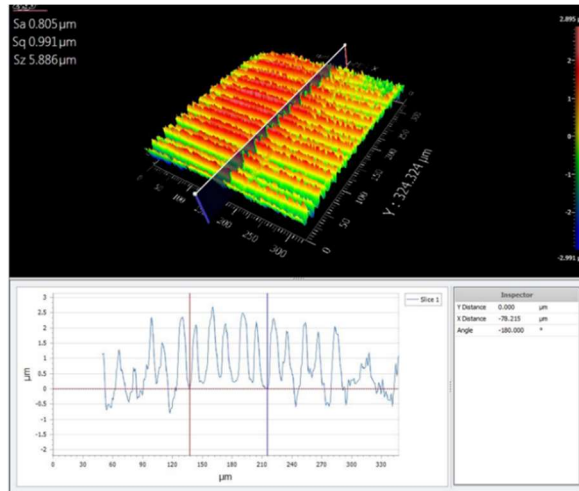


Figure 78: Profilometer surface profile and line profile of embossed segments of 1st MG ring.

The second MG ring was pressed to the center of the custom mandrel using a hydraulic arbor press. The hot plate was at 480°C and the aluminum block was at 430°C. The first segment of the ring was embossed with the leadscrew turning at 10 rpm, the second segment at 5 rpm and the last segment at 2.4 rpm. That corresponded to the motor controller set to high range and the dial at 50, 30 and 20 respectively. Also, to the MG ring moving across the Ni mold at 0.423 mm/s for segment 1, 0.2116 mm/s for segment 2 and 0.1016 mm/s for segment 3. The MG ring was cut at the segment borders for analysis (Figure 79).



Figure 79: The three segments of the MG ring and motor controller.

The depth of embossing was around 2 μm for segment 1, 6.8 μm for segment 2 and 11 μm for segment 3 as seen in the profilometer surface profile and line profile shown in Figure 80.

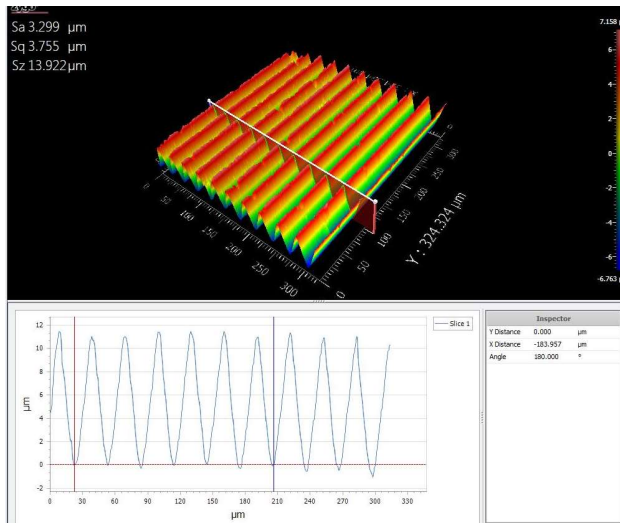
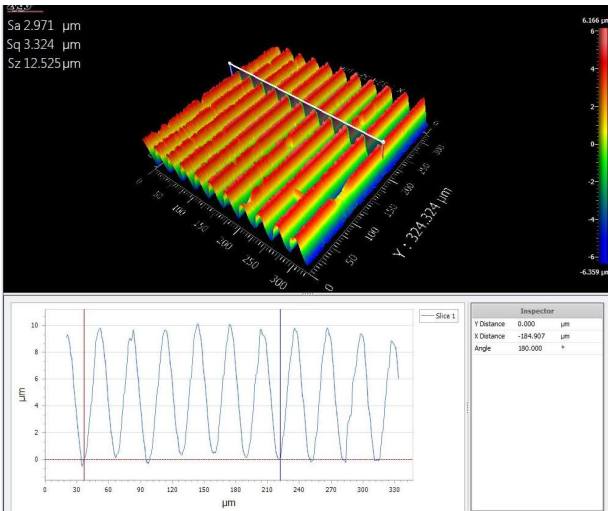
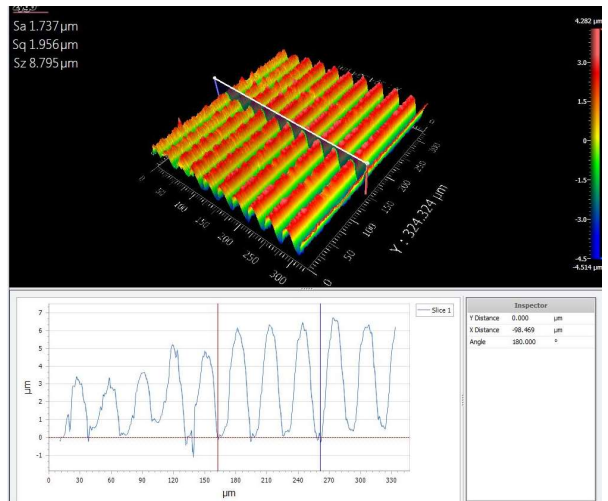


Figure 80: Profilometer surface profile and line profile of embossed segments of 2nd MG ring.

The operating parameters for embossing are temperature, pressure and time of contact. Time of contact is a function of surface speed of the roller across the master mold. If the contact time with the hot master mold is too short the MG surface will not be heated to T_g and soften to fill the mold features. If it is too long the MG will distort and begin to crystalize. The graph of embossing depth verses surface speed in Figure 81 shows the relationship of contact time to embossing quality.

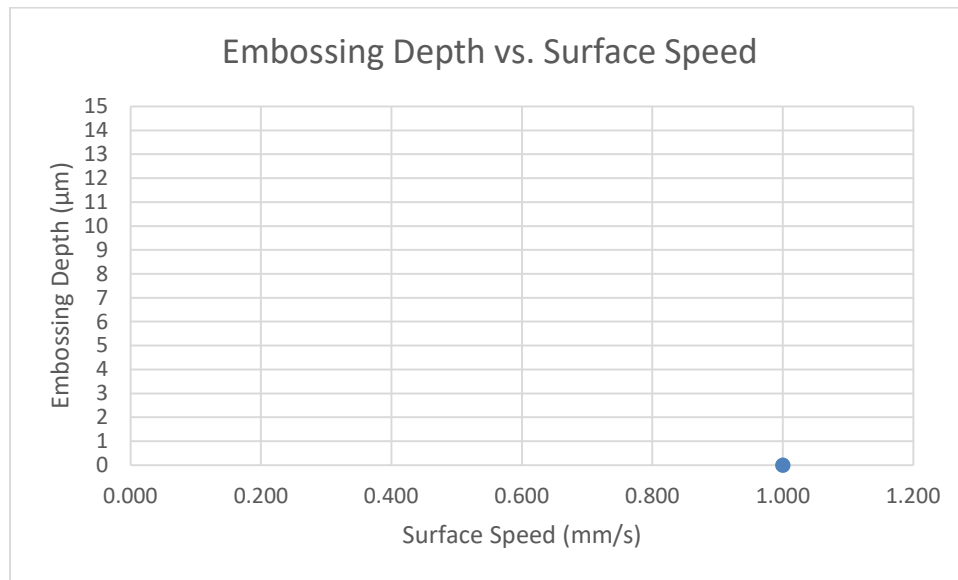


Figure 81: Graph of embossing depth vs. surface speed.

During the first two experiments the top of the steel cart that the hot roller embossing mechanism was on got quite hot and it was difficult for the hotplate to reach and maintain 500°C so a sheet of glass and high temperature ceramic wool insulation were placed under the mechanism. This not only kept the steel cart cool; it improved and stabilized the temperature regulation of the hotplate (Figure 82).



Figure 82: Glass plate and ceramic wool insulation under the hot roller embossing mechanism.

A third MG ring was pressed onto the mandrel for embossing. This ring was to be used on the calender roller for embossing extruded polymer. The hotplate was heated to 500°C and the Al block was at 455°C (Figure 83). With the temperature stable at these higher temperatures, it was decided to run the embossing with the leadscrew turning at 5 rpm. The Ni mold, having been used several times, was slightly curled and did not lie flat on the Al block (Figure 84).



Figure 83: Hotplate temperature controller and Al block thermocouple display.

This reduced the heat transfer to the mold and the MG ring was only embossed to a 6 μm depth or less as seen in Figure 85 so a fourth MG ring was prepared and run with the leadscrew slowed to 2.4 rpm.



Figure 84: The nickel mold curled.

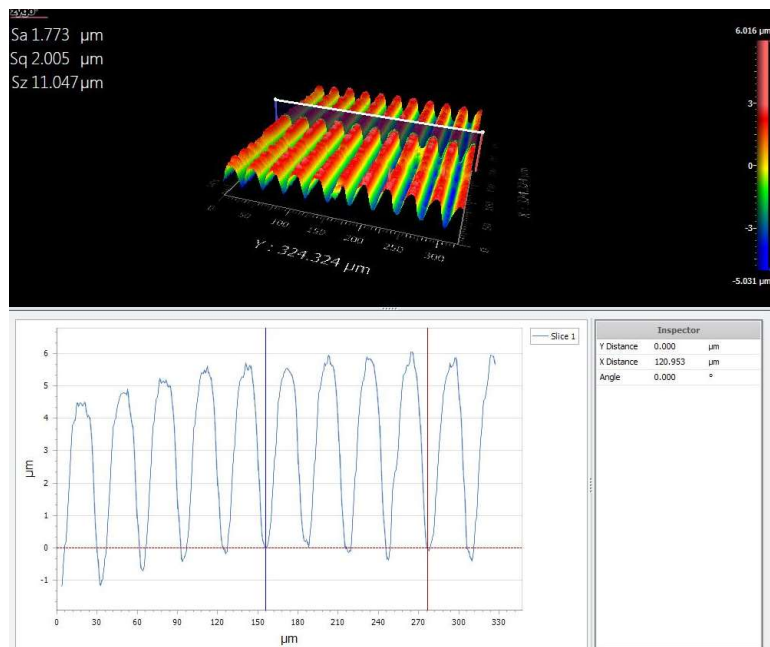


Figure 85: The Ni mold curled and the Profilometer surface profile and line profile of the 3rd ring.

A fourth MG ring was pressed onto the mandrel for embossing. The hotplate was again heated to 500°C and the Al block was at 455°C and the embossing was run with the leadscrew turning at 2.4 rpm. The embossing of the MG ring was very good but could have been better. The depth of impressions was 12 μm (full embossing) around most of the ring (Figure 86) but as low as 6 μm in one area.

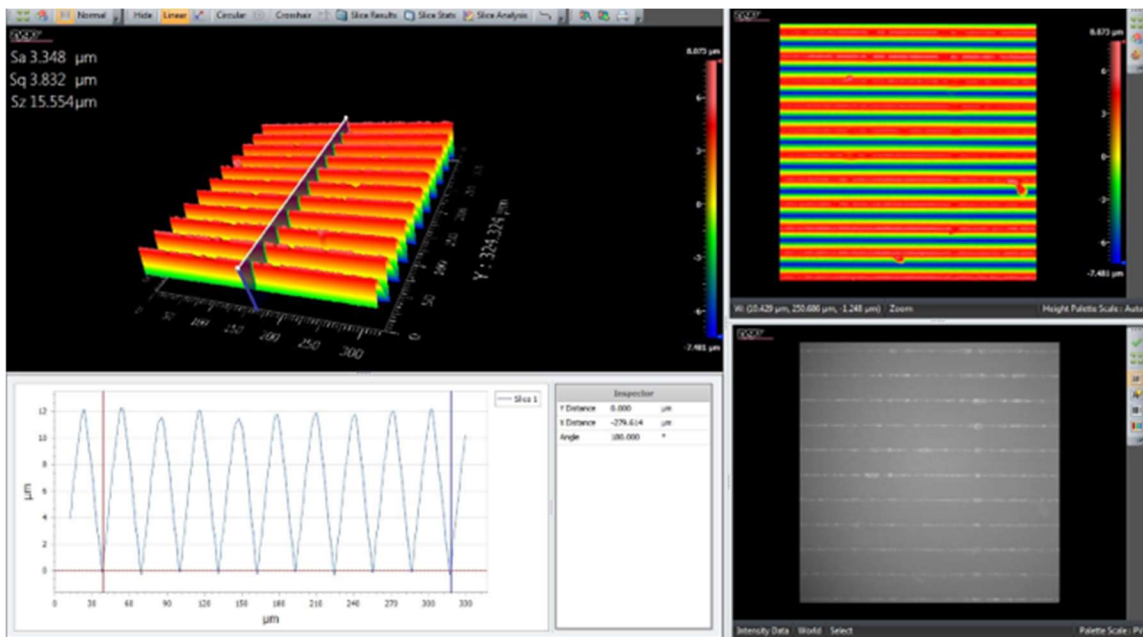


Figure 86: Profilometer analysis of 4th MG ring.

7.4 Roll-to-Roll embossing of extruded LDPE with the MG ring

To use a section of the injection molded MG cylinder with 40 mm OD and 1 mm thick walls in the continuous extrusion-to-embossing process a rolling mill with 40 mm diameter rollers was adapted to serve as a calender. A top roller was annealed and machined to a diameter of 38 mm to support the MG ring. Aluminum cylindrical parts were

machined to be pressed onto the roller mandrel on either side of the MG ring to form a continuous 40 mm diameter surface (Figure 87).

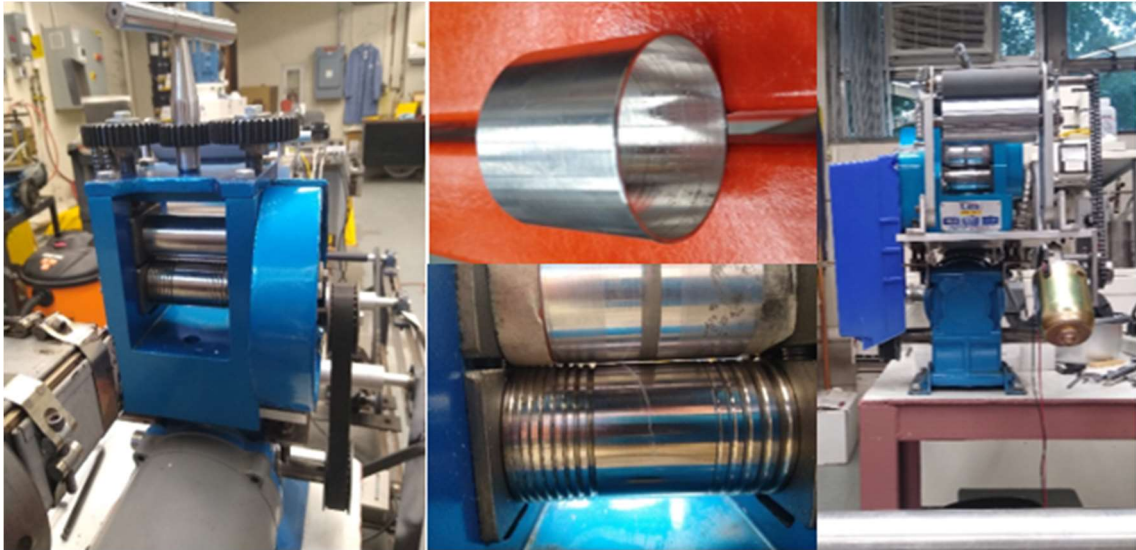


Figure 87: Rolling mill with 40 mm diameter rollers adapter to serve as a calender.

The temperatures of the four extruder barrel zones were set to 180 C. The extruded HDPE web exiting the die was run to meet the mold at the roller nip, through the cooling roller and then through about 2 feet of air to a winder or take up shaft (Figure 88).



Figure 88: Path of LDPE web through the calender, over the cooling roller and to the winder.

Samples of the resulting LDPE ribbon was examined with an optical microscope (OM) and analyzed with the profilometer. OM images are shown in Figure 89.

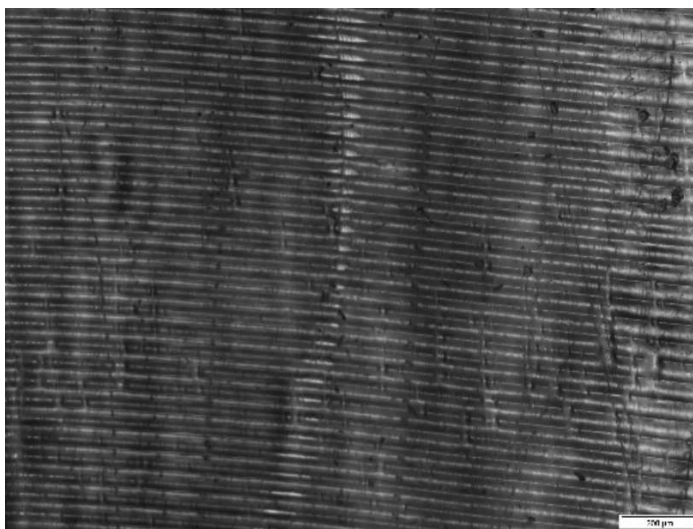
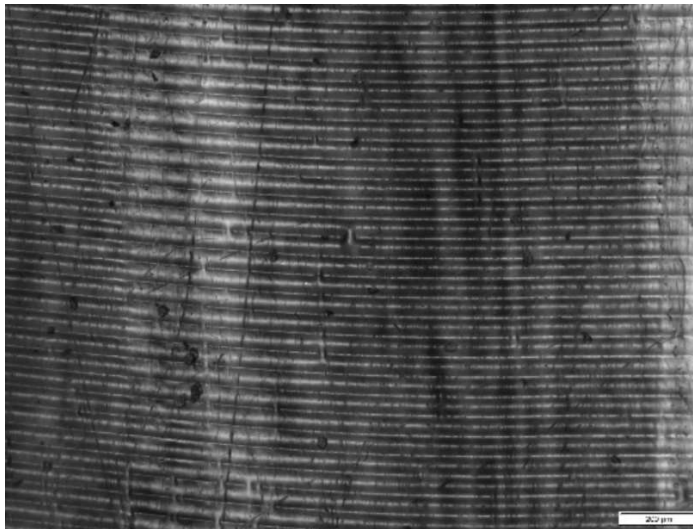
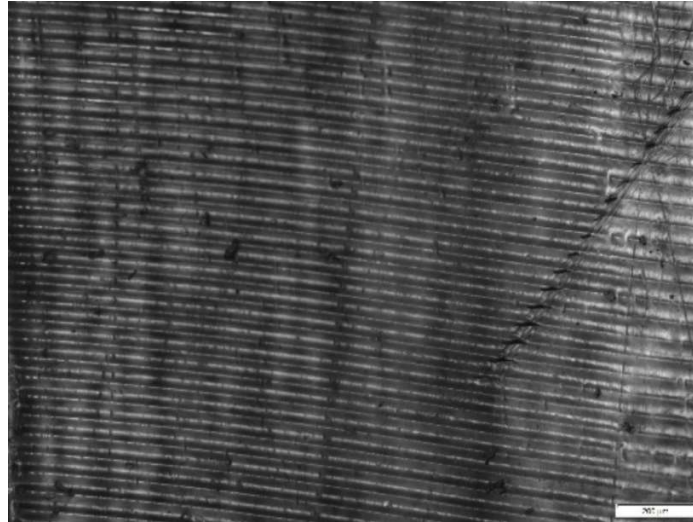


Figure 89: Three OM images of the LDPE ribbon.

The depth of embossing can be seen in the profile views of embossed samples of the LDPE ribbon in Figure 90. The embossed pattern is only between 7 and 9 μm peak to trough and is rounded at both. The fidelity to the 12 μm saw tooth pattern is not there. This is probably a combination of the extrudate not filling the unheated MG mold ring and the LDPE not being adequately cooled before separation from the mold. Raising the takeoff roller to keep the polymer ribbon against the roller mold and slowing down the process may improve the results and will be tested.

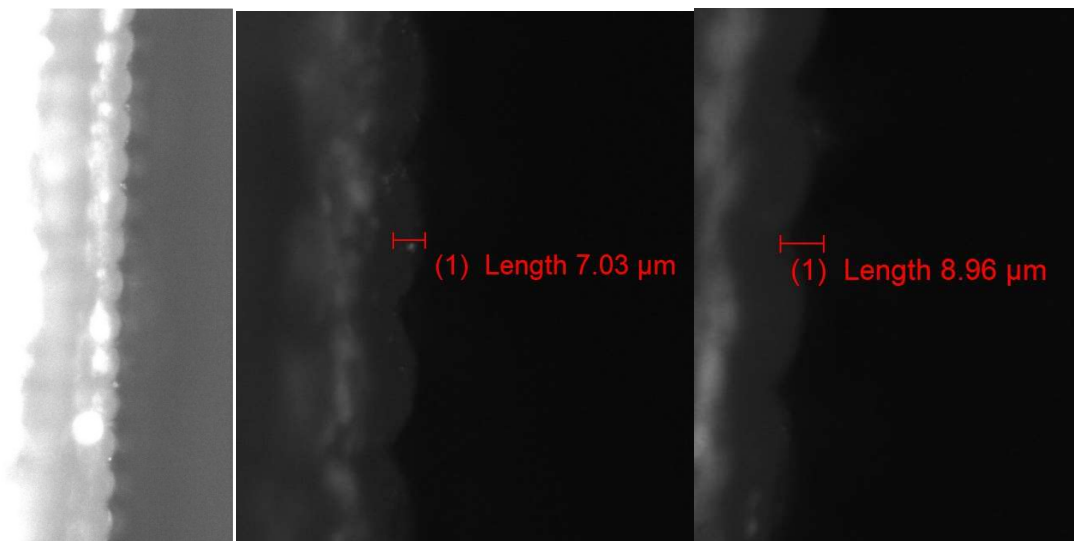


Figure 90: Profile views of embossed LDPE

CHAPTER 8

CONCLUSIONS

This research presented and demonstrated a method for advancing the art of T-NIL by directly embossing extruded polymers on a laboratory scale. Microscale and nanoscale features were imprinted directly onto extruded polymer film at a rate of 10 to 12 meters per second, three to over one hundred times the throughput of current R2R processes and orders of magnitude faster than planar processes [34] [37] [45]. The big challenge was in developing a suitable mold that could yield the thermal changes needed to emboss viscoelastic material successfully.

The use of a thin metallic ribbon as the mold for roll-to-roll thermal imprint lithography was shown to have significant advantages. First, the ribbon mold could be rapidly heated beyond the melt temperature of the extrudate using induction heating. This enabled the polymer melt to fully fill the micro and nano patterns on the surface of the ribbon for high fidelity embossing. Second, the low thermal mass of the thin ribbon allowed for rapid cooling of the mold and the polymer by the high thermal mass of the calender rollers. In an actual production environment, the rollers would have to be cooled. The imprinted polymer film was effectively cooled before release from the belt mold, thereby minimizing feature distortion caused by viscoelastic recovery. The results show that the belt mold temperature plays a profound role in affecting the replication quality. Belt mold temperature above the polymer melting temperature is needed for complete replication of the of the features on the mold belt, especially the sharp corners. Second, Ribbon mold

belts are scalable for the production of large-area micro- and nanostructures on polymer substrates.

The feasibility of creating ribbon mold belts using a Polyethylene terephthalate (PET) film, with surface nano features formed by a R2R UV NIL process developed by the Center for Hierarchical Manufacturing, as a mandrel for metal forming techniques was shown. Although the ribbon belts were successfully employed in the continuous embossing of extruded polymer further investigation in nickel plating metallurgy needs to be done to improve the ductility and durability of the ribbon belts and UV curable epoxy resists that can be dissolved or more easily removed from the metal formed nickel ribbon mold should be investigated.

The crystallin structure of metals limits how small mold features could be and thermally embossing most durable metals at reasonable temperatures for the use as master molds is a problem. For this reason, much effort and attention has been given to using metal glass (MG) as a mold material for R2R embossing of polymers. In this research, a mechanism was designed and built to thermally emboss a roller with a MG surface using a flat master mold. The apparatus was designed to be usable in a vacuum or inert gas over at temperatures close to T_g of MG as well as at room temperature.

Sections of a 40 mm diameter extruded MG cylinder were used to determine the operating parameters for embossing the MG and a 5 mm wide ring cut from the MG cylinder was successfully embossed using the designed apparatus. The embossed ring was then used in the calender of the laboratory scale film manufacturing setup as a mold to emboss continuously extruded polymer successfully.

Future work will include embossing a roller and then a metal ribbon belt with a cold sprayed MG surface with micro and nano features and then using the roller for R2R NIL. Cold spraying the surface of a roller or a metal ribbon mold belt is scalable to industrial applications.

BIBLIOGRAPHY

- [1] R. J. Daniello, N. E. Waterhouse and J. P. Rothstein, "Drag reduction in turbulent flows over superhydrophobic surfaces," *PHYSICS OF FLUIDS*, vol. 21, p. 085103, 2009.
- [2] A. Mall, P. R. Jelia, A. Agrawal, R. K. Singh and S. S. Joshi, "Design of Arrayed Micro-Structures to get Super-Hydrophobic Surface for Single Droplet and Bulk Flow Conditions," *Proceedings of the COMSOL Conference 2009 Bangalore*, 2009.
- [3] K. Kurihara, Y. Suzuki, K. Suto, N. N. Shiba, T. and J. Tominaga, "Wettability control using large-area nanostructured film," *Microelectronic Engineering*, vol. 87, p. 1424–1427, 2010.
- [4] J. Brandrup, E. H. Immergut and E. A. Grulke, "Polymer Handbook," in *Polymer Handbook*, New York , Wiley, 1999.
- [5] B. H. D. E. Ganesan, "A Lab Scale Polymer Micro-Embossing Machine for Process Control Research," Singapore-MIT Alliance (SMA), 2004.
- [6] E. Michaeli, B. Fink and P. Blomer, "Dynamic controll of roll temperatures," in *Kunststoffe-Plast Europe 2005*, 2005.
- [7] W. Michaeli, S. Eilbracht, M. Scharf, C. Hartmann, K. Bobzin, N. Bagcivan and S. Theiss, "Application of variothermal heating concepts for the production of microstructured films using the extrusion embossing process," *Journal of Polymer Engineering*, vol. 32, pp. 95-101, 2012.
- [8] C. Hopmann, E. Michaeli, S. Eilbracht, K. Bobzin, N. Bagcivan, S. Theiss, C. Hartmann and J. Holtkamp, "Extrusion embossing of hydrophobic films - a study on process characteristics and surface properties," *Journal of Plastics Technology*, vol. 8, pp. 302-330, 2012.

- [9] D. Yao, P. Nagarajan, L. Li and A. Yi, "A two-station embossing process for rapid fabrication of surface microstructures on thermoplastic polymers," *Polymer Engineering and Science*, vol. 47, pp. 530-539, 2007.
- [10] D. Yao, P. Nagarajan, L. Li and A. Yi, "A strategy for rapid thermal cycling of molds in thermoplastic processing," *Journal of Manufacturing Science and Engineering-Transactions of the ASME*, vol. 128, pp. 837-843, 2006,, .
- [11] D. Yao, S. Chen and B. Kim, "Rapid Thermal Cycling of Injection Molds: An Overview on Technical Approaches and Applications," *Advances in Polymer Technology*, vol. 27, p. 233+255, 2008.
- [12] J. Dumond and H. Low, "Recent developments and design challenges in continuous roller micro- and nanoimprinting," *Journal of Vacuum Science & Technology B*, vol. 30, p. 010801, 2012.
- [13] S. Seo, T. Kim and H. Lee, "Simple fabrication of nanostructure by continuous rigiflex imprinting," *Microelectronic Engineering*, vol. 84, pp. 567-572, 2007.
- [14] M. D. Fagan and B. H. Kim, "A Novel Process for Continuous Thermal Embossing of Large-Area Nanopatterns onto Polymer Films," *Advances in Polymer Technology*, vol. 28, no. 4, pp. 246-256, 2009.
- [15] T. Huang, J. Ciou, P. Huang, K. Hsieh and S. Yang, "Fast fabrication of integrated surface-relief and particle-diffusing plastic diffuser by use of a hybrid extrusion roller embossing process," *Optics Express*, vol. 16, pp. 440-447, 2008.
- [16] J. Schroers, T. Nguyena, S. O’Keeffe and A. Desai, "Thermoplastic forming of bulk metallic glass—Applications for MEMS and microstructure fabrication," *Materials Science and Engineering A*, p. 449–451 (2007) 898–902, 2006.
- [17] W. Liu, D. Wu, Y. Liu and X. Zheng, "The research of the extrusion hot embossing process," *Materials Processing Technology*, vol. 337, pp. 323-327, 2011.

- [18] J. J. Kelly and S. Goods, "X-ray Lithography Techniques, LIGA-Based Microsystem Manufacturing: The Electrochemistry of Through-Mold Deposition and Material Properties," in *Nanostructure Science and Technology, Electrochemistry at the Nanoscale*, Springer Science+Business Media, LLC, 2009, pp. 79-138.
- [19] E. W. Backer, W. Ehrfeld, D. Münchmeyer, H. Betz and A. Heuberger, "Production of separation-nozzle systems for uranium enrichment by a combination of X-ray lithography and galvanoplastics," vol. 69, no. 11, pp. 520-523, 1982.
- [20] A. Kolew, D. Münch, K. Sikora and M. Worgull, "Hot embossing of micro and sub-micro structured inserts for polymer replication," *Microsystems Technology*, vol. 17, pp. 609-618, 2010.
- [21] Z. Cui, "LIGA," in *Encyclopedia of Microfluidics and Nanofluidics*, Springer-Verlag, 2008.
- [22] S. Chou, P. Krauss and P. Renstrom, "Imprint Lithography with 25-Nanometer Resolution," *Science*, vol. 272, pp. 85-87, 1986.
- [23] "Nanoimprint lithography," [Online]. Available: http://en.wikipedia.org/wiki/Nanoimprint_lithography. [Accessed 28 8 2011].
- [24] T. Mappes, M. Worgull, M. Hecke and J. Mohr, "Submicron polymer structures with X-ray lithography and hot embossing," *Microsystems Technology*, vol. 14, p. 1721–1725, 2008.
- [25] L. Lin, Y. Cheng and C. Chiu, "Comparative study of hot embossed micro structures fabricated by laboratory and commercial environments," *Microsystem Technologies*, vol. 4, pp. 113-116, 1998.
- [26] J. Wang, W. Xue and T. Cui, "A combinative technique to fabricate hot embossing master for PMMA tunneling sensors," *Microsystem Technologies*, vol. 10, pp. 329-333, 2004.
- [27] T. E. Kimerling, W. Liu and B. H. Kim, "Rapid hot embossing of polymer microfeatures," *Microsystem Technology*, vol. 12, p. 730–735, February 2006.

- [28] S. R. Nugen, P. J. Asiello and A. J. Baeumner, "Design and fabrication of a microfluidic device for near-single cell mRNA isolation using a copper hot embossing master," *Microsystem Technologies*, vol. 15, no. 3, pp. 477-483, 2008.
- [29] L. Q. Chen, M. B. Chan-Park, Y. H. Yan, Q. Zhang, C. M. Li and J. Zhang, "High aspect ratio silicon nanomoulds for UV embossing fabricated by directional thermal oxidation using an oxidation mask," *Nanotechnology*, vol. 18, 2007.
- [30] X. Fu, Q. Chen, X. Chen, L. Zhang, A. Yang and Y. Cui, "A Rapid Thermal Nanoimprint Apparatus through Induction Heating of Nickel Mold," vol. 10, no. 334, 2019.
- [31] J. Lee, S. Park, K. Choi and G. Kim, "Nano-scale patterning using the roll typed UV-nanoimprint lithography tool," *Microelectronic Engineering*, vol. 85, pp. 861-865, 2008.
- [32] O. Nezuka, "REPLICATION OF MICROSTRUCTURES BY ROLL-TO-ROLL UV-CURING EMBOSSING," Amherst, 2007.
- [33] S. H. Ahn, "HIGH-THROUGHPUT, CONTINUOUS NANOPATTERNING TECHNOLOGIES FOR DISPLAY AND ENERGY APPLICATIONS," 2010.
- [34] S. H. Wang and Z. F. Ng, "Hot roller embossing for microfluidics: process and challenges," *Microsystem Technology*, vol. 15, pp. 1149-1156, 2008.
- [35] H. Suzuki, K. Nagato, S. Sugimoto, K. Tsuchiya, T. Hamaguchi and M. Nakao, "Iterative imprint for multilayered nanostructures by feeding, vacuum forming, and bonding of sheets," *Journal of Vacuum Science & Technology B*, vol. 26, no. 5, p. 1753, 2008.
- [36] L. P. Yeo, S. H. Ng, Z. F. Wang, H. M. Xia, Z. P. Wang and V. S. Thang, "Investigation of hot roller embossing for microfluidic devices," *JOURNAL OF MICROMECHANICS AND MICROENGINEERING*, vol. 20, p. 015017 (10pp), January 2010.

- [37] T. Velten, F. Bauerfeld, H. Schuck, S. Scherbaum, L. C. Landesberger and K. Bock, "Roll-to-roll hot embossing of microstructures," *Microsystem Technology*, vol. 17, p. 619–627, 2010.
- [38] S. H. Ahn and L. J. Guo, "Large-Area Roll-to-Roll and Roll-to-Plate Nanoimprint Lithography: A Step toward High-Throughput Application of Continuous Nanoimprinting," *ACS NANO*, vol. 3, no. 8, pp. 2304-2310, 2008.
- [39] M. Matschuk, H. Bruus and N. B. Larsen, "Nanostructures for all-polymer microfluidic systems," *Microelectronic Engineering*, vol. 87, pp. 1379-1382, 2010.
- [40] S. Hattori, K. Nagato, T. Hamaguchi and M. Nakao, "Rapid injection molding of high-aspect-ratio nanostructures," *Microelectronic Engineering*, vol. 87, pp. 1546-1549, 2010.
- [41] M. Worgull, M. Hecke and W. K. Schomburg, "Large-scale hot embossing," *Microsystems Technology*, vol. 12, p. 110–115, 2005.
- [42] H. Taylor, D. Boning, C. Iliescu and B. Chen, "Computationally efficient modelling of pattern dependencies in the micro-embossing of thermoplastic polymers," *Microelectronic Engineering*, vol. 85, pp. 1453-1456, 2008.
- [43] S. Stoyanov, T. Tilford, F. Amalaou and S. Cargill, "Modeling and optimization study on the fabrication of nanostructures using the imprint of forming process," vol. 28, no. 1, p. 93, 2011.
- [44] Y. Ren and J. K. Good, "THE NIP MECHANICS OF NANO-IMPRESSION LITHOGRAPHY IN ROLL-TO-ROLL PROCESS MACHINES," 2017.
- [45] N. Unno and T. Mäkelä, "Thermal Nanoimprint Lithography—A Review of the Process, Mold Fabrication, and Material," *Nanomaterials*, vol. 13, no. 14, 8 July 2023.
- [46] T. Kimerling, W. Liu, B. Kim and D. Yao, "Rapid hot embossing of polymer microfeatures," *Microsystem Technologies-Micro-and Nanosystems-Information Storage and Processing Systems*, vol. 12, pp. 730-735, 2006.

- [47] H. Tan, A. Gilbertson and S. Chou, "Roller nanoimprint lithography," *Journal of Vacuum Science & Technology*, vol. B, no. 16, pp. 3926-3928, 1998.
- [48] S. Liu and W. Chen, "Nanofeatured Anti-Reflective Films Manufactured Using Hot Roller Imprinting and Self-Assembly Nanosphere Lithography," *Optics & Laser Technology*, no. 48, pp. 226-234, 2013.
- [49] V. Rudnew, R. Loveless, R. Cook and M. Black, *Handbook of Induction Heating*, New York, USA: Marcel Dekker, Inc., 2003.
- [50] K. Takenaka, N. Saidoh, N. Nishiyama and A. Inoue, "Fabrication and nano-imprintabilities of Zr-, Pd- and Cu-based glassy alloy thin films," *Nanotechnology*, vol. 22, p. 105302 (6pp), 2011.
- [51] Ziff Davis, "process technology," [Online]. Available: <https://www.pcmag.com/encyclopedia/term/process-technology>. [Accessed 6 June 2023].
- [52] "INTERNATIONAL TECHNOLOGY ROADMAP FOR SEMICONDUCTORS," 2010.
- [53] Wikipedia, "Photolithography," 21 07 2011. [Online]. Available: <http://en.wikipedia.org/wiki/Photolithography>. [Accessed 30 7 2011].
- [54] A. N. Broers, "Fabrication Limits of Electron Beam Lithography and of UV, X-Ray and Ion Beam Lithographies," in *Perspectives on the Limits of Fabrication and Measurement*, 1995.
- [55] H. S. Jang, G. H. Kim, J. Lee and K. B. Choi, "Eliminating the undercut phenomenon in interference lithography for the," *Current Applied Physics*, vol. 10, no. 6, pp. 1436-1441, 17 May 2010.
- [56] J. M. Kohler and W. Fritzsche, *Nanotechnology: an introduction to nanostructuring techniques*, Weinheim: Wiley--VCH Verlag GmbH & Co., 2007.
- [57] MicroChemicals, "Exposure of Photoresists," MicroChemicals GmbH, 27 1 2010. [Online]. Available: www.microchemicals.eu/technical_information. [Accessed 7 8 2011].

- [58] Q. Xiea, M. Honga, H. Tanb, G. Chenb, L. Shia and T. Chong, "Fabrication of nanostructures with laser interference lithography," *Journal of Alloys and Compounds*, vol. 449, no. 1 - 2, pp. 261-264, 31 January 2008.
- [59] H.-G. Park, J.-J. Lee, K.-Y. Dong, B.-Y. Oh, Y.-H. Kim, H.-Y. Jeong, B.-K. Ju and D.-S. Seo, "Homeotropic alignment of liquid crystals on a nano-patterned polyimide surface using nanoimprint lithography," *Soft Matter*, vol. 7, pp. 5610-5614, 2011.
- [60] N. P. Pham, E. Boellard, P. M. Sarro and J. N. Burghartz, "Spin, Spray coating and Electrodeposition of photoresist for MEMS structures – A comparison," *Euroensors*, pp. 86-86, 2002.
- [61] N. P. Pham, T. L. Scholtes, R. Klerks, E. Boellaard, P. M. Sarro and J. N. Burghartz, "Direct spray coating of photoresist – a new method for patterning 3-D structures," in *Euroensors XVI*, Prague, 2002.
- [62] K. Cooper, K. Cook and B. Whitney, "LITHOGRAPHIC CHALLENGES AND SOLUTIONS FOR 3D INTERCONNECT," in *IWLPC*, San Jose, CA, 2008.
- [63] G. A. LUURTSEMA, "SPIN COATING FOR RECTANGULAR SUBSTRATES," 1997.
- [64] G. Perçin, T. H. Soh and B. T. Khuri-Yakub, "Resist deposition without spinning by using novel inkjet technology and direct lithography for MEMS," *IEEE TRANSACTIONS ON SEMICONDUCTOR MANUFACTURING*, vol. 16, no. 3, August 2003.
- [65] S. Chakraborty, *Microfluidics and Microfabrication*, New York Dordrecht Heidelberg London: Springer, 2010, pp. 197-199.
- [66] P. Jalonen and A. Tuominen, "The Applicability of Electrodeposited Photoresist in Producing Ultra-fine Lines Using Sputtered Seeding Layers," *2000 Int'l Symp on Electronic Materials & Packaging*, 2000.
- [67] R. M. Kubacki, "Plasms Deposited Selective Wetting Material". USA Patent 20040197488 A1, 7 October 2004.

- [68] T. W. Weidman and A. M. Joshi, "New photodefinable glass etch masks for entirely dry photolithography: Plasma deposited organosilicon hydride polymers," *Applied Physics Letters*, vol. 62, no. 4, pp. 372-374, January 1993.
- [69] P. R. Kanikella, "Process development and applications of a dry film photoresist," University of Missouri-Rolla, Rolla, 2007.
- [70] E. KOUKHARENKO, M. KRAFT, G. J. ENSELL and N. HOLLINSHEAD, "A comparative study of different thick photoresists for MEMS applications," *Journal of Materials Science: Materials in Electronics*, vol. 16, no. 11-12, pp. 741-747, November 2005.
- [71] C. A. Bower, K. H. Gilchrist, M. R. Lueck and B. R. Stoner, "Microfabrication of fine-pitch high aspect ratio Faraday cup arrays in silicon," *Sensors and Actuators*, vol. A, no. 137, pp. 296-301, 2007.
- [72] M. Gower, "Laser micromachining for manufacturing MEMS devices," in *Proceedings of SPIE Vol. 4559 (2001)*, 2001.
- [73] S. Chen, V. Kancharla and Y. Lu, "Laser-based microscale patterning of biodegradable polymers for biomedical applications," *International journal of materials & product technology*, vol. 18, no. 4/5/6, pp. 457-468, 2003.
- [74] H. Zhang, D. W. Hutmacher, F. Chollet, A. N. Poo and E. Burdet, "Microrobotics and MEMS-Based Fabrication Techniques for Scaffold-Based Tissue Engineering," *Macromolecular Bioscience*, no. 5, pp. 477-489, 2005.
- [75] P. Dyer, S. Maswadi, C. Walton, M. Ersoz, P. Fletcher and V. Paunov, "157-nm laser micromachining of N-BK7 glass and replication for microcontact printing," *Applied Physics A - Materials Science & Processing*, pp. 391-394, 2003.
- [76] D. D. Karnakis, "Ultrafast Laser Nanomachining: Doing More With Less," Oxford Lasers Ltd, Didcot Oxfordshire, 2007.
- [77] I.-B. Baeka, J.-H. Yang, W.-J. Cho, C.-G. Ahn, K. Im and S. Lee, "Electron beam lithography patterning of sub-10 nm line using hydrogen," *Journal of Vacuum Science and Technology*, vol. B 23, no. 6, pp. 3121-3123, 2005.

- [78] W. Hu, W. Hu, K. Sarveswaran, M. Lieberman and G. H. Bernstein, "High-Resolution Electron Beam Lithography and DNA Nano-Patterning for Molecular QCA," *IEEE TRANSACTIONS ON NANOTECHNOLOGY*, vol. 4, no. 3, May 2005.
- [79] C. Vieu, F. Carcenac, A. Pe'pin, Y. Chen, M. Mejias, A. Lebib, L. Manin-Ferlazzo, L. Couraud and H. Launois, "Electron beam lithography: resolution limits and applications," *Applied Surface Science*, no. 164, pp. 111-117, 2000.
- [80] A. A. Tseng, K. Chen, C. D. Chen and K. J. Ma, "Electron Beam Lithography in Nanoscale Fabrication: Recent Development," *IEEE TRANSACTIONS ON ELECTRONICS PACKAGING MANUFACTURING*, vol. 26, no. 2, pp. 141-149, April 2003.
- [81] P. S. Spinney, D. Howitt, R. L. Smith and S. D. Collins, "Nanopore formation by low-energy focused electron beam machining," *Nanotechnology*, vol. 21, 2010.
- [82] Malek, F. T. Hartley and C. Khan, "Nanometer X-ray Lithography," *Design, Characterization and Packaging for MEMS and Micro Electronics*, 29 October 1999.
- [83] NanoMatrix, Inc., "NanoMatrix," NanoMatrix, Inc., [Online]. Available: <http://www.nanomatrix.com/index.html>. [Accessed 25 8 2011].
- [84] M. J. Jackson, "Non-Traditional machining using pulsed water jets," *International journal of manufacturing technology and management*, vol. 7, no. 2/3/4, pp. 127-141, 2005.
- [85] J. John, Y. Tang, J. P. Rothstein, J. J. Watkins and K. R. Carter, "Large-area, continuous roll-to-roll nanoimprinting with PFPE composite molds," *Nanotechnology*, vol. 24, p. 505307, 27 November 2013.
- [86] NSF Center for Hierarchical Manufacturing at the University of Massachusetts - Amherst , "Center for Hierarchical Manufacturing," [Online]. Available: <http://chm.pse.umass.edu/>. [Accessed 12 6 2023].
- [87] I. Kim and P. F. Mentone, "Electroformed nickel stamper for light guide panel in LCD back light unit," *Electrochimica Acta*, vol. 52, no. (2006) 1805–1809, 2006.

- [88] P. T. Tang, M. E. Benzon, J. P. Rasmussen and F. S. Fontenay, "Important Parameters and Applications for Nickel Electroforming," in *American Electroplaters and Surface Finishers Society. Annual Technical Conference. Proceedings*, 1996.
- [89] G. A. Di Bari, "Electroforming," in *Electroplating Engineering Handbook - Fourth*, L. J. Durney, Ed., New York, Van Nostrand Reinhold Company, 1984.
- [90] N. Li, J. Pan, Z. Liu and L. Liu, "Metallic glass nanostructures: Forming strategies and functional applications," *materialstoday ADVANCES*, vol. 15, no. August, p. 100253, 2022.
- [91] Y. Saotome, S. Miwa, T. Zhang and A. Inoue, "The microformability of Zr-based amorphous alloys in the supercooled liquid state and their application to micro-dies," *Journal of Materials Processing Technology*, vol. 113, no. 1-3, pp. 64-69, June 2001.
- [92] D. Wang, G. Liao, J. Pan, Z. Tang, P. Peng, L. Liu and T. Shi, "Superplastic micro-forming of Zr₆₅Cu_{17.5}Ni₁₀Al_{7.5} bulk metallic glass with silicon mold using hot embossing technology," *Journal of Alloys and Compounds*, vol. 484, no. 1-2, pp. 118-122, 18 September 2009.
- [93] L. Jiang, T. Huang, C. Chiu, C. Chang and S. Yang, "Fabrication of plastic microlens arrays using hybrid extrusion rolling embossing with a metallic cylinder mold fabricated using dry film resist," *Optics Express*, vol. 15, pp. 12088-12094, 2007.